RESONANT CAVITY FIBRE BRAGG GRATING

SENSOR INTERROGATION

GLYNN DAVID LLOYD

Doctor of Philosophy

ASTON UNIVERSITY

December 2004

ASTON UNIVERSITY

RESONANT CAVITY FIBRE BRAGG GRATING SENSOR INTERROGATION

GLYNN DAVID LLOYD

Doctor of Philosophy, December 2004

ABSTRACT

This thesis presents a novel high-performance approach to time-division-multiplexing (TDM) fibre Bragg grating (FBG) optical sensors, known as the resonant cavity architecture.

A background theory of FBG optical sensing includes several techniques for multiplexing sensors. The limitations of current wavelength-division-multiplexing (WDM) schemes are contrasted against the technological and commercial advantage of TDM. The author's hypothesis that 'it should be possible to achieve TDM FBG sensor interrogation using an electrically switched semiconductor optical amplifier (SOA)' is then explained.

Experimental work shows that when electrically switched, a single SOA provides the combined functions of optical source, amplifier and gate, to TDM closely space low-reflectivity FBG sensors. Exceptional optical performance is achieved using a broadband, chirped FBG to cycle the sensor reflection signals in a virtual 'laser-like' resonant cavity. Several alternative optical circuit configurations for this resonant cavity architecture are provided, which enable compatibility with numerous wavelength detection components. An analysis of cavity signal evolution, an evaluation of sensor crosstalk and preliminary work to demonstrate operation with sensors less than one metre apart using a dual-pulse WDM / TDM hybrid, are also included.

Research and development of a commercially viable optical sensor interrogator based on the resonant cavity architecture forms the remainder of this thesis. A fully programmable SOA drive system allows interrogation of sensor arrays 10km long with a spatial resolution of 8cm and a variable gain system provides dynamic compensation for fluctuating system losses. Ratiometric filter- and diffractive-element spectrometer-based wavelength measurement systems are developed and analysed for different commercial applications. The ratiometric design provides a low-cost solution that has picometre resolution and low noise using 4% reflective sensors, but is less tolerant to variation in system loss. The spectrometer design is more expensive, but delivers exceptional performance with picometre resolution, low noise and tolerance to 13dB system loss variation.

Finally, this thesis details the interrogator's peripheral components, its compliance for operation in harsh industrial environments and several examples of commercial applications where it has been deployed. Applications include laboratory instruments, temperature monitoring systems for oil production, dynamic control for wind-energy and battery powered, self-contained sub-sea strain monitoring.

Key words

Optical fibre sensing, time-division-multiplexing, semiconductor optical amplifier

To all of my family and friends, I could not have done this without you.

3

ACKNOWLEDGEMENTS

I would like to acknowledge a few of the many people who have contributed to this thesis.

Firstly, I would like to express a big thank you to my two supervisors, Ian Bennion at Aston University and Kate Sugden at Indigo Photonics. They both invested their time in me and have provided tremendous help, support and encouragement throughout the happier and harder times at University, Indigo, Insensys and outside. Over these past few years we have become good friends and I thank them both for that. I'd also like to thank Mark Volanthen, Martin Jones and Chris Shannon from Insensys for their encouragement and for allowing me to complete this work. Acknowledgements also go to EPSRC for their financial support and to my colleagues and friends at Aston Photonics Research Group, Indigo Photonics and Insensys for their help, advice, humour and encouragement; in particular a special thank you to John Mitchell, who knows what a PhD in Industry is really like! I'd also like to thank my family and friends, past and present, for their understanding; I've been very preoccupied with this work for a long time, but without them I could not have done it.

Finally, not withstanding the enormous support from everyone else, the person I'd like to thank most, and the person who has made such a difference, is Lorna Everall. Lorna helped with some of the early experimental work and manufactured many of the gratings used for the proof of concept experiments, but most importantly Lorna has provided immeasurable support, encouragement and advice throughout. There were many times when I may have appeared ungrateful, but I truly thank her so much, for everything.

TABLE OF CONTENTS

TABLE OF FIGURES

15

17

TABLE OF TABLES

1 INTRODUCTION

1.1 Fibre Bragg grating based optical fibre sensing

1.1.1 The development of optical fibre technology

Over the past 25 years optical fibre has established itself as the most efficient, cost effective and versatile transport medium for data signals. Examples of applications that now employ optical fibre technology include instrumentation for non-invasive diagnosis and treatment in medicine, fly-by-light control systems for the latest generation of aircraft, laser delivery systems for use in material machining and instrumentation for distributed astronomical research. However, by far the greatest sector to commercially drive and apply optical fibre technology to-date has been telecommunications [1].

The ever-increasing bandwidth required to satisfy a continued market demand for new telecommunications services has ensured a sustained academic and commercial investment into the development of new optical fibre technology. The application of this technology within telecommunications now ranges from the delivery of data, voice and video signals between continents using multi-million dollar silica-based fibre systems, through to the distribution of clock signals across printed circuit boards using multimode polymer cabling at a cost of a few dollars. The result of this exponential success for the technology has meant that components for the generation and detection of optical signals, for signal conditioning, amplification, attenuation, routing, coupling, gating, switching and diagnostics have now reached a high level of maturity.

1.1.2 Optical fibre sensing

Optical fibre sensing (OFS) is one of the sectors to benefit from the numerous technological advances that have occurred as a result of telecommunications [2]. For more than fifteen years the area has received considerable research interest and has grown to cover a vast range of technical disciplines, applications and systems.

Some of the proposed benefits of using optical fibre based measurement technology arise from the host fibre itself. The fibre is manufactured from low attenuation glass, it provides a close material match for embedding into a large variety of composites, is chemically inert, has good electrical insulating properties and it is not affected by, nor

21

does it generate, electromagnetic interference; all features that make it an ideal transport medium for low loss, remote, passive sensing.

The fibre is, however, only a small part of a complete optical system and the optical sensors themselves can also provide numerous key advantages. A number of optical sensor transducer types exist, of which each is sensitive to particular ranges of physical or chemical measurands and of which each is able to deliver the measured output using a different physical approach.

Many simple, and often low-cost, optical sensor systems provide measurement using intensity-based techniques. Typical configurations utilise light from an optical source that is guided into one end of an optical fibre, such that it passes through the optical sensor and onto a photosensitive detector located at the far end of the fibre. The optical sensor is constructed such that it provides a level of optical signal attenuation that is proportional to the magnitude of the measured disturbance. Through calibration of the sensor and source, and by measurement of the intensity of the light received at the detector, an optical method of remotely assessing the value of the measurand experienced by the sensor, is then achieved.

Other common optical sensor systems utilise interference based measurement principles. In these configurations a coherent light signal is often split into two optical paths, one of which is subjected to an external measurand such that the effective optical path length experienced by the light is affected. Recombining the two optical signals at the far end of the system allows interference to occur, the extent of which can be used to assess the magnitude of the path-length disturbance, and hence determine the value of the external measured.

Unfortunately however, despite the simplicity of these and many other optical sensing approaches, difficulties can arise with regard to sensitivity, long-term stability, accuracy and manufacturability. In particular, intensity based systems can often suffer from fluctuation in the optical source output power, which can be misinterpreted at the photodetector as a change in the measured disturbance. Similarly small temperature changes or vibrations can often manifest as undesired path-length errors in interferometric systems, the result of which is a reduction in the measurement accuracy.

22

1.1.3 Fibre Bragg gratings

It is partially as a result of these errors and shortcomings of interferometric- and intensity-based relative-measurement optical sensor techniques that one of the largest sections of the diverse optical sensing arena, that has remained active for over ten years, is dedicated to the research and development of transducers and systems based around the absolute-measurement advantage of fibre Bragg gratings (FBGs).

FBGs are entirely passive, in-fibre devices that are manufactured within a host optical fibre through exposure of the silica core to intense radiation from an ultraviolet laser [3, 4, 5]. In their simplest form they can be considered as miniature in-line mirrors, which can strongly reflect optical signals over a narrow (user definable) range of wavelengths, yet cause little attenuation to the transmission of signals at all other wavelengths. This versatile optical filtering property has meant that FBGs have been very successfully employed in a range of signal conditioning applications within telecommunications, but ever since their initial discovery the devices have also been noted for their excellent sensing properties. An increase of either the ambient temperature or the external strain that is applied to an FBG will result in a shift of the optical filtering profile of the device towards longer wavelengths. As such, by illuminating an FBG using a broadband optical source and measuring the wavelength of the resulting reflection signal, an assessment of the physical conditions experienced by the device is possible [6, 7]. When operated in this manner FBGs form highly sensitivity, passive, all-optical, absolute-measurement sensors, which allow remote measurement of temperature or strain.

Furthermore, FBGs also have the advantage that they can be used to form the basis of more complex transducers, which provide measurement of other environmental, physical, chemical and electrical variables. Some examples of applications that have employed such sensors have included the detection of gases and liquids [8], the measurement of strain [9], temperature [10], salinity [11] and corrosion [12] and the analysis of pressure [13], vibration [14], inclination [15] and fluid flow [16].

However, it is not only the diversity of measurands recorded using FBGs that make them important devices for optical fibre sensing; one of the most fundamental benefits is their inherent potential for multiplexing. Since FBGs are typically employed as wavelength selective reflectors, multiple transducers can be independently operated within a single length of optical fibre. The only requirement for this mode of operation

is that the wavelength interrogation equipment is able to identify the individual reflection signals returned from each sensor.

1.1.4 Wavelength-division-multiplexing

Numerous techniques have been proposed that have the potential for multiplexing FBG sensors within a single fibre, but of these by far the simplest and most commonly exploited is wavelength-division-multiplexing (WDM) [6, 7], as shown in Figure 1.1. This approach employs application-specific sensor arrays, which contain FBGs that are each manufactured to operate within a different wavelength window. The sensors are typically illuminated from a single continuous wave, broadband optical source, such that the reflections from all sensors are returned simultaneously to the wavelength measurement system. Since each of the reflection signals is of distinct wavelength the identification of individual sensors can occur with relative ease if the correct detection components are chosen. Such WDM systems can be developed with common bench-top laboratory equipment and can provide adequate performance for many research applications.
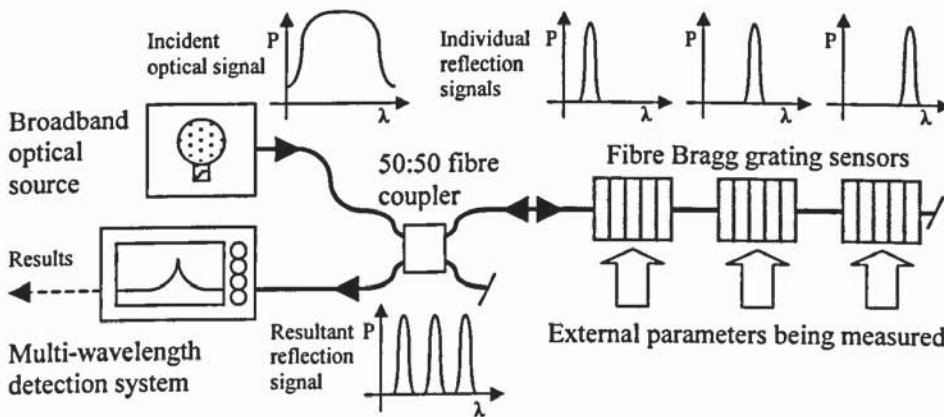
Figure 1.1 The general arrangement for a wavelength-division-multiplexed fibre Bragg grating sensor interrogation system

Unfortunately however, despite the simplicity of the WDM technique, there are a number of disadvantages that limit its performance and commercial viability. Since each of the FBGs is required to operate within a distinct optical window, the maximum number of sensors that can be multiplexed onto a single optical fibre is often fewer than 10; the finite operating bandwidth of both the optical source and the wavelength measurement components means that a trade-off exists between the measurement range of each sensor and the total number of sensors that can be used. The requirement for bespoke array design, such that each FBG is of a unique wavelength (chosen according to the desired sensor range) also causes considerable increases in costs; sensor yields

are reduced while the fabrication time is greatly increased as a result of continuous tooling changes, stock inventories become more complex and delivery lead-times are increased. Finally, the WDM requirement for individual identification of multiple, simultaneously received reflection signals places a limit on the variety of wavelength measurement techniques that can be employed; some of the lower cost, passive approaches cannot be used [17, 18].

1.1.5 Time-division-multiplexing

As a result of the limitations of the WDM technique, several other approaches have been proposed for multiplexing FBG sensors, of which time-division-multiplexing (TDM) is perhaps the most common [6, 7]. In contrast to WDM, which identifies each of the sensors by their unique wavelength, TDM employs sensors that are all at the same nominal wavelength and of low reflectivity. Individual sensors are uniquely identified by measuring the time of flight of the reflections generated from illumination of the sensors by a pulsed optical source. The sensors at more distance positions in the sensor array will have reflections that arrive at the wavelength interrogation system later in time, as shown in Figure 1.2.
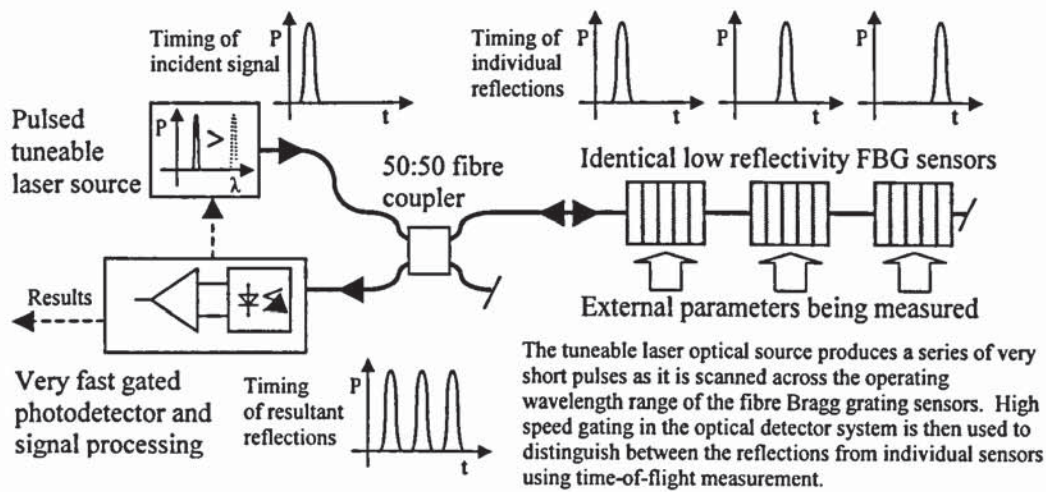
Figure 1.2 The general arrangement for a time-division-multiplexed fibre Bragg grating interrogation scheme

The TDM approach has a number of key advantages that arise from its use of identical wavelength, low reflectivity sensors. Firstly, the maximum number of sensors that can be supported is far higher than for WDM systems, as the bandwidth of the source and detector do not have to be divided between the sensors. Bespoke sensor array design is not required as all sensors can operate with the full working range of the system. The actual cost of array manufacture is therefore significantly cheaper since no tooling changes are needed and only low reflectivity FBGs are required; such factors remove

25

the requirement for expensive manual intervention, allow the use of through-coating fabrication [19] and greatly increase yield. Large spools of identical sensors can be manufactured in a single operation and can then be used for many different installations. This approach exploits economies of scale, enables a reduction in the diversity of the stock inventory and decreases the project lead-time.

Unfortunately however, despite the advantages of using TDM for multiplexing FBG sensors onto a single optical fibre, very few demonstration systems have actually been reported and no commercially viable solutions have existed until now. This lack of research and development has been due to the difficulty in identifying the individual reflections from sensors. Since the optical signals travel at over 200 million metres per second in the fibre, interrogation systems that use low reflectivity sensors spaced at 2m intervals will produce reflections that are very low in power, are less than 20ns long and arrive at the wavelength detector just 20ns apart. Very fast gating and sensitive detectors are therefore required to measure individual sensors without crosstalk.

To-date two primary approaches have been proposed for isolating individual sensor reflections:

Electronic gating has attempted to separate out signals after they have been converted into the electrical domain using a photodetector [20]. This approach has the disadvantage that fewer wavelength measurement techniques can be employed, but at first sight it appears to provide a low cost and simple solution. Unfortunately, in reality the technique requires very high-bandwidth, high-gain electronics, which means that it is fundamentally limited by noise and provides poor performance. Therefore, to-date, no systems have been demonstrated that utilise electronic gating of closely spaced, low reflectivity sensors.

Optical gating is a significantly more effective approach and has been demonstrated with many tens of low reflectivity, closely spaced sensors [21]. By using the combination of a high extinction-ratio optical modulator and an erbium-doped fibre amplifier (EDFA) individual reflection signals can be isolated and amplified directly in the optical domain. This allows wavelength detection using a broad range of techniques with minimal crosstalk between sensors and results in excellent system performance. Unfortunately however, commercial viability of the approach is severely

26

limited as the EDFA and optical modulator components are bulky, expensive and electrically inefficient.

1.1.6 The commercial success of FBG based fibre optic sensing

Until now, only a few commercial sensor interrogation systems have been developed that provide a facility for multiplexing of multiple sensors, and of these all have employed WDM techniques. They have all required the use of expensive bespoke sensor arrays, have been limited to a few sensors per fibre and have shown little development from the original laboratory demonstrations; despite being commercial in nature, many of the available interrogators have not been designed to operate in harsh industrial environments. They have often been bulky, fragile and electrically inefficient and have not been provided with appropriate hardware or software control and communication interfaces.

Therefore, despite the significant academic achievement that has occurred in FBG based optical fibre sensing, and in contrast to telecommunications, mass uptake of the technology has not occurred. Due to the low performance and high cost of the interrogation equipment, commercial applications have often only delivered modest economic returns. True commercial investment has remained small and so rather than developing interrogation equipment, research has largely focused on deploying existing sensors in new ways, to provide measurement in a wider range of disciplines. The result of this has been that the arena has been broadened, rather than strengthened and overall market acceptance has remained relatively poor.

It is therefore pleasing that the work in this thesis has helped to bring a significant change to the market acceptance for FBG sensing technology and has thus created a substantially greater commercial uptake. This change has been achieved through the realisation of a low cost, low power, high performance, environmentally robust, TDM interrogation system that can operate with low reflectivity, closely spaced FBG sensors. To-date around 75 of these interrogation systems have been deployed, while the sales for 2005 are expected to rise exponentially as customers complete their initial development work and begin deploying devices into their next generation of volume products.

27

1.2 The resonant cavity architecture

This unique interrogation system is based on a novel resonant cavity architecture, whose conception, experimental verification and development form the basis of this thesis. The system utilises the high-speed switching capabilities of a semiconductor optical amplifier (SOA) to perform the combined functions of sensor illumination, optical gating and optical amplification in a single active component. Through the use of a broadband reflector, a cyclic optical signal is produced in a resonant 'laser-like' cavity around the SOA. This provides a true TDM demultiplexer that delivers an exceptionally high signal level, a high optical signal to noise ratio (OSNR) and a minimum crosstalk from large arrays of closely spaced, low reflectivity, identical 'commodity' FBG sensors.

To-date two wavelength detection techniques have been successfully researched, developed and employed with the resonant cavity interrogator. Each provides a different set of key performance characteristics, to cater for different applications. Use of the ratiometric wavelength detection technique results in a very low cost, high-speed interrogation system that has a high resolution with a modest operating range, but is less able to support a large variation in system loss. The superior diffractive element spectrometer-based alternative provides an exceptional performance and has been commercially verified with 160 sensors. It has a large operating range, high resolution, low noise and good polarisation insensitivity, but is more expensive.

However, as stated within this thesis mass acceptance of fibre sensor technology requires more than just a superior level of optical performance. Delivery of a product that is environmentally qualified, industrially robust and compatible with a wide range of commercial and industrial power and control systems is also essential. By focusing on the research and development of a core interrogation module that can be deployed in a wide range of environments, the economies of scale, development efficiency and the benefit of cross application experience have all been achieved. With only a minimum of additional engineering effort the product has been deployed in applications as diverse as battery-power sub-sea strain measurement, for dynamic control in wind turbines and for distributed temperature monitoring in oil production.

1.3 Thesis overview

The work in this thesis has been carried out whilst working within a commercial engineering environment and, as such, has been strongly driven by commercial goals.

28

Therefore, whilst methodical scientific research has been the key to engineering success, the development of the most commercially attractive results has taken precedence over coverage of all avenues of enquiry. In contrast to some research that covers a broad range of topics, this work is vertically integrated and covers only one key topic. It extends from the initial hypothesis, through the proof of concept, to the development of a commercial product with its qualification and final application.

The structure and the methods used for reporting within this thesis are intentionally aimed at both an academic and an engineering audience since the novelty of the invention can be utilised and extended on many levels. Understanding of the core optical architecture, its levels of performance, the configurations that have been most successful and those that have proved difficult will all be of great value to an academic audience, who may wish to extend the design at a fundamental level. Additionally, an understanding of the reasons and methods employed during the design and development of the overall engineered product will appeal to readers from a variety of disciplines, who may wish to deploy, control or enhance the system at a higher level.

Chapter 2 provides a background summary of the extensive research and development that has been carried out within optical fibre sensing. It highlights the benefits of using the technology and a history of the development of FBGs. Included are several of the most common FBG fabrication techniques and a discussion of the advantages that can be gained from using low reflectivity, identical wavelength devices. Numerous multiplexing schemes and their benefits and limitations are also introduced, including several WDM and TDM approaches and a few less common methods. An overview of the SOA is then provided, with reference to its usual CW mode of operation and some prior work on utilising the device as an optical switch. Finally the author's original hypothesis, 'that it may be possible to use a semiconductor optical amplifier to time-division-multiplex fibre Bragg grating sensors', is introduced.

Chapter 3 concentrates on the numerous 'proof of concept' experiments that were conducted to verify the use of an SOA for multiplexing FBG sensors. Included is the initial proof that a single device could be used as the optical source, amplifier and gate. The notion of cycling the pulses to form a resonant cavity is then covered, as are a number of variations on the architecture that allow extraction of the cavity signal from a number of locations in the optical circuit. The key characteristics of each scheme are provided and a discussion is given as to the most appropriate wavelength detection

technique to use with each variant. Then, following research into the evolution of the cavity signal and the performance of the system with low reflectivity devices, a more complex pulsing scheme is introduced that provides a hybrid WDM and TDM interrogation architecture, which allows for a reduction in the spacing of the sensors. Finally, the chapter concludes with a discussion of the commercial viability of the scheme, the application for patent protection of the idea and an analysis of the components that were considered essential for a commercially viable interrogation system.

Chapter 4 concentrates on the research and development of the pulsed SOA driver sub-system. This was the most important part of the interrogator design, as high-speed delivery of accurately timed, variable length SOA drive pulses was essential to the commercial success of the product. The chapter begins with a discussion of the laboratory equipment that was used for the original proof of concept experiments, which employed sensors that were spaced 65m apart. It then details a series of iterative research and development steps that finally resulted in the novel driver design. This final design not only provides accurate timing of the SOA switching profile, but also dynamically adjusts the gain of the system to allow operation under variable loss conditions with sensors only one metre apart.

Chapter 5 covers the development of the two wavelength measurement sub-systems. The first utilises a ratiometric approach and is based around a commercial filter component, while the second is based on a diffractive element spectrometer. The chapter describes the bespoke electronics and software that were developed to control and interface each of these detection methods into the remainder of the system. An analysis of the performance of the final interrogation solution was then carried out to assess the commercial viability of each approach. The results show that the ratiometric technique provides a low cost solution with a good level of performance under stable conditions, but that limitations are experienced with increased cavity loss. The diffractive element spectrometer is shown to provide excellent performance for a wider variety of applications.

Chapter 6 provides coverage of the hardware and software interface components developed to enable deployment of the interrogator in a wide range of industrial applications. Details are also included regarding the environmental performance criteria to which the system was designed and the results of the qualification tests that

were conducted to verify compliance. Finally, an overview is provided of a range of applications where the resonant cavity interrogator has been deployed, with a selection of results.

Finally, chapter 7 summarises the significance of the work that is contained in this thesis and suggests possible areas for future study, while chapter 8 provides a listing of the publications that have arisen as a result of this research.

1   J. M. Senior, *'Optical Fibre Communications: Principles and Practice'* (2nd Edition), Prentice Hall, London (1992)

2   K. T. V. Grattan, T. Sun, 'Fibre optic sensor technology: an overview', *Sensors and Actuators A*, **82**, 2000, pp.40-61

3   I. Bennion, J. A. R. Williams, L. Zhang, K. Sugden and N. J. Doran 'UV-written in-fibre Bragg gratings', *Optical and Quantum Electronics*, **28**, 1996, pp.93-113

4   K. O. Hill and G. Meltz 'Fiber Bragg grating technology fundamentals and overview', *J. Lightwave Technol.*, **15**, 1997, pp.1263-1276

5   C. R. Giles, 'Lightwave applications of fiber Bragg gratings', *J. Lightwave Technol.*, **15**, 1997, pp.1391-1404

6   A. D. Kersey, M. A. Devis, H. J. Patrick, M. LeBlanc, K. P. Koo, C. G. Askins, M. A. Putnam and E. J. Friebele, "Fiber grating sensors", *J. Lightwave Technol.*, **15**, 1997, pp.1442-1463

7   Y. J. Rao, 'In-fibre Bragg grating sensors', *Meas. Sci. Technol.*, **8**, 1997, pp.355-375

8   A. MacLean, C. Moran, W. Johnstone, B. Culshaw, D. Marsh, P. Parker, 'Detection of hydrocarbon fuel spills using a distributed fibre optic sensor', *Sensors and Actuators A*, **109**, 2003, pp.60-67

9   R. Maaskant, T. Alavie, R. M. Measures, G. Tadros, S. H. Rizkalla, A. Guha-Thakurta, 'Fibre-optic Bragg grating sensors for bridge monitoring', *J. Cement Concrete Compos.*, **19**, 1997, pp.21-23

10   V. M. Murukeshan, P. Y. Chan, L. S. Ong, L. K. Seah, 'Cure monitoring of smart composites using Fiber Bragg Grating based embedded sensors', *Sensors and Actuators A*, **79**, 2000, pp.153-161

11   J. Cong, X. Zhang, K. Chen, J. Xu, 'Fiber optic Bragg grating sensor based on hydrogels for measuring salinity', *Sensors and Actuators B*, **87**, 2002, pp.487-490

12   Y. L. Lo, Y. Y. Yan, 'Multiplexing Intensity-Based Corrosion Sensors Based on Multiple Pairs of Fiber Bragg Gratings', *14th Conference on Optical Fibre Sensing,* 2000, pp.170-173

13   T. Yamate, R. T. Ramos, R. J. Schroeder, E. Udd, 'Thermally Insensitive Pressure Measurements up to 300 degree C using Fiber Bragg Gratings Written onto Side

Hole Single Mode Fiber', *14th Conference on Optical Fibre Sensing*, 2000, pp.628-631

14   W. Jin, Y. Zhou, P. K. C. Chan, H. G. Xu, 'A fibre-optic grating sensor for the study of flow-induced vibrations', *Sensors and Actuators A*, **79**, 2000, pp.36-45

15   Y. Zhao, J. Yang, B. J. Peng, S. Y. Yang, 'Experimental research on a novel fiber optic cantilever-type inclinometer', *Optics and Laser Technol.*, In press

16   S. Takashima, H. Asanuma, H. Niitsuma, 'A water flowmeter using dual fiber Bragg grating sensors and cross-correlation technique', *Sensors and Actuators A*, **116**, 2004, pp.66-74

17   S. M. Melle, K. Liu, R. M. Measures, 'A passive wavelength demodulation system for guided-wave Bragg grating sensors', *Photon. Technol. Lett.*, **4**, 1992, pp.516-518

18   M. A. Davis, A. D. Kersey, 'All-fiber Bragg grating strain-sensor demodulation technique using a wavelength division coupler' *Electron. Lett.*, **30**, 1994, pp.75–77

19   D. S. Starodubov, V. Grubsky and J. Feinberg, 'Efficient Bragg grating fabrication in a fibre through its polymer jacket using near-UV light', *Electron. Lett.*, **33**, 1997, pp.1331-1333

20   Y. J. Rao, A. B. L. Ribeiro, D. A. Jackson, L. Zhang, I. Bennion, 'Simultaneous spatial, time, and wavelength division multiplexed in-fibre grating sensing network', *Opt. Commun.*, **125**, 1996, pp.53-58

21   D. J. Cooper, T. Coroy, P. W. E. Smith, 'Time division multiplexing of large serial fiber-optic Bragg grating sensor arrays', *Appl. Opt.*, **40**, 2001, pp.2643-2654

2 BACKGROUND

2.1 Chapter overview

From a research and commercial perspective, the area of optical fibre sensing is both broad and deep. Therefore, it is not the intention of this chapter to detail all aspects of the topic, but rather to provide a background that covers those parts of fibre optic sensing that have had greatest influence on the conception, research, development and commercialisation of the resonant cavity fibre sensor interrogator.

The chapter begins with an overview of fibre Bragg gratings (FBG), since variants of these devices formed signal conditioning components and individual sensor elements in the interrogator system. The mode of operation, the unique application advantages and the intrinsic sensitivity to temperature and strain offered by these devices is covered, as are modelling techniques and methods of fabrication often used in manufacture.

Several common methods of interrogating FBGs are also discussed, including simple passive techniques appropriate for single sensor systems and more complex options capable of operating with multiple sensors. Primary multiplexing schemes are then discussed, with focus given to the advantages, disadvantages and level of commercial opportunity exploited from each technique.

An outline of the operation and general application of semiconductor optical amplifiers (SOA) is then provided. This includes reference to research conducted on application of these devices as optical switches. Finally the author's original hypothesis is given, since it formed the conception of this whole body of work; that it may be possible to exploit the switching property of an SOA to provide time-division-multiplexing (TDM) of FBG sensors.

2.2 Fibre Bragg gratings

Fibre Bragg gratings are now an established technology and have been covered in a range of review articles [1, 2, 3]. Devices are commercially manufactured in volume and are used as the basis for a large range of components and modules. The variety of these devices is extensive and cannot be covered in depth, but the more notable industrial sector applications are highlighted below. References are also provided for external sources of detailed information.

- Telecommunications remains the largest industry sector to utilise fibre Bragg gratings. Filter components range from narrowband devices used in laser locking and blocking [4, 5], through broadband routing components for distributed wavelength-division-multiplexing (WDM) [6, 7], to very wide, arbitrary profile, gain-flatting and equalisation elements for erbium-doped-fibre amplifiers. Fixed and tuneable chromatic dispersion compensating devices that use either chirped or etalon gratings have also become highly important for the provision of very high bit rate (40G bits/s) systems [8, 9, 10], as have pump rejection and re-circulation filters for distributed amplifiers [11, 12]

- The manufacture of efficient industrial-sized fibre-lasers for material cutting and manufacturing has also become lucrative recently. Gratings with complex profiles are used to produce distributed mirrors that are capable of operating with the intense radiation delivered by these high power devices [13]

- Microwave photonics utilises gratings for combining, routing, phasing and demodulation of radar, video and telecommunications signals conveyed over sub-carrier optically distributed radio systems. The advantages that optical fibre provides when compared to copper cables means that these systems are now being employed in an increasing number of commercial and military applications [14, 15, 16]

- Optical sensing and instrumentation is the other increasingly important industry sector to employ gratings [17, 18]. Applications include the use of gratings as sensors to directly measure temperature [19] or strain in smart structures [20, 21, 22, 23], as sensors to indirectly measure many other physical, chemical or electrical quantities [24, 25] or as cavity mirrors for distributed interferometric measurement of minute vibrations [26] and acoustic disturbances in military sonar systems [27]

2.2.1 Fibre Bragg grating theory

A fibre Bragg grating is a device that can be formed within the core of a fibre optic cable through exposure of the silica fibre to a periodic pattern of intense ultra-violet (UV) radiation. Permanent FBGs were first reported by Hill *et al* in 1978 [28, 29], and in their simplest form can be described as a uniform sinusoidal variation in the refractive index of the fibre core material, along the lengthwise axis $n(z)$,

$$n(z) = n_{core} + \delta n \left[1 + V \cos\left(\frac{2 \cdot \pi \cdot z}{\Lambda} \right) \right]$$

Equation 2.1

where n_{core} is the refractive index of the core prior to exposure, δn is the amplitude of the induced refractive index change, Λ is the period of the modulation and V is the UV fringe visibility.

The magnitude of the refractive index perturbation is typically very small ($<10^{-4}$), but the number of fringes is large (~ 2000 per mm for gratings designed to operate at 1550nm). Each of the fringes can be considered as a partial reflector, such that constructive interference from the many thousands of minute reflections occurs for light incident on the structure that is close to the Bragg wavelength, λ_B,

$$\lambda_B = 2 \cdot n_{eff} \cdot \Lambda$$

Equation 2.2

where n_{eff} is the effective refractive index of the fibre core and Λ is the period of the grating structure.

When broadband light is injected into the fibre to illuminate a grating structure, a narrowband spectral component around the Bragg wavelength will be reflected back to the source. The remainder of the incident radiation will propagate with minimal attenuation and will result in a transmitted signal that takes the form of the source, but with the reflected spectral component removed. This is shown in Figure 2.1.
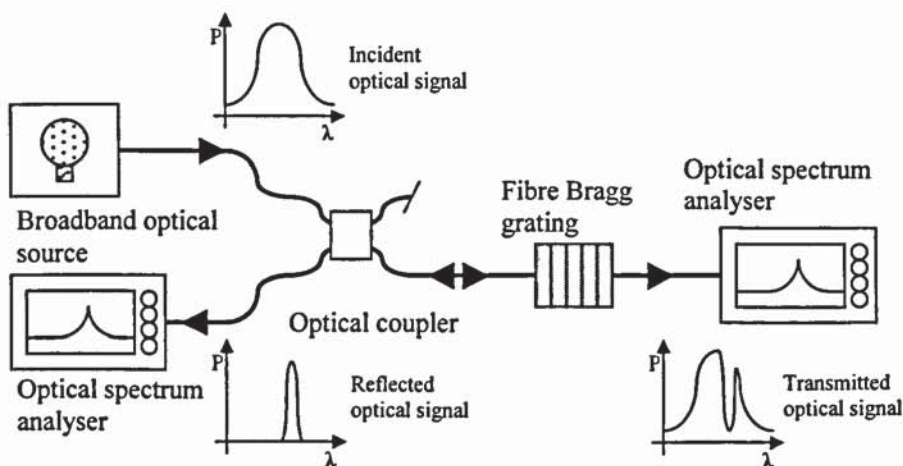
Figure 2.1 The basic response of a fibre Bragg grating to incident broadband radiation, showing the reflected and transmitted optical signals

35

It is possible to evaluate the full transmission and reflection profiles of simple uniform period refractive index Bragg structures using a technique known as coupled mode theory [30, 31]. The maximum reflectivity (R) occurs at the Bragg wavelength, but its exact value is governed by a parameter known as the coupling coefficient (κ), which is proportional to the magnitude of the index change, and by the length of the grating structure (L),

$$R = \tanh^2(\kappa L)$$
<div align="right">Equation 2.3</div>

Gratings with increased reflectivity may be obtained by increasing the magnitude of the refractive index change through increased UV radiance or by creation of longer structures.

The full-width at half-maximum (FWHM) bandwidth of a grating is defined as the difference between the two wavelengths, either side of Bragg condition, where reflectivity falls to half its maximum. This parameter is also related to κ and L and so a trade-off exists between the bandwidth and the reflectivity that can be provided by a uniform period FBG. Gratings with high peak reflectivity (~100%) have bandwidths largely determined by the coupling coefficient, such that increased κ results in increased bandwidth. But, length has the greater influence for low reflectivity FBGs, such that an increase in L results in a reduction in the FWHM bandwidth.

Due to this cross-relationship limitation, and as a result of improvements made to manufacturing techniques, modern FBGs are often fabricated with complex, non-uniform refractive index modulations. This allows tailoring of reflection and transmission profiles to meet the requirements of specific applications, but the theoretical modelling and design of these FBGs requires methods of greater complexity than provided by the basic coupled-mode approach. Chirped gratings, which have a structure of increased periodicity with length, have been modelled as a set of coupled-mode equations with phase (ϕ) and κ terms dependent on z [32, 33]. While, for refractive index structures with combined chirp, tapering and phase shift, other versatile approaches have concentrated on treatment of the complete grating as a series of connected, short, uniform structures. Each unit contribution is defined using a transfer matrix and then all contributions are combined using powerful numerical matrix multiplication techniques [34,35].

2.2.2 Manufacturing methods

The first reported FBGs [28, 29] were produced in 1978 from within the fibre core by launching radiation from an Argon-ion laser into one end of the fibre. The launched light propagated through the fibre and was partially reflected from the silica-air boundary at the far end. Interaction of the incident and counter-propagating radiation created a standing wave along the length of the fibre. After several minutes of exposure, strong reflection of the incident light was observed as the properties of the core material were permanently modified by the presence of the standing wave. Unfortunately however, these FBGs were of limited practical significance and created little research interest since the Bragg wavelength was always the same as the wavelength of the laser used for the exposure.

Meltz *et al* [36] in 1989 reported the first significant breakthrough in fibre Bragg grating fabrication with the demonstration of the holographic interferometric technique, as shown in Figure 2.2. This approach allowed creation of FBGs by UV radiation delivered into the fibre core from the side, through the cladding layer. Most significantly, the period of the induced fringe pattern was not solely a function of the writing laser wavelength, but was also dependent on the angle of incidence of the interfering beams. This angle could be adjusted over a wide range and so the wavelength of the resulting Bragg reflectors could be freely tailored.
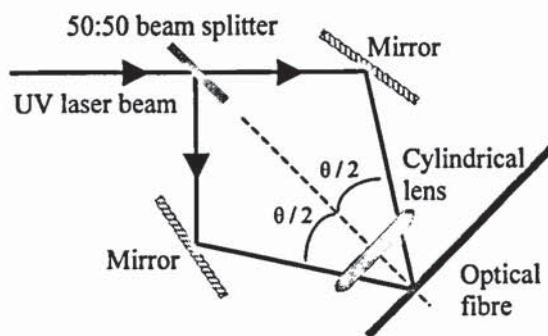
Figure 2.2 The holographic interferometric technique for fibre Bragg grating fabrication

The relationship between the laser wavelength λ_{UV}, the beam interference angle θ and the resulting period of induced refractive index change Λ, was shown to be,

$$\Lambda = \frac{\lambda_{UV}}{2.\sin(\theta/2)}$$

Equation 2.4

37

Unfortunately limitations of the technique included the requirement for a laser with high spatial and temporal coherence to allow longer grating exposure time and greater exposure length, and the disadvantage of inherent self-chirping of the grating structure, which resulted from an uneven exposure due to the beam shape.

Despite these limitations, research interest continued and in 1990 Kashyap *et al* [37] demonstrated the first FBGs designed for operation around 1550nm. This significant step opened the opportunity for design and manufacture of in-fibre grating components for use in telecommunication systems that operated in this window. This caused a dramatic increase in academic and commercial research as companies battled to service this high revenue market.

In 1993 Hill *et al* [38] reported a new technique for grating fabrication using a phase mask. The phase mask was constructed from a flat, UV transparent, silica substrate into which a periodic pattern of corrugations was etched using photolithography. UV radiation incident on the mask was diffracted by the pattern of corrugations into two primary orders, as shown in Figure 2.3. By placing the phase mask in near contact with the fibre, interference between the primary orders produced a periodic pattern within the fibre, which in turn created a refractive index perturbation similar to that produced using other techniques.
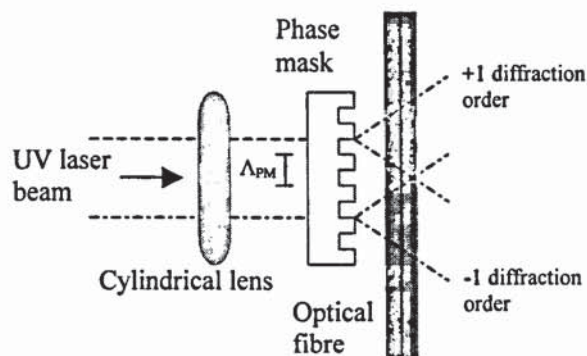
Figure 2.3 The phase mask technique for fibre Bragg grating fabrication

The phase mask approach had a number of significant advantages. The temporal and spatial coherence requirements of the UV laser were less stringent, while the period of the photo-induced pattern (Λ) was wholly dependant on the period of the mask corrugations (Λ_{PM}) and not the wavelength of the writing beam or the angle of any mirrors,

$$\Lambda = \frac{\Lambda_{PM}}{2}$$

Additionally, since diffraction of the incident UV beam occurred at all points on the mask, researchers quickly demonstrated that the mask and fibre could be laterally translated relative to the beam to create gratings with lengths limited only by the mask size and not the beam width [39, 40]. Complex chirped, phase shifted and apodised profiles could also all be produced in the phase mask pattern, for direct reproduction into each grating [41, 42, 43]. These factors allowed a significant improvement in the mass production of gratings with high parameter repeatability. Later additions to this technology included the 'dither' method of producing arbitrarily apodised gratings and the direct writing technique for the manufacture of very long gratings.

However, an unfortunate side effect of all of these side-writing techniques was a requirement to remove the outer protective polymer coating from the fibre to expose the bare silica to the UV radiation. Removal was required as the coating was opaque and so absorbed radiation at the usual writing wavelengths around 244nm. Removal, grating exposure and subsequent recoating of the protective polymer layer was time-consuming and therefore expensive, and could significantly reduce the mechanical strength of the fibre. This increased the risk of breakage during manufacture and of premature failure in the field. The first alternative to removal of the coating was demonstrated by Dong *et al* [44] and Askins *et al* [45, 46], who showed that simple, low reflectivity sensors could be produced prior to the initial application of the protective coating, by writing directly on the draw-tower during the fibre manufacture process.

A second more versatile and commercially viable alternative to coating removal was demonstrated in 1997 by Starodubov *et al* [47, 48] and other researchers [49]. They showed that gratings could be written through the fibre coating using longer wavelength near-UV radiation at 334nm. Their techniques eliminated the requirement for coating removal and so reduced manufacturing cost and improved yield. Unfortunately however, due to the reduced photosensitivity of silica at longer wavelengths, highly reflective gratings were not easily fabricated in standard fibre, so more expensive Boron or Germanium doped speciality fibres were used.

2.2.3 Sensitivity to temperature and strain

The Bragg wavelength of a fibre Bragg grating is inherently sensitive to changes in the external temperature and strain exerted on the device. A variation in either, or both, of these parameters manifests as a change to the Bragg condition, that in turn results in a shift in the wavelength of the reflected and transmitted optical filter signals.

This sensitivity to external physical disturbance is exploited in most of the application areas in which FBGs are employed. For example, in telecommunications temperature and strain tuning are often used to set or adjust the operating region of components and modules, while in fibre lasers the operating wavelength may be adjusted by tuning the strain on an FBG.

In optical sensing, this inherent sensitivity of the Bragg wavelength to external force forms the fundamental reason for choosing FBGs as sensors. Remote monitoring of the reflected or transmitted optical signals from an FBG sensor, via the optical fibre cabling, allows direct, self-referenced measurement of the physical forces experienced by the sensor. This topic is well established and covered by a range of review articles [4, 18, 50, 51, 52].

The actual changes to the fibre grating Bragg condition, as a function of temperature and strain, arise as the result of both direct and indirect physical effects on the grating structure, according to the following relationship [4]:

$$\Delta\lambda_B = 2 \cdot n \cdot \Lambda \left(\left\{ 1 - \left(\frac{n^2}{2} \right) \cdot \left[P_{12} - v \cdot (P_{11} + P_{12}) \right] \right\} \cdot \varepsilon + \left[\alpha + \frac{\left(\frac{dn}{dT} \right)}{n} \right] \cdot \Delta T \right) \quad \text{Equation 2.6}$$

where $\Delta\lambda_B$ is the shift in the Bragg wavelength for an applied strain ε or temperature change ΔT. P_{11} and P_{12} are known as the components of the fibre optic strain tensor, v is the Poisson's ratio, α is the coefficient of thermal expansion of the material, n is the effective refractive index of the fibre core and Λ is the period of the refractive index perturbation.

The term $\left(\dfrac{n^2}{2}\right)\cdot\left[P_{12} - v\cdot(P_{11} + P_{12})\right]$ is known as the effective photoelastic coefficient (P_e) and has a typical value of ~0.22 for standard telecommunications grade single-mode optical fibre.

Some experimental measurements of the actual strain and temperature response of FBG sensors (written in standard telecommunications fibre) have also been conducted, with normalised results found to be as follows:

$$\frac{1}{\lambda_B}\cdot\frac{\partial\lambda_B}{\partial\varepsilon} = 0.78\times10^{-6}\,\mu\varepsilon^{-1} \qquad\qquad \text{Equation 2.7}$$

$$\frac{1}{\lambda_B}\cdot\frac{\partial\lambda_B}{\partial T} = 6.67\times10^{-6}\,{}^{\circ}C^{-1} \qquad\qquad \text{Equation 2.8}$$

These results indicate that for typical FBG sensors operating at around 1550nm, a temperature change of 1°C or a strain change of 8µε will both result in a Bragg wavelength shift of around 10pm. Therefore, by converse, these results also imply that for an optical measurement system that has a wavelength measurement resolution of 1pm, temperature discrimination to 0.1°C or strain detection of <1µε can be expected.

However, a high sensitivity to both temperature and strain are not the only desirable properties of FBGs when used as sensors. Optical fibre sensing using fibre Bragg grating sensors has many other distinct advantages over the electrical and mechanical alternatives, which include:

- Optical fibre is mainly manufactured for use in long-haul telecommunications systems. It is therefore the ideal transmission medium for low loss, long distance remote sensing

- A single fibre can provide the power to the remote FBG transducer and return the optically encoded result

- Often many FBG sensors can be multiplexed onto a single fibre

41

- Manufactured from the insulating materials of polymer and glass, optical fibre provides inherent electrical isolation between the FBG transducers and the interrogation instrument

- In a multiplexed sensor system, the FBG sensors are also electrically isolated from one another

- Since all signals are transmitted optically no electrical interference is generated and crosstalk to other optical fibres or electrical systems does not occur. This allows many fibres to run in close proximity to one another and with other sensitive electrical systems (such as radio receivers, heart pacemakers or aircraft avionics). It also makes unauthorised 'tapping' of sensitive information, or malicious tampering of sensor data very difficult. It has been suggested that this latter issue may be valuable in long distance remote sensing systems

- Optical signals are not subject to electrical interference. This is essential in power generation systems where distributed sensors are placed in contact with high voltage, high current power lines, without interference

- Optical transducers do not use electrical power and do not pose the risk of creating sparks. This makes them ideal for use in oil and gas production

- Optical fibre and in-fibre optical transducers can be manufactured without any metallic content. This makes them ideal for use in structures that are at risk from lightening strikes (e.g. optical strain sensors in wind turbine blades), for use in high electric fields (e.g. current sensors in electrical generating and distribution equipment) or for use in high magnetic fields (e.g. magnetic resonance imaging scanners)

- Glass is chemically inert to all but the most volatile of acids. Fibre transducers are therefore ideal for inert operation in bio-medical applications (e.g. intravenous temperature sensing) or industrial process control (e.g. chemical concentration sensing, fluid level detection, temperature sensing or pressure sensing). Additionally, embedding fibres into structures does not affect the chemical properties of the host material

- Optical fibre provides a close physical match to many composite materials and so embedding does not adversely effect the overall structural strength

42

- FBGs are in-fibre devices so no connectors are required between the transmission medium and the sensor

- Having a diameter of only 250μm optical fibre is small and unobtrusive

- Optical fibre and components are designed to meet stringent environmental performance criteria required by telecommunications systems; often guaranteeing maintenance free operation for 25 years

- Standard telecommunications grade fibre is low cost (7 pence/metre in 2km lengths)

2.2.4 Sensitivity to other physical, chemical and electrical measurands

In addition to their direct high sensitivity to temperature and strain, FBGs are also frequently employed as the final measurement element within specially designed mechanical or chemical transducer systems, such to provide assessment of a diverse range of other measurands. The use of such mechanical and chemical transducer systems includes:

- Measurement of acoustic disturbance for civil and naval sonar applications using pairs of FBGs to form Fabry-Perot cavities [27]

- Measurement and analysis of strain induced vibration in numerous industrial and medical applications [26, 53, 54]

- Measurement of pressure, through either the measurement of strain on a diaphragm or by detection of peak splitting in a specially formed 'side-hole' fibre; these are often used for the monitoring of oil in pipelines and sub-sea reserves [55, 24]

- Measurement of water depth and flow direction by measurement of pressure and hence strain, for use in remote river management

- Measurement of fluid flow rate by detection of ultrasonic strain vibrations in a pipeline [56]

- Measurement of inclination by measurement of strain on a cantilever pendulum [57]

- Measurement of torsion using FBGs in high-birefringence fibre [58]

- Measurement of shear forces through measurement of strain in an angularly embedded FBG sensor [59]

- Detection of fuel leaks in industrial pipelines and installations by measurement of the strain induced in a fibre that has been coated with an hydro-carbon absorptive material [25, 60]

- Measurement of salinity by measurement of the strain induced in a fibre coated with an absorptive hydrogel material [61]

2.2.5 Overcoming the dual sensitivity to temperature and strain

Since FBGs are sensitive to both temperature and strain it is difficult isolate the effects of each; it is not always clear if a change in the Bragg wavelength is the result of actual strain experienced by a structure or simply a change in the ambient temperature. To date most commercial applications rely on additional strain-free FBG sensors to provide temperature referencing, but a diversity of other solutions have been reported. These range in both complexity and commercial practicality and include:

- The use of two FBGs of greatly different wavelength (800nm and 1300nm) (and correspondingly different response to temperature and strain), such that effects of each can be resolved by solving pairs of simultaneous equations [62]

- The use of two FBGs, each in fibres of different diameter, spliced together such that the strain response of each is independently resolved [63]

- The combination of an FBG and a long period grating that each have distinctly different responses to strain and temperature [64]

- The combination of a standard (type IIa) FBG and a type Ia FBG, which each have different responses to temperature [65, 66]

- A variety of solutions that combine the temperature dependant properties of rare-earth doped fibres and the properties of FBGs written in them [67, 68, 69]

2.3 Single fibre Bragg grating sensor interrogation techniques

Recovery of the value of the measurand from an FBG based sensor system requires that the optically encoded signal from the sensor is detected and measured. The exact nature of encoding the measurement onto the optical signal varies according to the detection and sensor system employed, but the most common techniques use one or

more of the following optical parameters: wavelength, amplitude, phase, dispersion or polarisation. The resolution, accuracy, stability and speed of these optical measurement systems varies considerably depending on the sensors and interrogation techniques employed, as does the cost and the complexity of the final implementation.

Some interrogation systems provide support for just one sensor, as shown in Figure 2.4. These systems are often very simple and claim to be low cost, but unfortunately also commonly suffer from environmentally instability or have other significant operating limitations.
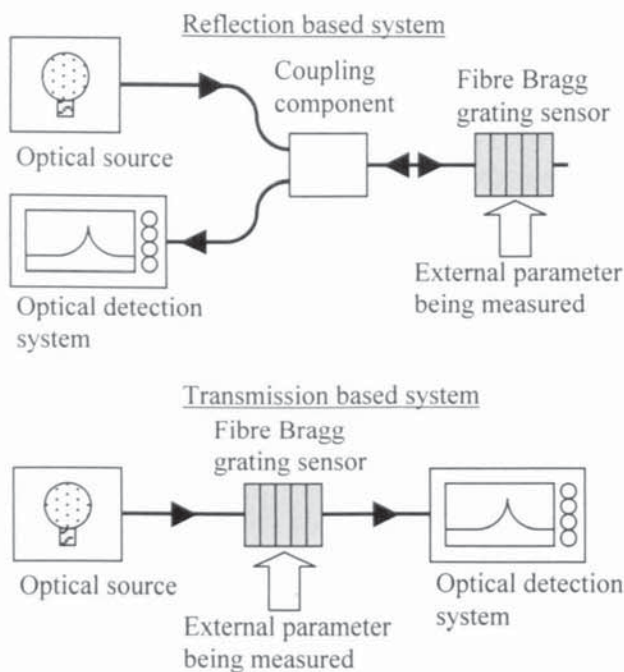
Figure 2.4 The general reflection based and transmission based circuit arrangements for a single sensor fibre Bragg grating sensor interrogation system

A few reported examples of single-sensor interrogation systems have included:

1. The use of a wavelength matched (overlapping) pair of FBGs, which operate using a power or intensity measurement technique. In these systems light from a laser or LED is incident on the sensor FBG, such that it is reflected (or transmitted) to interact with the separate, second, measurement FBG. The second FBG is then interactively strained or temperature tuned to match the wavelength of the sensor device and so minimise (or maximise) the transmitted optical signal delivered to a single photodiode [70, 71, 72], as shown in Figure 2.5.
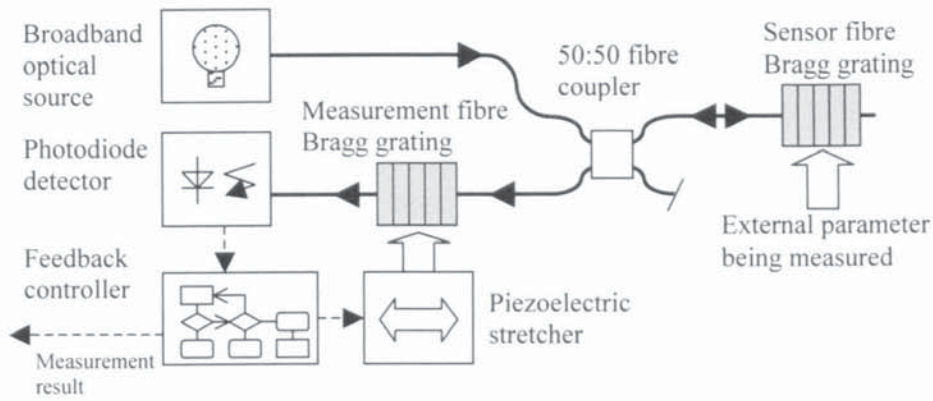
Figure 2.5 A typical single fibre Bragg grating sensor interrogation scheme using matched-grating detection

2. Other systems have employed in-fibre interferometer interrogation schemes. These have been noted for very high dynamic resolution, but have also suffered from significant environmental effects [73, 74, 75], as shown in Figure 2.6.

A fibre path length imbalance of less than the effective coherence length of the sensor grating (<10mm) is maintained between the arms of the interferometer. This results in an interferometer transfer function of the form $1 + \cos(\theta)$, where θ is dependant on both the imbalance and the grating wavelength. Small changes in sensor wavelength are then easily detected as large variations in the power recorded by the two photodiodes

Figure 2.6 A typical single fibre Bragg grating sensor interrogation system using interferometric detection

3. Ratiometric and edge-filter wavelength detection approaches have also offered the potential for low cost interrogation systems of modest resolution, but they have also been shown to suffer from variations in optical loss or source intensity, or require difficult calibration schemes when used in real-world applications [76, 77, 78, 79]. A typical example of the ratiometric approach is shown in Figure 2.7.

Light reflected from the fibre Bragg grating sensor is routed via the two couplers into two paths. One path is directly incident on a photodiode, whereas the other is first passed through a ramp or edge filter that has a transmission profile that varies with wavelength. By taking the numerical ratio of the optical power recorded by the photodiodes a wavelength measurement, independent of absolute power, is possible.

Figure 2.7 A typical single fibre Bragg grating sensor interrogation scheme using ratiometric detection

4. The use of a polarisation maintaining fibre loop mirror for interferometric wavelength detection has also been demonstrated. This approach provided a greater level of environmental stability than other interferometric methods, but does not appear to have been taken further [80].

5. Further novel schemes have been demonstrated to measure the wavelength of an optical signal by monitoring the 'transparent-current' in a partially biased laser diode [81] or through the use of electro-absorption filter components [82]. The results from these demonstrations were encouraging, but commercial exploitation seems, as yet, unlikely.

2.4 Wavelength-division-multiplexed fibre Bragg grating sensor interrogation techniques

One of the greatest advantages of using fibre Bragg gratings as sensors is that they provide a range of possible options for multiple devices to be independently operated in a single length of fibre. Extensive research in this field has ensured that numerous different multiplexing configurations have been reported. However, of these many variants, most can be categorised into one of two primary forms; those that employ some form of wavelength-division-multiplexing (WDM) and those of a time-division-multiplexing (TDM) nature.

The simplest and most widely reported FBG sensor multiplexing technique is WDM. Using this approach a number of FBG sensors can be written serially into a single

length of optical fibre. The FBGs are designed such that under zero strain and at room temperature they each have a different central (Bragg) wavelength. Strain or temperature applied to each FBG then causes a shift in the Bragg reflection wavelength, such that the signal from the sensor varies within the devices own wavelength window, but does not encroach into the operating window of other sensors. Using this approach the interrogation equipment is required to provide illumination for each sensor and undertake detection and measurement of the wavelength-encoded measurands that are returned. Figure 2.8 shows the general arrangement for such a WDM based FBG sensor system.
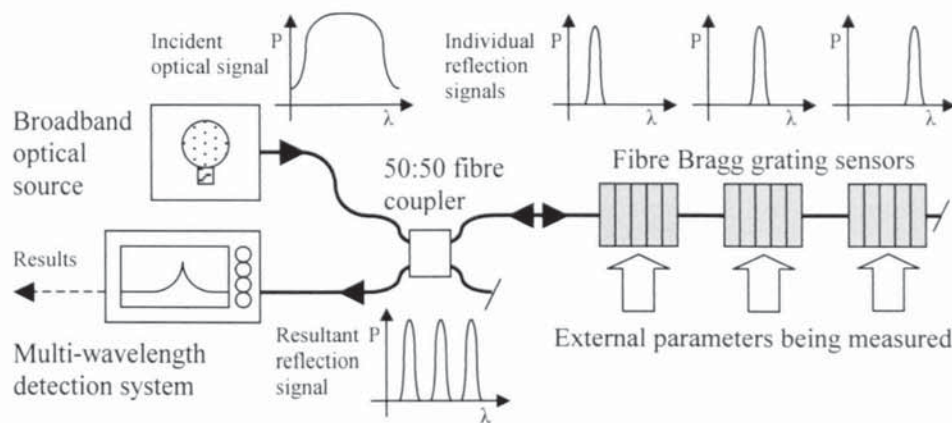
Figure 2.8 The general arrangement for a wavelength-division-multiplexed fibre Bragg grating sensor interrogation system

Examples of reported WDM based fibre optic sensor systems have included:

1. Numerous configurations that have employed fibre or bulk Fabry-Perot (FP) filters. These interrogation systems typically operated the FP filters using ramped or triangular electrical waveforms, such that a narrow optical pass-band was swept across the full wavelength range of the sensors while a photodiode sampled the reflected signal. Peaks in the reflected signal were detected and used to provide a measurement of the strain or temperature of each of the sensors [83, 84].

2. One configuration extended the basic single-sensor matched filter approach (described previously) by using multiple matched filters, such that each sensor FBG (in the serial array) was matched by a separate parallel-configured measurement FBG and photodiode. The approach required many photodiodes and couplers and was optically inefficient, but it did provide independent operation for each of the sensors [85]. A further variation on the matched filter

concept employed two serial arrays, one containing the sensor FBGs (in the usual manner) and a second containing the measurement FBGs. This approach differed from the previous design in that the match condition was detected from the transmitted signal through all of the measurement FBGs using just a single coupler and photodiode. This approach was therefore simpler, cheaper and more optically efficient, but also suffered from greater limitation in the sensor operating speed [86].

3. An extension of the single-sensor interferometric approach was reported that used a telecommunications WDM splitter to provide a four-channel sensor system. This maintained the advantages of high resolution and response to dynamic strain, but in common with the single-sensor design also suffered from environmental drift [87].

4. Two demonstrations of WDM sensor systems have employed acousto-optic filters. These tracked the wavelength signals from sensors either sequentially or simultaneously by adjustment of the RF modulation to the filter and were therefore novel. Unfortunately they were also prone to drift and required expensive components [88, 89].

5. Numerous configurations have been reported that have employed FBG sensors as reflectors in active fibre laser cavities or have used external scanning fibre lasers to illuminate and measure reflections from serial arrays of FBG sensors. These approaches have provided considerably higher signal power and lower noise when compared with other broadband-illuminated WDM alternatives [90, 91, 92] and have been employed in commercial designs.

6. Other reported configurations have used spectrometers to detect and simultaneously measure the reflection signals from each of the WDM sensors in a serial array. These offer solid state advantages, but are limited by the cost and stability of components [93, 94, 95, 96, 97].

2.4.1 The advantages of wavelength-division-multiplexing

There are a number of advantages to using wavelength-division-multiplexing to provide multi-sensor interrogation, including:

49

- The fact that, in a well-designed array, the sensors each operate in separate and distinct wavelength windows, which ensures they are inherently free of crosstalk. This behaviour occurs since arrays are intentionally designed such that the zero-strain wavelength of each FBG sensor is well separated from all others

- Once the array has been designed in this manner, the sensors are also simple to set-up. This is because no information is required as to the spatial position of each device. The measurement results and individual sensors are determined and identified solely from the reflected wavelengths that are returned in the fibre

- There is also little limitation on the minimum separation that is allowed between sensors. The limit is solely based on the particular sensor manufacturing technique that is employed, but is typically only a few centimetres

- Since the FBGs operate in distinct wavelength windows they can also be made ~100% reflective without risk of interference. The total reflected power from the sensors is therefore high, which means that reasonable levels of system loss can be supported before signal noise becomes problematic

2.4.2 The disadvantages of wavelength-division-multiplexing

Unfortunately employing simple WDM techniques also has a number of disadvantages. These include the following:

- As all of the FBG sensors in a WDM array are intentionally at different wavelengths, most manufacturing systems require skilled and time-consuming operator intervention to continually change the fabrication parameters or tooling of the machinery. This means that sensor arrays are often very expensive to produce

- As each FBG is required to operate in a distinct wavelength window, the bandwidth of the optical source and detector components (which is typically <70nm) often limits the number of sensors that can be used to less than 10 per fibre. This is because sensors with an operational range of 5000$\mu\varepsilon$ each deviate by ~6nm due to an applied signal, plus a ~1nm of guard spacing is required between adjacent sensors to allow for manufacturing and installation tolerance.

50

Therefore, although an increase in the total system sensor count can often be achieved using multiple fibres, the cost and complexity is substantially increased

- To maximise efficient use of the source and detector optical bandwidth application-specific array design is usually required. This is very expensive, increases lead times, complicates installation and increases stock inventory. The result is a large increase in system cost and a difficulty in scaling for mass manufacture

- Since the reflected signals from the FBG sensors are simultaneously delivered to the wavelength detector, the range of measurement techniques that can be employed is limited. Most commercial system vendors appear to adopt scanning Fabry-Perot filters, but these are bulky, expensive and often have limited scanning speeds

- Due to the limited number of sensors supported per fibre and the requirement for application specific design of the arrays, it is often difficult to extend installed systems at a later date; future-proofing is difficult

2.5 Time-division-multiplexed fibre Bragg grating sensor interrogation techniques

To overcome some of the disadvantages of WDM a number of time-division-multiplexing systems have been proposed. In these systems the FBGs are all of low reflectivity, nominally of the same wavelength and operate in the same optical window. Identification of individual sensors is not achieved using wavelength, but instead is carried out using time-of-flight measurements from a pulsed optical source. Figure 2.9 shows the general arrangement for a TDM system.

51

The tuneable laser optical source produces a series of very short pulses as it is scanned across the operating wavelength range of the fibre Bragg grating sensors. High speed gating in the optical detector system is then used to distinguish between the reflections from individual sensors using time-of-flight measurement.
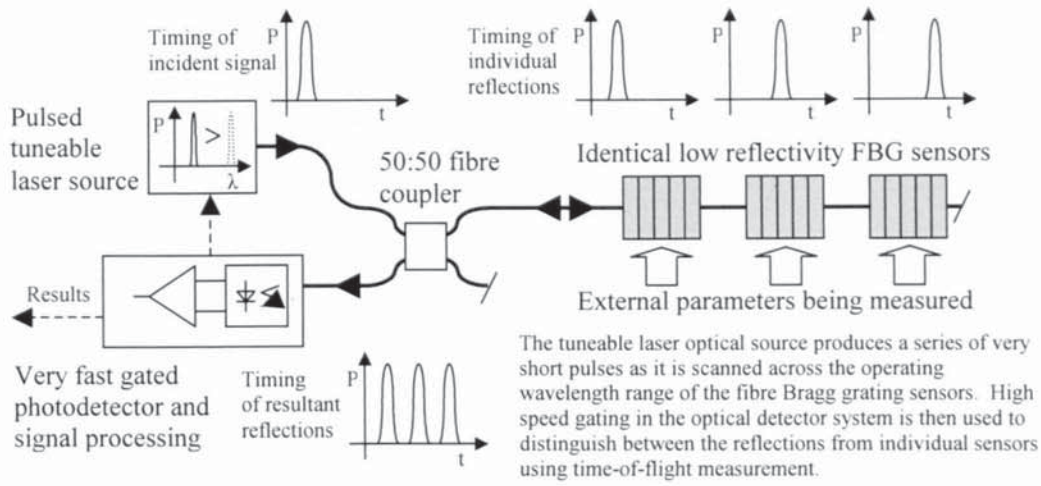
Figure 2.9 The general arrangement for a time-division-multiplexed fibre Bragg grating interrogation scheme

2.5.1 Time-division-multiplexing theory

The velocity of light in a medium v can be determined from the universal constant for the velocity of light in a vacuum C and effective refractive index of the fibre material n_{eff} using the simple relationship,

$$v = \frac{C}{n_{eff}}$$

Equation 2.9

It follows that the time taken in seconds t for an optical pulse to travel a distance d metres in a fibre can be found using the relationship,

$$t = \frac{d \cdot n_{eff}}{C}$$

Equation 2.10

Therefore, for a short optical pulse launched into a fibre that is incident on a series of FBG sensors spaced at x metre intervals, the time delay τ between the arrival of reflections from adjacent sensors will be,

$$\tau = \frac{2 \cdot x \cdot n_{eff}}{C}$$

Equation 2.11

This is true for the reflections, since the incident pulse travels in both directions in the fibre and so covers twice the distance of the separation between the adjacent sensors.

Therefore, for a TDM system employing FBG sensors fabricated in standard single-mode telecommunications fibre that are spaced at 2m intervals, the delay between the arrival of successive reflections from a short pulsed optical signal will be,

$$\tau = \frac{2 \times 2 \times 1.48}{3 \times 10^8} = 19.7\text{ns} \qquad \text{Equation 2.12}$$

2.5.2 The advantages of time-division-multiplexing

The notion of using TDM to allow access to multiple FBG sensors in a single fibre has many potential advantages, which include:

- Since all sensors operate at nominally the same wavelength, the number of sensors in a TDM system is not limited by the operating bandwidth of the source or detector components. TDM systems therefore have the potential to support tens or even hundreds of sensors per fibre

- Since all sensors operate in the same wavelength window, each sensor can use the full operating bandwidth of the optical source and detector. Different sensors can also operate over different strain or temperature ranges without the requirement for changes to the sensor wavelength spacing

- Since all FBG sensors are identical and of low reflectivity they can be produced at significantly reduced cost. Operator intensive tooling changes are not required between sensors, whilst the requirement for only low reflectivity means that through-coating [47, 48] and online at the draw-tower [44, 45, 46] fabrication techniques can be employed. These are cheaper and maintain the maximum mechanical strength of the fibre

- Since application specific array design is not required, this reduces cost, stock inventory and system delivery lead-time. Rather than having to maintain a stock of many different array types or having to design on a system-by-system basis, a reel of hundreds of identical sensors can be purchased, which can then be simply cut to length and used for all applications

- Since all arrays and sensors are identical, system extension is possible after initial deployment. This means that once a customer has purchased the basic system, additional sensors can added later as required

2.5.3 Disadvantages of time-division-multiplexing

Unfortunately there are also a number of fundamental issues when employing TDM techniques to interrogate sensors. These issues do not stop effective use of the technology, but do require attention and compromise during the initial system design phase. These issues and the solutions required are discussed in a number of papers [17, 98, 99], and include:

1. The fact that in a TDM system, as all sensors operate with nominally identical wavelength, a style of crosstalk known as 'multiple-reflection interference' can occur, as shown in Figure 2.10. This arises when the pulsed signal from the source, which is intentionally reflected from a distant sensor, is also repeatedly reflected between other closer sensors, in such a manner that both the desired and interfering reflections arrive at the wavelength detection system simultaneously. The extent and severity of this interference is dependant on the reflectivity of the sensors, such that a reduction in the reflectivity of the FBGs results in a lower level of interference. Complete elimination of this detrimental effect is also possible (in some applications) by careful selection of the sensor spacing, or by increasing the number of available timeslots through an increase in gating speed.
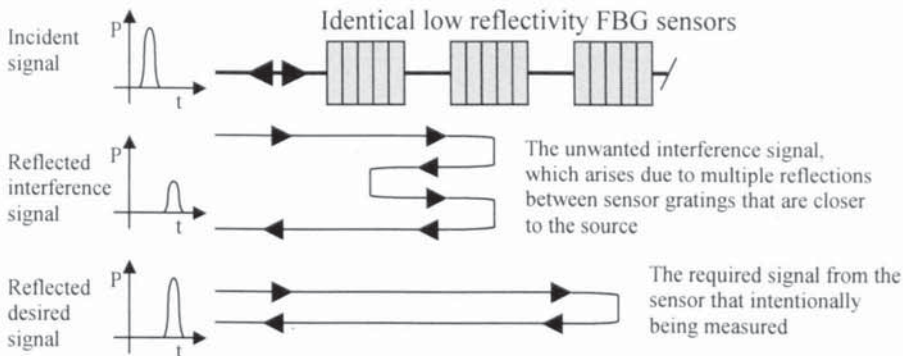
Figure 2.10 An illustration of 'multiple-reflection interference' in a TDM sensor interrogation system

2. A second interference effect known as 'wavelength shadowing' can also cause crosstalk and measurement inaccuracy in a TDM system. This interference is caused by attenuation of the propagating optical signal, to and from a distant sensor, through interaction with one or more sensors closer to the source, as shown in Figure 2.11. Modelling shows that this effect is most severe when the wavelength separation between the measured and interfering sensors is near to

54

the FWHM bandwidth of the gratings and can be over 1µε for >5% reflective devices. This interference is fundamentally unavoidable if all sensors operate in the same wavelength window within the same fibre, but its detrimental effect can be significantly reduced by using lower reflectivity or narrower bandwidth sensors or though mathematical (curve fit based) profile correction at the wavelength detector
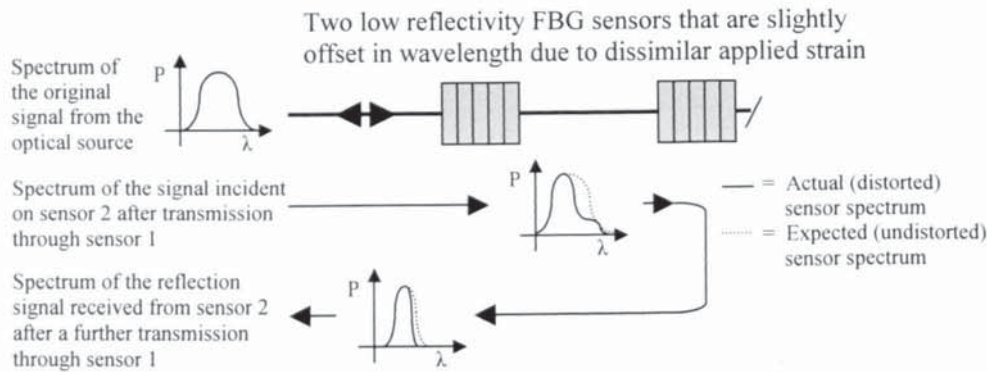
Figure 2.11 A highly exaggerated illustration of 'wavelength shadowing' interference in a TDM sensor interrogation system

In addition to these fundamental issues there are also a number of other difficulties that arise during implementation of TDM based interrogation systems, which include the following:

- From Equation 2.12 it can be seen that producing a true, commercially useful TDM system requires the successful gating and separation of returned reflection signals at very high speed. For a 2m-spaced FBG array these reflections occur at ~20ns intervals, while for sensors spaced closer, even faster gating is required and operating at such speeds is very demanding

- The fact that TDM systems are also required to operate with very short, pulsed optical sources, and with low reflectivity FBGs, means that the mean optical power returned from each sensor is very low. This makes wavelength detection difficult and results in increased noise. There is often a harsh trade-off between the measurement resolution and speed that can be achieved

- Where high-speed electronic gating is used to separate out the sensor reflections, the electronic amplifiers are required to have high gain, strong linearity and high bandwidth. These are conflicting requirements, which result in systems that can be plagued by noise and crosstalk, or have limited resolution

- Electrically gated systems are also limited to using basic wavelength detection techniques, which can lead to further limitations as a result of component and system imperfections. A typical example of such a limitation is the variation from linearity that can occur due to ripples in the edge-filter profiles used in ratiometric detection schemes

- Optical gating of the reflection signals from each sensor eases the difficulties associated with using high bandwidth, high gain electrical amplifiers and also allows the use of a greater range of wavelength measurement techniques. Unfortunately however, optical gating requires the use of high-speed, high extinction-ratio optical modulators. These components are bulky, environmentally sensitive, electrically inefficient and expensive

- To aid with the general trade-off between gain and bandwidth, successful implementation of TDM usually requires high-power optical sources, but unfortunately these components are also bulky, electrically inefficient and expensive

These design issues and implementation difficulties have meant that setting up (even basic) experimental TDM systems in a lab environment has been difficult. This in turn has resulted in limited research and slowed the progress in this branch of optical sensing. As such, the full extent of research, development and commercial exploitation of true TDM based interrogation has been significantly lower than for that of WDM technology.

2.5.4 Reported implementations of time-division-multiplexing

It can be considered that some reported research systems are variants of the basic TDM concept, but they actually use methods of sensor identification that do not require gating of pulsed reflection signals. Demonstrations of this nature have included Fourier analysis of interference [100], code-division multiple access (CDMA) [101] and frequency modulated continuous wave (FMCW) [102]. However, these techniques all have practical limitations and have not been exploited commercially.

Some predominantly WDM systems have been reported that included gated TDM extensions to enable hybrid operation. However, these have either lacked actual detailed implementation [103, 104, 105] or have provided only limited TDM

performance using widely spaced sensors [106, 107, 108]. They have not been appropriate for sole TDM operation in a commercial environment.

For systems operating using a true TDM approach two principle methods have been employed for gating reflections from the sensors at high speed; either electronic gating, using high bandwidth, high gain electrical amplifiers [109] or optical gating, using optical modulators [110, 111]. The electrical gating approach has been shown to be the significantly cheaper option to implement, but to-date has delivered poor measurement resolution and has required high power pulsed sources, larger spacing between sensors and low system loss. By contrast, the most effective optically gated TDM implementations have been shown to deliver high resolution and low noise from tens of low reflectivity sensors.

Apart from the author's resonant cavity approach, Cooper *et al* reported another successful experimental TDM system in 2001 [111, 112]. Their design was based on the standard optical gated TDM concept, but the implementation was considerably more expensive than previous electrical or optical gated alternatives. This increased cost was due to the inclusion of an optical modulator and optical signal amplification. By using optical gating to achieve a high sampling speed and Erbium doped fibre amplifiers (EDFAs) for increased signal power with low detector noise, a number of advantages were highlighted. These included compatibility with a wide range of measurement techniques, close spacing of sensors and strong performance under non-ideal real-world conditions. However, despite this high performance, commercial viability was hampered by the inherent complexity, large power consumption, increased size and high cost of the system and as such there does not appear to be any intention of taking the design into mass production.

2.5.5 Commercial TDM fibre sensor interrogation systems

In spring 2003 the author's resonant cavity fibre sensor interrogator became the first mass-produced commercial TDM system and to-date remains the only commercial TDM interrogator to operate with low reflectivity identical sensors for delivery of high resolution and low noise measurement under harsh environmental conditions. Although a second (partial) TDM system was later released commercially in 2004, its specifications indicate that it actually uses the standard electrically gated approach and will only operate with widely spaced, high reflectivity, WDM style sensors [113]. To-date, no other true TDM commercial systems are known to exist.

2.6 Semiconductor optical amplifiers

A semiconductor optical amplifier (SOA) is a small opto-electronic component that is manufactured from a layered structure of doped Indium-Phosphide (InP) or Indium-Gallium-Arsenide-Phosphide (InGaAsP). In both design and operation the SOA is essentially very similar to a semiconductor laser, but in place of the two high reflectivity end facets used in a laser, in an SOA anti-reflection coatings are employed. As such the component amplifies externally injected rather than internally generated optical signals through the action of stimulated emission [114]. This process is depicted in Figure 2.12 where it can been that the electrical pump current creates a charged carrier distribution that on the arrival of a single photon causes a cascade of stimulated emission and corresponding all-optical coherent amplification.
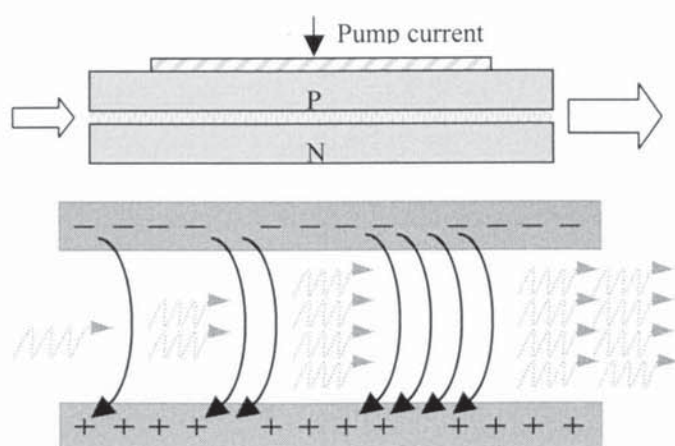
Figure 2.12 An outline of the stimulated emission amplification process in a semiconductor optical amplifier

As a result of the considerable research effort and commercial success of semiconductor lasers for telecommunications, SOAs have also become the focus of significant attention in recent years. They also benefit from a small size, a broad and tailored spectral bandwidth, simple electrical pumping and provide the opportunity for tight device integration and low cost through mass production.

2.6.1 Applications of semiconductor optical amplifiers

Despite the attractive features of SOAs and their natural place as amplifiers in telecommunications, they are not currently the preferred choice for high bit rate, long haul transmission systems; here Erbium doped fibre amplifiers (EDFA) remain dominant. Instead, the use of SOAs as simple amplifiers only generally occurs within short-reach, low bit rate, metro and optical local area networks (OLAN).

The reason for this limited deployment within high data rate systems is the fact that the gain dynamics of SOAs are effectively either too slow or too fast compared to the bit-interval of the conveyed data. As a data bit arrives at the device and is amplified, charged carriers are consumed within the active region as the electrons in the excited conduction band are depleted. This reduction in the density of excited charge causes two effects; the amplifier gain is reduced and the refractive index of the waveguide changes. If this effect and its subsequent recovery was to occur in a time significantly shorter or considerable longer than the bit-interval (as with EDFAs where recovery is measured in milliseconds) little consequence would result, but unfortunately in SOAs this time period is measured in hundreds of picoseconds. The effect of this dynamic gain and index change (both during and shortly beyond each bit-interval) is a distortion and patterning of the optical data signal and a significant reduction in the bit error rate (BER); a stream of data 1's will initially suffer increasingly lower gain as the devices population inversion attempts to re-establish equilibrium and then a steadily increasing background noise will follow after the arrival of a stream of 0's.

Fortunately however, despite the complexities of modelling the dynamic gain and refractive index behaviour of an SOA (under the influence of a pulsed optical signal) [115, 116] a number of very important optical techniques have been identified and utilised that are only possible in this highly non-linear regime. The concepts of cross-gain modulation (XGM), cross-phase modulation (XPM) and four-wave mixing (FWM) have been easily achieved in an SOA and focused research has successfully demonstrated numerous novel configurations for achieving all-optical switching [117, 118, 119], optical packet routing, 2R and 3R signal regeneration [120] and wavelength conversion [121].

2.6.2 The application of semiconductor optical amplifiers as switches

All of the previously discussed applications employ SOAs that are operated with a continuous and constant electrical current. As such all of the charged carriers depleted by photon emission are quickly replenished by the action of electrical pumping and so optical amplification is continuously maintained. By contrast, a few applications have demonstrated the use of SOAs as electrically controllable switches. These demonstrations have shown that when SOAs are actively pumped they provide optical gain for any required signals, but that in the absence of pumping significant photon absorption occurs, such that the devices can also be used to provide high-level optical attenuation for signal blocking.

59

The commercial use of SOAs for the formation of electrically controlled optical switches was first noted by the author in a presentation at the *27th European Conference on Optical Communications (ECOC)* in 2001 by Khalfallah *et al* [122]. In this system 16 SOA devices were electrically controlled to provide active signal switching for a multi-wavelength packet router. The system demonstrated that low distortion optical switching with very high extinction ratio could be achieved in around 5ns using SOA technology. Later research by Gallep *et al* [123] also demonstrated that by using complex drive current profiles SOA switching times of ~10ps could also be possible in the future.

Furthermore, research and development into quantum-dot based SOAs has since shown that in contrast to older bulk and quantum well (QW) configurations these new devices have the potential to provide the simultaneous combination of high signal gain (>40dB) and high saturated output power (>20dBm). These enhanced levels of performance are considered highly likely to increase the range of applications and the importance of SOAs in the future.

2.7 Time-division-multiplexing of fibre Bragg grating sensors using the optical switching properties of an SOA

On discovery of the use of SOAs for optical switching in a packet routing system, the author supposed that it should be possible to use the same technology to optically gate the reflection signals from sensors in a time-division-multiplexed fibre Bragg grating sensor interrogation system. It was envisaged that such a system would operate in a manner similar to other optically gated TDM configurations that employed optical modulators, but that an SOA variant would be cheaper and smaller, and would provide inherent signal amplification.

It was this hypothesis, that it should be possible to use the latest telecommunication technology to overcome existing difficulties in implementing high performance TDM sensor interrogation, that has formed the foundation for the work contained in this thesis.

2.8 Chapter conclusion

This chapter has provided an historical overview of the advances made in fibre Bragg grating technology over the last 25 years. It introduced the operation, design and

manufacture of fibre Bragg gratings and highlighted the significant inherent advantages of using these components as sensors. A large variety of applications using FBGs for the measurement of temperature, strain and many other physical, chemical and electrical parameters were also discussed.

Two primary techniques for multiplexing numerous FBG sensors onto a single fibre optic cable were considered. It was shown that whilst wavelength-division-multiplexing has been the most successful technology to-date, time-division-multiplexing provides a wealth of commercial advantages that can be exploited, if the technical challenges surrounding successful implementation are overcome.

The chapter then provided an overview of the semiconductor optical amplifier, which was shown to provide a unique range of features under both continuous and switched operation conditions.

Finally, the author's hypothesis, that the characteristics of a switched semiconductor optical amplifier could be used to provide a novel implementation of optically gated time-division-multiplexing, was presented. This hypothesis formed the foundation for the work discussed within the remainder of this thesis.

1   I. Bennion, J. A. R. Williams, L. Zhang, K. Sugden and N. J. Doran 'UV-written in-fibre Bragg gratings', *Optical and Quantum Electronics*, **28**, 1996, pp.93-113

2   K. O. Hill and G. Meltz 'Fiber Bragg grating technology fundamentals and overview', *J. Lightwave Technol.*, **15**, 1997, pp.1263-1276

3   C. R. Giles, 'Lightwave applications of fiber Bragg gratings', *J. Lightwave Technol.*, **15**, 1997, pp.1391-1404

4   J. L. Zyskind, V. Mizrahim, D. J. DiGiovanni, J. W. Sulhoff, 'Short single frequency erbium-doped fibre laser', *Electron. Lett.*, **28**, 1992, pp.1385-1387

5   G. A. Ball, W. W. Morey, 'Continuously tunable single-mode erbium fibre laser', *Opt. Lett.*, **17**, 1992, pp.420-422

6   T. J. Cullen, H. N. Rourke, C. P. Chew, S. R. Baker, T. Bricheno, K. C. Byron, A. Fielding, 'Compact all-fibre wavelength drop and insert filter', *Electron. Lett.*, **30**, 1994, pp.2160-2162

7   K. Sugden, L. Zhang, J. A. R. Williams, R. W. Fallon, L. A. Everall, K. E. Chisholm, I. Bennion, 'Fabrication and characterisation of bandpass filters based on concatenated chirped fibre gratings', *J. Lightwave Technol.*, **15**, 1997, pp.1424-1432

8   J. A. R. Williams, L. A. Everall, I. Bennion, N. J. Doran, 'Fibre Bragg Grating fabrication for dispersion slope compensation', *Photon. Technol. Lett.*, **8**, (9), 1996, pp.1187-1189

9   M. Durkin, M. Ibsen, M. J. Cole, R. I. Laming, '1m long continuously-written fibre Bragg gratings for combined second and third order dispersion compensation', *Electron. Lett.*, **33**, (22), 1997, pp.1891-1893

10   X. Shu, K. Sugden, P. Rhead, J. Mitchell, I. Felmeri, G. Lloyd, K. Byron, Z. Huang, I. Khrushchev, I. Bennion, 'Tunable Dispersion Compensator Based on Distributed Gires-Tournois Etalons', *Photon. Technol. Lett.*, **15**, (8), 2003, pp.1111-1113

11   I. Riant, P. Bousselet, P. Sansonetti, P. Garabediam, J. L. Beylat, '20% pump power saving using photoinduced intracore fibre Bragg grating in erbium doped fibre amplifier', *Electron. Lett.*, **30**, 1994, pp.221-223

12   M. Farries, C. M. Ragdale, D. C. J. Reid, 'Broadband chirped fibre Bragg filters for pump rejection and recycling in erbium doped fibre amplifiers', *Electron. Lett.*, **28**, 1992, pp.487-489

13   Y. Jeong, J. K. Sahu, S. Baek, C. Alegria, D. B. S. Soh, C. Codemard, V. Philippov, D. J. Richardson, D. N. Payne, J. Nilsson, 'Ytterbium-doped double clad large core fibre lasers with kW-level continuous-wave output power' Paper CMS1, *Proc. Conference of Lasers and Electro-optics 2004*, San Francisco, USA

14   A. Molony, C. Edge, I. Bennion, 'Fibre grating delay element for phased array antennas', *Electron. Lett.*, **31**, 1995, pp.1485-1486

15   J. L. Cruz, B. Ortega, M. V. Andres, B. Gimeno, D. Pastor, J. Capmany, L. Dong, 'Chirped fibre Bragg gratings for phased array antennas', *Electron. Lett.*, **33**, 1997, pp.545-546

16   W. Zhang, J. A. R. Williams, L. A. Everall, I. Bennion, 'Tuneable radio frequency filtering using linearly chirped fibre gratings', *European Conference on Optical Communications 1998*, Madrid, Spain

17   A. D. Kersey, M. A. Devis, H. J. Patrick, M. LeBlanc, K. P. Koo, C. G. Askins, M. A. Putnam and E. J. Friebele, 'Fiber grating sensors', *J. Lightwave Technol.*, **15**, 1997, pp.1442-1463

18   M. A. Davis and A. D. Kersey, 'Fiber Bragg grating sensors for infrastructure sensing', Paper WL15, *Conference on Optical Fiber Communications 1997*, USA, pp.177-178

19   V. M. Murukeshan, P. Y. Chan, L. S. Ong, L. K. Seah, 'Cure monitoring of smart composites using Fiber Bragg Grating based embedded sensors', *Sensors and Actuators A*, **79**, 2000, pp.153-161

20   R. Maaskant, T. Alavie, R. M. Measures, G. Tadros, S. H. Rizkalla, A. Guha-Thakurta, 'Fibre-optic Bragg grating sensors for bridge monitoring', *J. Cement Concrete Compos.*, **19**, 1997, pp.21-23

21   C. K. Y. Leung, 'Fiber optic sensors in concrete: the future?', *N. D. T & E. International*, **34**, 2001, pp.85-94

22   K. Lau, L. Yuan, L. Zhou, J. Wu, C. Woo, 'Strain monitoring in FRP laminates and concrete beams using FBG sensors', *Composite Structures*, **51**, 2001, pp.9-20

23   K. Wood, T. Brown, R. Rogowski, B. Jensen, 'Fiber optic sensors for health monitoring of morphing airframes: I. Bragg grating strain and temperature sensor', *Smart Mater. Struct.*, **9**, 2000, pp.163-169

24   T. Yamate, R. T. Ramos, R. J. Schroeder, E. Udd, 'Thermally Insensitive Pressure Measurements up to 300 degree C using Fiber Bragg Gratings Written onto Side Hole Single Mode Fiber', *14th Conference on Optical Fibre Sensing*, 2000, pp.628-631

25   A. MacLean, C. Moran, W. Johnstone, B. Culshaw, D. Marsh, P. Parker, 'Detection of hydrocarbon fuel spills using a distributed fibre optic sensor', *Sensors and Actuators A*, **109**, 2003, pp.60-67

26   S. P. Christmas, D. A. Jackson, P. J. Henderson, L. Zhang, I. Bennion, T. Dalton, P. Butler, R. Kenny, 'High-resolution vibration measurements using wavelength-demultiplexed Fibre-Fabry-Perot sensors', *14th Conference on Optical Fibre Sensing*, 2000, pp.744-747

27   N. Takahashi, K. Yoshimura, S. Takahashi, K. Imamura, 'Development of an optical fibre hydrophone with Fibre Bragg grating', *Ultrasonics.*, **38**, 2000, pp.581-585

28   K. O. Hill, Y. Fujii, D. C. Johnson, B. S. Kawasaki, 'Photosensitivity in optical fibre waveguides: Application to reflection filter fabrication', *Appl. Phys. Lett.*, **32**, (10), 1978, pp. 647-649

29   B. S. Kawasaki, K. O. Hill, D. C. Johnson, Y. Fujii, 'Narrow-band Bragg reflectors in optical fibres', *Opt. Lett.*, **3**, 1978, pp.66-68

30   H. Kogelnik, 'Coupled Wave Theory for Thick Hologram Gratings', *Bell Syst. Tech. J.*, **48**, (9), 1969, pp.2909-2947

31   A. Yariv, 'Coupled-mode theory for guided-wave optics', *IEEE J. Quantum Electron.*, **QE-9**, (9), 1973, pp.919-933

32   K. O. Hill, 'Aperiodic distributed-parameter waveguides for integrated optics', Appl. Opt., **13**, 1974, pp.1853-1856

33   H. Kogelnik, 'Filter response of non-uniform almost-periodic structures', *Bell Syst. Tech. J.*, **55**, (1), 1976, pp.109-125

34   M. Yamada, K. Sakuda, 'Analysis of almost-periodic distributed feedback slab waveguides via a fundamental matrix approach', *Appl. Opt.*, **26**, 1987, pp.3474-3478

35   S. Radic, N. George, G. P. Agrawal, 'Analysis of non-uniform distributed feedback structures: Generalized transfer matrix method', *IEEE J. Quantum Electron.*, **31**, (7), 1995, pp.1326-1336

36   G. Meltz, W. M. Morey, W. H. Glenn, 'Formation of Bragg gratings in optical fibres by a transverse holographic method', *Opt. Lett.*, **14**, (15), 1989, pp.823-825

37   R. Kashyap, J. J. Armitage, R. Wyatt, S. T. Davey, D. L. Williams, 'All-fibre narrowband reflection gratings at 1550nm', *Electron. Lett.*, **26**, 1990, pp.730-731

38   K. O. Hill, F. Bilodeau, B. Malo, D. C. Johnson, J. Albert, 'Bragg gratings fabricated in monomode photosensitive optical fibre by UV exposure through a phase mask', *Appl. Phys. Lett.*, **62**, (10), 1993, pp.1035-1037

39   J. Martin, F. Ouellette, 'Novel writing technique of long and highly reflective in-fibre gratings', *Electron. Lett.*, **30**, (10), 1994, pp.811-812

40   H. N. Rourke, S. R. Baker, K. C. Byron, R. S. Baulcomb, S. M. Ojha, S. Clements, 'Fabrication and characterisation of long, narrowband fibre gratings by phase mask scanning', *Electron. Lett.*, **30**, (16), 1994, pp.1341-1342

41   J. J. Pan, Y. Shi, 'Steep skirt fibre Bragg grating fabrication using a new apodised phase mask', *Electron. Lett.*, **33**, (22), 1997, pp.1895-1896

42   J. Albert, K. O. Hill, B. Malo, S. Theriault, F. Bilodeau, D. C. Johnson, L. E. Erickson, 'Apodisation of the spectral response of fibre Bragg gratings using a phase mask with variable diffraction efficiency', *Electron. Lett.*, **31**, 1995, pp.222-223

43   J. Albert, K. O. Hill, D. C. Johnson, F. Bilodeau, M. J. Rooks, 'Moiré phase masks for automatic pure apodisation of fibre Bragg gratings', *Electron. Lett.*, **32**, (24), 1996, pp.2260-2261

44   L. Dong, J. L. Archambault, L. Reekie, J. St. P. Russel, D. N. Payne, 'Single pulse Bragg gratings written during fibre drawing', *Electron. Lett.*, **29**, 1993, pp.1577-1578

45   C. G. Askins, M. A. Putnam, G. M. Williams, E. J. Friebele, 'Stepped-wavelength optical-fiber Bragg grating arrays fabricated in line on a draw tower', *Opt. Lett.*, **19**, 1994, pp.147-149

46   C. G. Askins, M. A. Putnam, H. J. Patrick, E. J. Friebele, 'Fibre strength unaffected by on-line writing of single-pulse Bragg gratings', *Electron. Lett.*, **33**, 1997 pp.1333-1334

47   D. S. Starodubov, V. Grubsky and J. Feinberg, 'Efficient Bragg grating fabrication in a fibre through its polymer jacket using near-UV light', *Electron. Lett.*, **33**, 1997, pp.1331-1333

48   D. S. Starodubov, V. Grubsky, J. Feinberg, B. Kobrin, S. Juma, 'Bragg gating fabrication in germanosilicate fibres by use of near-UV light: A new pathway for refractive-index changes', *Opt. Lett.*, **22**, (14), 1997, pp.1086-1088

49   R. P. Espindola, R. M. Atkins, D. A. Simoff, K. T. Nelson, M. A. Paczkowski, 'Fiber Bragg gratings written through a fibre coating', Paper PD4, *Conference on Optical Fiber Communications 1997*, USA

50   Y. J. Rao, 'Recent progress in applications of in-fibre Bragg grating sensors', *Optics and Lasers in Eng.*, **31**, 1999, pp. 297-324

51 Y. J. Rao, 'In-fibre Bragg grating sensors', *Meas. Sci. Technol.*, **8**, 1997, pp.355-375

52 K. T. V. Grattan, T. Sun, 'Fibre optic sensor technology: an overview', *Sensors and Actuators A*, **82**, 2000, pp.40-61

53 M. W. Hathaway, N. E. Fisher, D. J. Webb, C. N. Pannell, D. A. Jackson, L. R. Gavrilov, J. W. Hand, L. Zhang, I. Bennion, 'Combined ultrasound and temperature sensor using a fibre Bragg grating', *Optics Comm.*, **171**, 1999, pp.225-231

54 W. Jin, Y. Zhou, P. K. C. Chan, H. G. Xu, 'A fibre-optic grating sensor for the study of flow-induced vibrations', *Sensors and Actuators A*, **79**, 2000, pp.36-45

55 J. Yang, Y. Zhao, B. J. Peng, X. Wan, 'Temperature-compensated high pressure FBG sensor with a bulk-modulus and self-demodulation method', *Sensors and Actuators A*, In press

56 S. Takashima, H. Asanuma, H. Niitsuma, 'A water flowmeter using dual fiber Bragg grating sensors and cross-correlation technique', *Sensors and Actuators A*, **116**, 2004, pp.66-74

57 Y. Zhao, J. Yang, B. J. Peng, S. Y. Yang, 'Experimental research on a novel fiber optic cantilever-type inclinometer', *Optics and Laser Technol.*, In press

58 Y. L. Lo, B. R. Chue, S. H. Xu, 'Fiber torsion sensor demodulated by a high-birefringence fiber Bragg grating', *Optics Comm.*, **230**, 2004, pp.287-295

59 R. Suresh, S. C. Tjin, N. Q. Ngo, 'Shear force sensing by strain transformation using non-rectilinearly embedded fiber Bragg grating', *Sensors and Actuators A*, **116**, 2004, pp.107-118

60 V. V. Spirin, M. G. Shlyagin, S. V. Miridonov, F. J. Mendieta Jiménez, R. M. López Gutiérrez, 'Fiber Bragg grating sensors for petroleum hydrocarbon leak detection', *Optics Lasers Eng.*, **32**, 1999, pp.497-503

61 J. Cong, X. Zhang, K. Chen, J. Xu, 'Fiber optic Bragg grating sensor based on hydrogels for measuring salinity', *Sensors and Actuators B*, **87**, 2002, pp.487-490

62 M. G. Xu, J. L. Archambault, L. Reekie, J. P. Dakin, 'Discrimination between strain and temperature effects using dual-wavelength fiber grating sensors', *Electron. Lett.*, **30**, 1994, pp.1085-1087

63. S. W. James, M.L. Dockney, R. P. Tatam, 'Simulataneous independent temperature and strain measurement using in-fibre Bragg grating sensors', *Electron. Lett.*, **32**, 1996, pp.1133-1134,

64 H. J. Patrick, G. M. Williams, A. D. Kersey, J. R. Pedrazzani, A. M. Vengsarkar, 'Hybrid fiber Bragg grating/long period fiber grating sensor for strain/temperature discrimination', *Photon. Technol. Lett.*, **8**, 1996, pp.1223-1225

65 X. Shu, Y. Liu, D. Zhao, B. Gwandu, F. Floreani, L. Zhang, I. Bennion, 'Fiber grating dependence of temperature and strain coefficients and application to simultaneous temperature and strain measurement', *15th Conference on Optical Fibre Sensing*, 2002, pp.83-86

66 O. Frazao, M. J. N. Lima, J. L. Santos, 'Simultaneous measurement of strain and temperature using type I and type IIa fibre Bragg gratings', *J. Opt. A: Pure Appl. Opt.*, **5**, 2003, pp.183-185

67 J. Jung, H. Nam, J. H. Lee, N. Park, B. Lee, 'Simultaneous measurement of strain and temperature by use of a single-fiber Bragg grating and an erbium-doped fiber amplifier', *Appl. Opt.*, **38**, 1999, pp.2749-2751

68 D. I. Forsyth, S. A. Wade, T. Sun, X. Chen, K. T. V. Grattan, 'Dual temperature and strain measurement with the combined fluorescence lifetime and Bragg wavelength shift approach in doped optical fiber', *Appl. Opt.*, **41**, 2002, pp.6585-6592

69 S. A. Wade, S. F. Collins, K. T. V. Grattan, G. W. Baxter, 'Strain-Independent Temperature Measurement by Use of a Fluorescence Intensity Ratio Technique in Optical Fiber', *Appl. Opt.*, **39**, 2000, pp.3050-3052

70 C. Song, S. K. Lee, S. H. Jeong, B. H. Lee, 'Absolute strain measurements made with fiber Bragg grating sensors', *Appl. Opt.*, **43**, 2004, pp.1337-1341

71 R. W. Fallon, L. Zhang, A. Gloag, I. Bennion, 'Identical broadband chirped grating interrogation technique for temperature and strain sensing', *Electron. Lett.*, **33**, 1997, pp.705-707

72 A. B. Lobo Ribeiro, L. A. Ferreira, J. L. Santos. D. A. Jackson, 'Analysis of the reflective-matched fibre Bragg grating sensing interrogation scheme', *Appl. Opt.*, **36**, 1997, pp.935-939

73 A. D. Kersey, T. A. Berkoff, W. W. Morey, 'High resolution fiber Bragg grating based strain sensor with interferometric wavelength shift detection', *Electron. Lett.*, **28**, 1992, pp.236-238

74 A. D. Kersey, T. A. Berkoff, W. W. Morey, 'Fiber optic Bragg grating sensor with drift-compensated high resolution interferometric wavelength shift detection', *Opt. Lett.*, **18**, 1993, pp.72-74

75 W. W. Morey, 'Distributed fiber grating sensors', *Proc. OFS'90*, Sydney, Australia, 1990, pp.285

76 S. M. Melle, K. Liu, R. M. Measures, 'A passive wavelength demodulation system for guided-wave Bragg grating sensors', *Photon. Technol. Lett.*, **4**, 1992, pp.516-518

77 S. M. Melle, K. Lui, R. M. Measures, 'Practical fibre-optic Bragg grating strain gauge system', *Appl. Opt.*, **32**, 1993, pp.3601-3609

78 M. A. Davis, A. D. Kersey, 'All-fiber Bragg grating strain-sensor demodulation technique using a wavelength division coupler' *Electron. Lett.*, **30**, 1994, pp.75-77

79 K. Sugden, I. Bennion, 'Chirped gratings produced in photosensitive optical fibers by fiber deformation during exposure', *Electron. Lett.*, **30**, 1994, pp.440

80 S. Chung, J. Kim, B-A. Yu, B. Lee, 'A Fiber Bragg Grating Sensor Demodulation Technique Using a Polarization Maintaining Fiber Loop Mirror', *Photon. Technol. Lett.*, **13**, 2001, pp.1343-1345,

81 S. L. Lee, Y. Y. Hsu, C. T. Pien, 'High-Resolution Wavelength Monitoring Using Differential/Ratio Detection of Junction Voltage Across a Diode Laser', *Photon. Technol. Lett.*, **13**, 2001, pp.872-874

82 T. Coroy, R. M. Measures, 'Demodulation system for Bragg grating fiber optic sensors using a quantum well electroabsorption filtering detector', *Smart Mater. Struct.*, **7**, 1998, pp.265-271

83 A. D. Kersey, T. A. Kerkoff, W. W. Morey, 'Multiplexed fiber Bragg grating strain-sensor system with a fiber Fabry-Perot wavelength filter', *Opt. Lett.*, **18**, 1993, pp.1370-1372

84 Y. N. Ning, A. Meldrum, W. J. Shi, B. T. Meggitt, A. W. Palmer, K. T. V. Grattan, L. Li, 'Bragg grating sensing instrument using tunable Fabry-Perot filter to detect wavelength variations', *Meas. Sci. Technol.*, **9**, 1998, pp.599-606

85 D. A. Jackson, A. B. Lobo Ribeiro, L. Reekie, J. L. Archambault, 'Simple multiplexing scheme for a fiber-optic grating sensor network', *Opt. Lett.*, **18**, 1993, pp.1192-1194

86 M. A. Davis, A. D. Kersey, 'Matched-filter interrogation technique for fiber Bragg grating arrays', *Electron. Lett.*, **31**, 1995, pp.822-823

87 A. D. Kersey, T. A. Berkoff, 'Fiber Bragg grating array sensor system using a bandpass wavelength-division-multiplexer and interferometric detection', *Photon. Technol. Lett.*, **8**, 1996, pp.1522-1524

88 H. Geiger, M. G. Xu, N. C. Eaton, J. P. Dakin, 'Electronic tracking system for multiplexed fiber grating sensors', *Electron. Lett.*, **31**, 1995, pp.1006-1007

89 C. Boulet, D. J. Webb, M. Douay, P. Niay, 'Simultaneous Interrogation of Fiber Bragg Grating Sensors Using an Acousto-optic Tunable Filter', *Photon. Technol. Lett.*, **13**, 2001, pp.1215-1217

90 Y. Yu, L. Lui, H. Tam, W. Chung, 'Fiber-Laser-Based Wavelength-Division-Multiplexed Fiber Bragg Grating Sensor System', *Photon. Technol. Lett.*, **13**, 2001, pp.702-704

91 S. Kim, J. Kwon, S. Kim, B. Lee, 'Multiplexed Strain Sensor Using Fiber Grating-Tuned Fiber Laser with a Semiconductor Optical Amplifier', *Photon. Technol. Lett.* **13**, 2001, pp350-351

92 P. C. Peng, H. Y. Tseng, S. Chi, 'Long-Distance FBG Sensor System Using a Linear-Cavity Fiber Raman Laser Scheme', *Photon. Technol. Lett.*, **16**, 2004, p575-577

93 C. G. Askins, M. A. Putnam, 'Instrumentation for interrogating many-element fiber Bragg grating arrays embedded in fiber/resin composites', *Proc. SPIE Smart Sensing, Processing and Instrumentation*, 1995, **2444**, pp.257

94   C. G. Askins, M. A. Putnam, 'Optical spectrometer with improved geometry and data processing for monitoring fiber optic Bragg gratings', *US Patent 6233373*, May 2001

95   C. Jáuregui, A. Quintela, J. M. L. Higuera, 'Interrogation unit for fibre Bragg grating sensors that uses a slanted fiber grating', *Opt. Lett.*, 29, 2004, pp.676-678

96   A. G. Simpson, K. Zhou, L. Zhang, L. Everall, I. Bennion, 'Optical sensor interrogation using a blazed fibre Bragg grating and CCD linear array', *Appl. Opt.*, 43, 2004, pp.33-40

97   K. Zhou, A. G. Simpson, X. Chen, L. Zhang, I. Bennion, 'Fiber Bragg Grating Sensor Interrogation System Using a CCD Side Detection Method With Superimposed Blazed Gratings', *Photon. Technol. Lett.*, 16, 2004, pp.1549-1551

98   C. C. Chan, Y. J. Gao, K. T. Lau, H. L. Ho, L. M. Zhou, W. Jin, 'Characterisation of crosstalk of a TDM FBG sensor array using a laser source', *Optics and Laser Technol.*, 33, 2001, pp.299-304

99   A. D. Kersey, 'Analysis of intrinsic crosstalk in tapped serial and Fabry-Perot interferometric fiber sensor arrays', Proc. SPIE Fiber Optic Laser Sensors VI, 985, 1988, pp.113-116

100 Mark Froggatt, Jason Moore, 'Distributed measurement of static strain in an optical fiber using multiple Bragg gratings at nominally equal wavelengths', *Appl. Opt.* 37, 1998, pp1741-1746

101 H. Lee, 'Multiple fiber Bragg grating sensor system using code-division multiple access', *Appl. Opt.*, 41, 2002, pp.5245-5248

102 P. K. C. Chan, W. Jin, J. M. Gong, M. S. Demokan, 'Multiplexing of Fibre Bragg Grating Sensors using an FMCW Technique', *Photon. Technol. Lett.*, 11, 1999, pp.1470-1472

103 M. A. Putnam, M. L. Dennis, I. N. Duling III, C. G. Askins, E. J. Friebele, 'Broadband square-pulse operation of a passively mode-locked fiber laser for fiber Bragg grating interrogation', *Opt. Lett.*, 23, 1998, pp138-140

104 P. R. Morkel, K. P. Jedrzejewski, E. R. Taylor, D. N. Payne, 'Short-Pulse, High-Power Q Switched Fiber Laser', *Photon. Technol. Lett.*, 4, 1992, pp.545-547

105 X. Wan, H. F. Taylor, 'Spectrally scanned, repetitively pulsed erbium-doped fiber laser for spectral and temporal multiplexing of fiber Bragg grating sensors', *Opt. Lett.*, 28, 2003, pp1648-1650

106 Y. J. Rao, A. B. L. Ribeiro, D. A. Jackson, L. Zhang, I. Bennion, 'Simultaneous spatial, time, and wavelength division multiplexed in-fibre grating sensing network', *Opt. Commun.*, 125, 1996, pp.53-58

107 Y. J. Rao, A. B. L. Ribeiro, D. A. Jackson, L. Zhang, I. Bennion, 'Combined spatial- and time-division multiplexing scheme for fiber grating sensors with drift-compensated phase-sensitive detection', *Opt. Lett.*, 20, 1995, pp.2149-2151

108 T. A. Berkoff, M. A. Davis, D. G. Bellemore, A. D. Kersey, G. M. Williams, M. A. Putnam, 'Hybrid time and wavelength division multiplexed fibre grating array', *Proc. SPIE*, **V2444**, 1995, pp.288

109 W. Ecke, L. C. da S. Nunes, L. C. G. Valente, K. Schroeder, C. Chojetzki, R. Willsch, 'OTDR Multiplexed High-Birefringent Fiber Grating Sensor Network for Transversal Strain and Optochemical Monitoring', *Proc. SPIE OFS16*, 2003, pp.548

110 M. Zhang, C. C. Chan, D. N. Wang, J. M. Gong, W. Jin, M. S. Demokan, 'Time division multiplexed strain sensing system by the use of dual-wavelength fiber Bragg gratings', *Sens. Actuators. A*, **100**, 2002, pp.175-178

111 D. J. Cooper, T. Coroy, P. W. E. Smith, 'Time division multiplexing of large serial fiber-optic Bragg grating sensor arrays', Appl. Opt., 40, 2001, pp.2643-2654

112 D. J. F. Cooper, P. W. E. Smith, 'Simple high-performance method for large-scale time division multiplexing of fibre Bragg grating sensors', *Meas. Sci. Technol.*, **14**, 2003, pp.965-974

113 Smart Fibers Ltd., 'Time division multiplexed fibre sensor interrogators', 2004, http://www.smartfibres.com/T4_Range.htm

114 J. Mørk, M. L. Nielsen, T. W. Berg, 'The dynamics of Semiconductor Optical Amplifiers: Modelling and applications', Opt. Photon. News, **14**, 2003, pp.42-48

115 M. J. Connelly, 'Wideband Semiconductor Optical Amplifier Steady-State Numerical Model', *J. Quantum Electron.*, 37, 2001, pp.439-447

116 G. Talli, M. J. Adams, 'Gain Dynamics of Semiconductor Optical Amplifiers and Three-Wavelength Devices', *J. Quantum Electron.*, 39, 2003, pp.1305-1313

117 B. K. Mathason, H. Shi, I. Nitta, G. A. Alphonse, J. Abeles, J. C. Connolly, P. J. Delfyett, 'Multiwavelength All-Optical TDM Switching Using a Semiconductor Optical Amplifier in a Loop Mirror', *Photon. Technol. Lett.*, 11, 1999, pp.331-333

118 E. Jahn, N. Agrawal, M. Arbert, H. J. Ehrke, D. Franke, R. Ludwig, W. Pieper, H. G. Weber, C. M. Weinertg, '40 Gbit/s all-optical demultiplexing using a monolithically integrated Mach-Zehnder interferometer with semiconductor laser amplifier', *Electron. Lett.*, 31, 1995, pp.1857–1858

119 J. H. Kim, K. R. Oh, H. S. Kim, K. Cho, 'All-Optical Switching by Counterpropagating Operating in Cascaded Semiconductor Optical Amplifiers', *Photon. Technol. Lett.*, **12**, 2000, pp.513-515

120 I. Ogura, Y. Hashimoto, H. Kurita, T. Shimizu, H. Yokoyama, 'Picosecond All-Optical Gate Using a Saturable Absorber in Mode-Locked Laser Diodes', *Photon. Technol. Lett.*, **10**, 1998, pp.603-605

121 R. Sato, T. Ito, K. Magari, Y. Inoue, I. Ogawa, R. Kasahara, M. Okamoto, Y. Tohmori, Y. Suzuki, N. Ishihara, 'Low input power (-10dBm) SOA-PLC hybrid

integrated wavelength converter and its 8-slot equipment', *Proc. ECOC '01,* 2001, Paper 156-1

122 S. Khalfallah, B. Martin, J. Decobert, S. Fabre, C. Fortin, P. Peloso, I. Guillemot, J. Le Bris, M. Renaud, A. Göth, A. Dupas, L. Gilbert, D. Penninckx, 'First Optical Packet Switching Demonstration with Sixteen-Channel InP Monolithically Integrated Wavelength Selector Module', *Proc. ECOC '01,* 2001, Paper 19-1

123 C. M. Gallep, E. Conforti, 'Reduction of Semiconductor Optical Amplifier Switching Times by Preimpulse Step-Injected Current Technique', *Photon. Technol. Lett.,* **14,** 2002, pp.902-904

3 THE PROOF OF CONCEPT EXPERIMENTS

3.1 Chapter introduction

In the previous chapter the hypothesis that a semiconductor optical amplifier (SOA) could be used as an optical gate to time-division-multiplex (TDM) a series of fibre Bragg gratings was introduced. This chapter describes a series of proof-of-concept experiments that were conducted to evaluate this idea.

The majority of these experiments were performed in the order in which they are described and before any decision was made to try to develop the concept into a commercial product. Therefore, due to limited time and financial budgets, only standard electrical and optical laboratory equipment, and a crudely modified semiconductor optical amplifier evaluation board were used.

However, as this chapter later describes, the resulting success of these early experiments resulted in the corporate decision to conduct a study into the commercial opportunity for a sensor interrogation system based on the switched SOA TDM idea. An encouraging market response then justified the compilation of a draft specification for such a device, and so an application for patent protection of the technology and a decision to continue research quickly followed. This all resulted in the development of some bespoke apparatus and further experimentation, which although actually conducted later in the project cycle, is also included here.

The chapter concludes with a discussion of the key sub-systems required to produce a viable fibre Bragg grating sensor interrogation system, so highlighting the design decisions that were made possible by these early experiments and the extent of the research and development that was still to be completed.

Although the majority of the experimental work described in this chapter is new and does not repeat existing work, it does build on a wealth of knowledge gained by previous researchers working in fibre Bragg grating based optical sensing and optical communications. Since many excellent review articles have covered earlier work [1, 2, 3, 4, 5] it is not the intention of this chapter to repeat this information. The reader is, however, encouraged to refer to chapter 2 for an overview of the theory, for the

hypothesis that formed the foundation of these experiments and for references to addition, external information.

3.2 The SOA evaluation board

When experimental work first began no practical experience of using SOAs existed within the company and so a decision was made to loan an evaluation board from a local SOA manufacturer (Kamelian Limited). The optical specification for the SOA is shown in Table 3.1. It should be noted that although the optical bandwidth is centred at 1491nm, the device is designed for optimised operation around 1540 to 1560nm.

Parameter	Typical value
Optical gain	23 dB (at 1550nm)
Optical bandwidth	55 nm
Optical central wavelength	1491 nm
Saturated output power	10.4 dBm (at 1550nm)

Table 3.1 The optical specification for the SOA provided on the evaluation board

3.2.1 Primary functions of the evaluation board

The complete evaluation board was constructed in an open 100x200mm (Eurocard) form factor and was designed for operation from a laboratory power supply with control from a PC. The primary components that it included are shown in Figure 3.1.

These components ensured that the SOA was kept at a constant temperature and provided with a smoothed and stable electrical supply. Unfortunately however, because the board was designed for use by telecommunications customers, the SOA was continuously enabled and there was no provision for switched or pulsed operation.
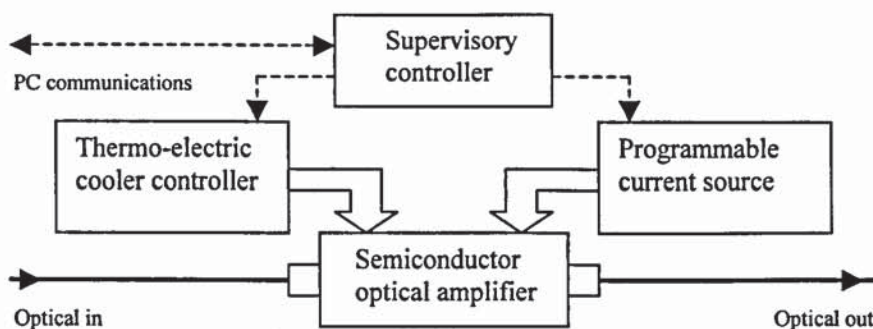
Figure 3.1 The primary components contained on the SOA evaluation board

3.2.2 Modification for pulsed operation

Figure 3.2 shows the original supply circuit for the SOA and a modified arrangement that was constructed using standard discrete components to allow basic switched operation. This modified arrangement was temporarily attached to the evaluation board, such that it could be easily removed later if required.
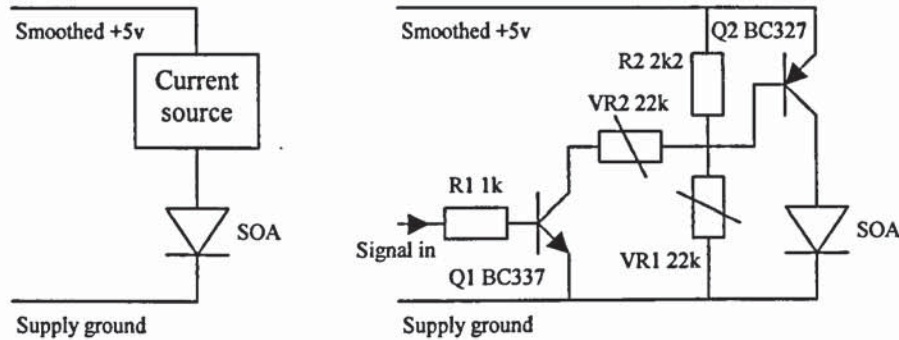
Figure 3.2 The original (left) and modified (right) SOA power supplies on the evaluation board

This alternative circuit provided adjustment for the current delivered to the SOA in the 'off' mode using VR1 and in the 'on' mode using VR2. Switching between 'on' and 'off' conditions was achieved using transistor Q1, which was connected to the output of the pulse generator system.

3.3 The original pulse generator system

It had been anticipated that evaluation of the SOA TDM system would require the ability to provide a chain of electrical pulses of reasonably short duration and variable frequency. The actual duration of the pulses was only expected to affect the minimum allowable sensor spacing and was of little significance in demonstrating a proof-of-concept, but a spacing of less than 100m was preferable due to difficulty handling large quantities of delicate fibre.

Figure 3.3 shows the connections that were made between two cascaded function generators and the modified evaluation board in order to provide the pulsed SOA operation that was used in many of the experiments. Figure 3.4 shows an idealised view of the signals at the points marked A and B. The actual delay that was experienced between the signals was dependent on the function generators and is explained in detail later.
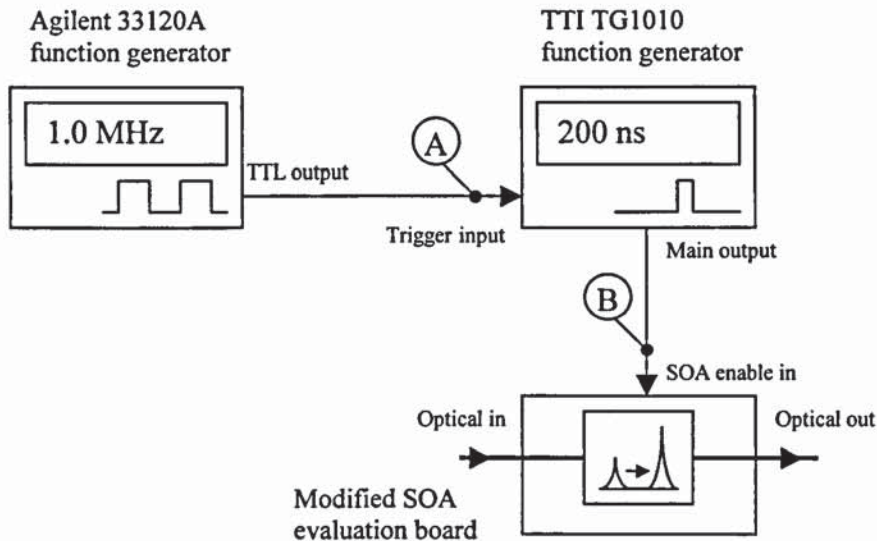
Figure 3.3 The connections between the two function generators and the modified SOA evaluation board, which were used to provide adjustable pulsed operation
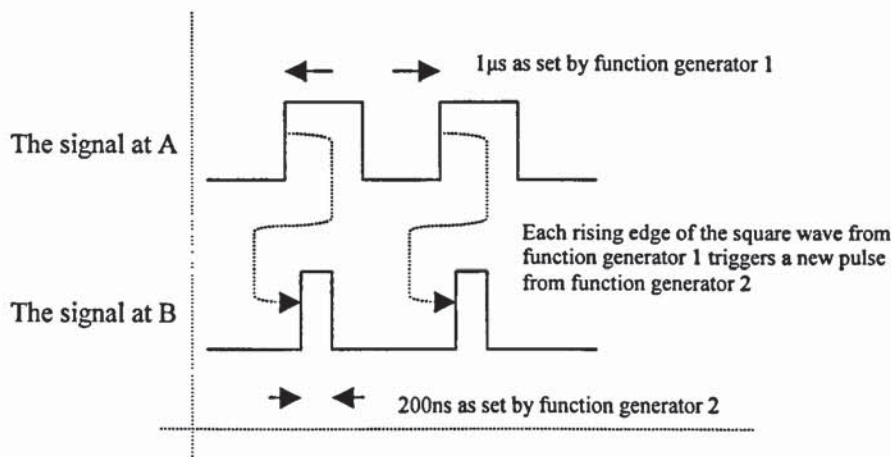
Figure 3.4 An idealised view of the signals at the locations marked A and B in Figure 3.3

The repetition frequency of the SOA drive pulses was dictated by an Agilent 33120A programmable function generator, which was configured to deliver a TTL compatible square wave. In most experiments the frequency was adjusted to match the time of flight of optical pulses in the fibre and was typically around 1MHz. The length of each of the SOA drive pulses was separately controlled by adjustment of a TTI TG1010 function generator. This was typically configured to produce a single 200ns pulse for each rising edge detected at its trigger input. The main output of this second instrument was configured to provide a 5V peak signal to the input of the modified SOA evaluation board, and in some experiments a secondary TTL output was also used to trigger an oscilloscope or light source.

74

3.4 Laboratory equipment for optical measurement

Measurements of optical signals were often required in the time or wavelength domains. A different equipment configuration was needed for each.

3.4.1 Measurement in the time domain

Measurement of optical pulse length and optical signal evolution over time was achieved using an amplified photodiode detector and an oscilloscope as shown in Figure 3.5. The detector used was a New Focus V1811, which had an electrical bandwidth from DC-125MHz, a 40,000 V/A transimpedance gain, operated from a standard bench power supply and was purchased for around $1000. The oscilloscope was a Tektronix TDS210 dual-channel digital storage model that had a sampling rate of 2G/s and an electrical bandwidth of 60MHz.
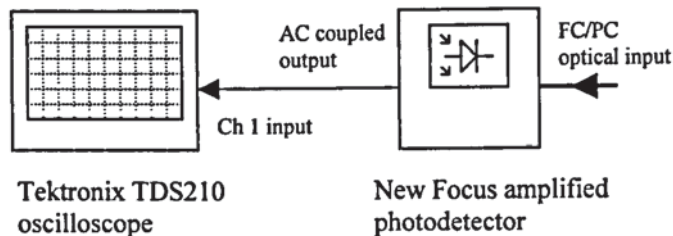
Figure 3.5 The equipment that was used to measure optical pulse length and signal evolution over time

3.4.2 Measurement in the wavelength domain

In all of the early experiments measurement of optical signals in the wavelength domain was carried out using an Ando AQ6331 optical spectrum analyser (OSA). This model had an adjustable filter bandwidth down to 50pm and a noise floor of around −90 dBm. The sweep speed could be adjusted by changing the number of sampling points or by using averaging. A typically scan over a 2nm range took around 3 seconds and was found to produce an adequately stable time-averaged recording from a pulsed optical signal.

Where measurement of the optical profile of a passive device was required (such as a coupler, length of fibre or FBG), illumination was provided using an Agilent 1550nm broadband super-luminescent light emitting diode (SLED) source.

3.5 Proof of unidirectional optical gating

The first proof-of-concept experiment that was conducted was intended to evaluate the optical gating properties of the SOA [6].

3.5.1 Circuit configuration

The optical and electronic circuit configuration used is shown in Figure 3.6. The two FBGs had 75% reflectivity, 1nm full-width-half-maximum (FWHM) optical bandwidth and central wavelengths of 1558.7nm and 1559.6nm respectively. They were spliced onto reels of standard SMF28 single mode optical fibre of lengths 65m and 130m and then connected to one arm of a fused fibre coupler via an FC/APC pigtailed connector. The opposite arms of the 50% transfer ratio coupler were then connected to the output of the SLED source and the input of the SOA. These two active devices were electrically connected for triggering from the cascaded function generators described earlier. Finally, the optical output from the SOA was monitored on the OSA via a standard patch cord.
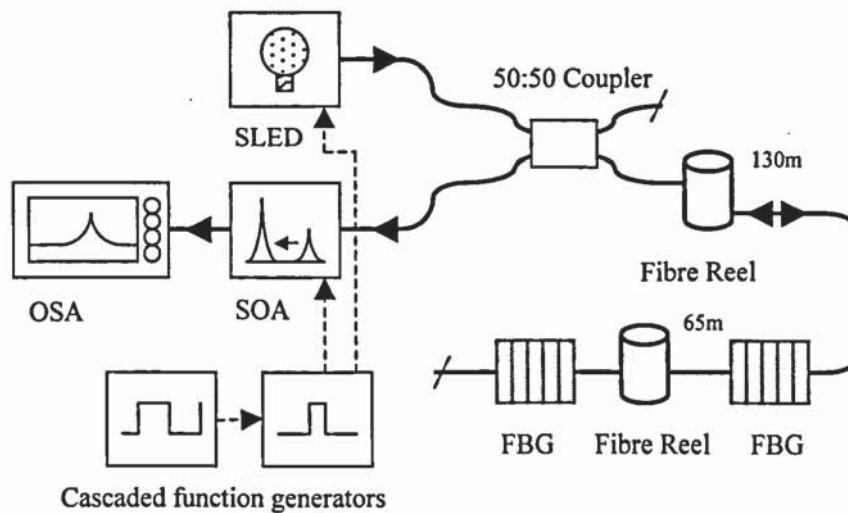
Figure 3.6 The equipment configuration that was used to assess unidirectional optical gating

3.5.2 Circuit operation

If the circuit was considered starting from the idle state with the SOA and SLED both in the 'off' condition, then the mode of operation was as follows:

- An initial electrical pulse was output from the cascaded function generators that resulted in the simultaneous output of an optical pulse from the SLED broadband source and the turn 'on' of the SOA. Turning 'on' of the SOA effectively 'opened' the optical gate

76

- When the electrical pulse ended, the SLED stopped emitting an optical signal and the SOA turned 'off', which closed the gate

- The broadband optical pulse generated by the SLED propagated into the left port of the coupler and was split with 50/50 ratio at the two right hand ports

- Half of the total input signal was therefore lost to the angle cleaved end, whilst the remainder propagated via the 130m fibre reel towards the two FBG sensors

- The electrical pulse lasted ≈200ns, so making the assumption that the optical pulse was of a similar duration, spatially the optical pulse occupied around 40m of fibre (from Equation 2.10)

- On reaching the first sensor, 75% of the incident optical signal (equal to the wavelength profile of the grating) was reflected by the FBG structure and began propagating back towards the coupler

- The remainder of optical signal continued in the direction of the second FBG via a further length of fibre

- On reaching this FBG, 75% of the remaining incident signal (equal to the wavelength profile of the grating) was also reflected back towards the coupler

- Since the FBG separation was 65m, the wave fronts from each of the two optical reflections were 130m apart in the fibre when they arrived back at the right hand port of the coupler

- Due to the 50/50 coupler ratio, half of the reflected signal that passed through the coupler entered the SOA input

- When the frequency of the first function generator was adjusted, such that the second function generator delivered a further electrical pulse to the SLED and SOA at a time coincident with the arrival of the first reflection, the reflected signal passed through the SOA and was amplified by around 20dB

- Due to the short pulse duration the SOA was turned 'off' again and the optical gate 'closed' before the arrival of the second reflection and hence only the signal from the first FBG arrived at the OSA

- This process was allowed to repeat with a continuous chain of pulses, such that for each pulse, the SLED emitted a new broadband illumination signal, whilst the SOA optically gated the reflection from the previous cycle

Adjustment of the pulse repetition frequency allowed selection between the reflection signals from either of the two FBGs when the period of repetition equalled the period of optical propagation between the SLED, the FBG sensor and back to the SOA.

Including the long initial lead fibre reel ensured that the optical path length to the second FBG could never be an integer multiple of the path length to the first FBG. Each sensor could therefore be tuned without interference from the other.

Having correctly adjusted the pulse repetition frequency for each sensor, the OSA was used to record a time-averaged profile of the optically gated reflection signal. A stable signal was possible from the OSA since its filter scan rate was more than three orders of magnitude lower than the gating of the reflection.

3.5.3 Experimental results

Table 3.2 shows the optimum settings for the pulse repetition frequency for selection of each FBG, while Figure 3.7 and Figure 3.8 show the recordings taken using the OSA for these settings.

Fibre Bragg grating number	Central wavelength [nm]	Optical propagation period [μs]	Pulse repetition frequency [kHz]
1	1558.73	1.35	740.7
2	1559.61	2.01	497.5

Table 3.2 The optimum function generator settings for selection of the two FBGs
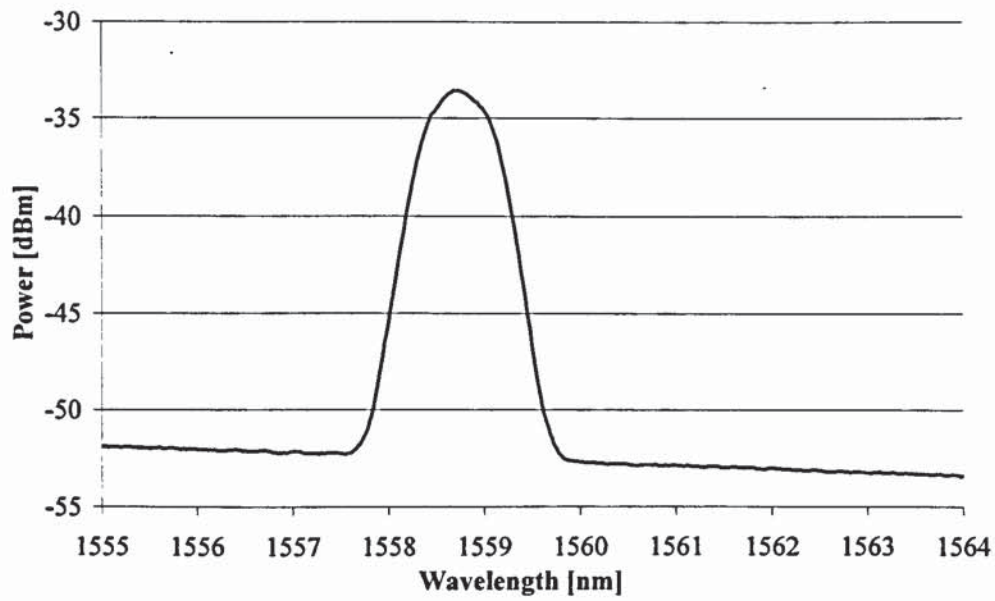
Figure 3.7 An OSA recording of the signal received when the system was adjusted to the optimum repetition period for FBG 1
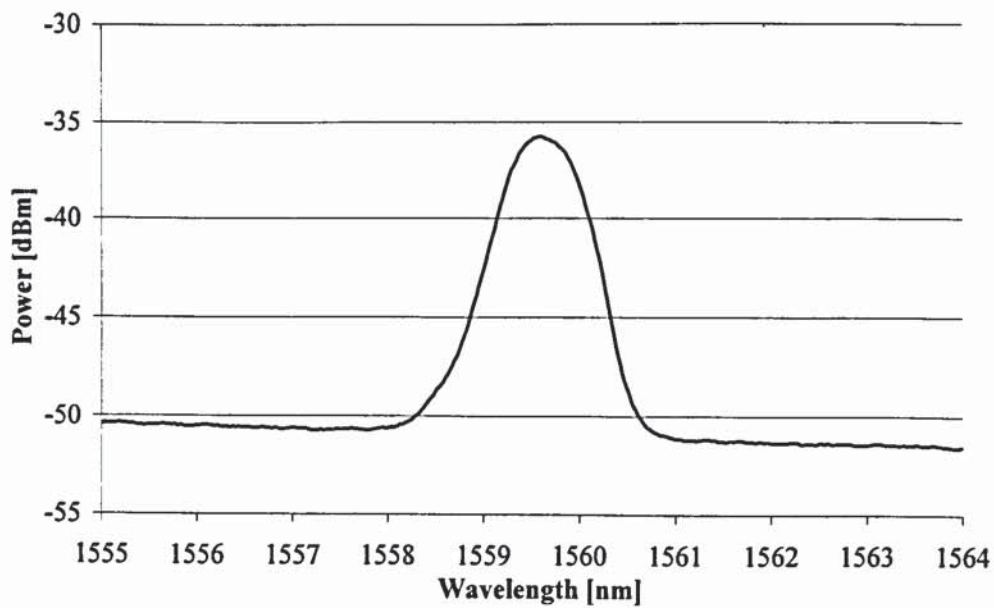
Figure 3.8 An OSA recording of the signal received when the system was adjusted to the optimum repetition period for FBG 2

The peak optical signal power, the mean level of the background noise and the ratio of the two values were taken from these OSA recordings and are shown in Table 3.3.

Fibre Bragg grating number	Peak optical signal power [dBm]	Mean background noise power [dBm]	Ratio of the values [dB]
1	-33.5	-53.0	19.5
2	-35.7	-51.3	15.6

Table 3.3 The parameters for the FBG signals (as taken from the OSA recordings)

An observation whilst conducting the experiment showed that the peak optical-signal-to-background-noise ratio (OSNR) increased steadily as the function generator was adjusted to the optimum setting for each FBG and that no apparent signal existed when the repetition period was adjusted to half way between the two optimum positions. Figure 3.9 therefore shows a plot of the variation in OSNR for the signals from each FBG as a function of repetition period.
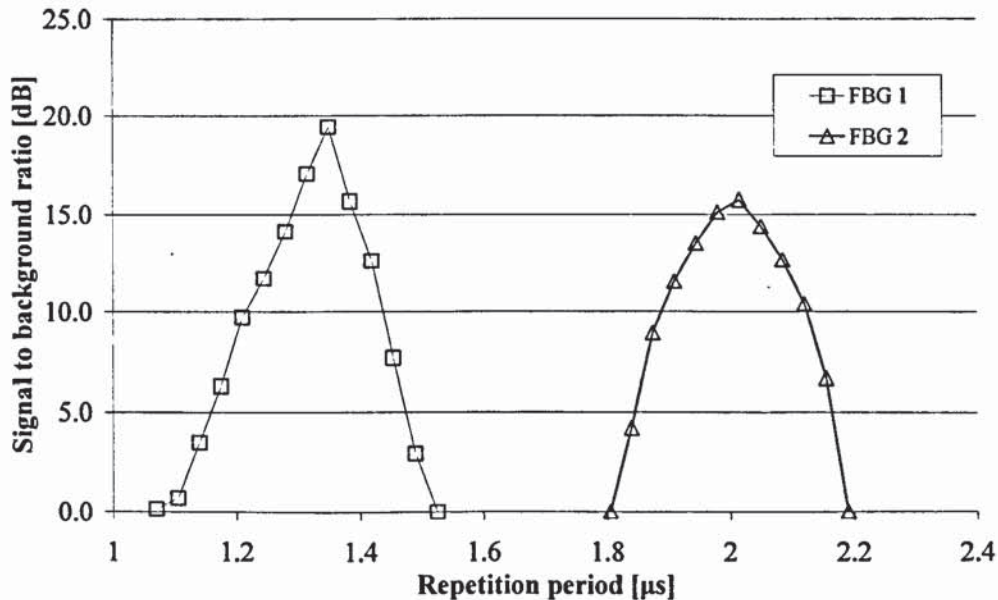
Figure 3.9 The optical signal-to-background-noise ratio for the signals received from each FBG, as a function of repetition period

Monitoring of a single FBG whilst applying strain also demonstrated that the reflected signal responded with a change in wavelength. Therefore, although no systematic analysis was conducted at this time, both FBGs were checked and found to exhibit an expected strain-related-wavelength-shift behaviour [1, 4].

A further observation showed that although the experiment had intended to use the SLED to provide the illumination for the FBG sensors, in reality a sufficiently strong broadband optical signal was emitted from the input port of the SOA (when it was

switched on) such that it was able to adequately illuminate the FBGs if the SLED was disabled.

3.5.4 Conclusions

The results of this first experiment proved that an SOA could be used as an optical gate to provide time-division-multiplexing of FBGs because with correct timing of the electrical drive signals only the reflection profile from one sensor could be seen on the OSA at a time. Equally importantly, when the SOA pulse timing was adjusted to block reflections from both FBG sensors no apparent grating profile was delivered to the OSA. This indicated that a high level of extinction occurred to those signals arriving when the optical gate was closed.

A further consequence of the experiment was the realisation of the effect of the amplified spontaneous emission (ASE) characteristically generated by an SOA. This was verified to manifest as a broadband optical signal emitted from both the input and output facets of the device. At the output of the SOA this ASE was found to have the detrimental effect of reducing the level of OSNR that could be obtained for the signal delivered to the OSA, while from the SOA input it had the positive effect of the providing broadband illumination of the FBG sensors, without the requirement for a separate SLED source.

3.6 The SOA as the optical gate and light source

Since the broadband source had been proven redundant as a result of the ASE generated by the SOA, the previous experiment was repeated without the coupler and SLED. It was considered that removal of the coupler would reduce the total signal loss from the source to FBG and back to the SOA by over 6dB.

3.6.1 Circuit configuration and operation

The circuit configuration used is shown in Figure 3.10. The operation was similar to that of the previous experiment, but with the exception that the SOA provided the combined functions of the pulsed optical source and the optical gate.
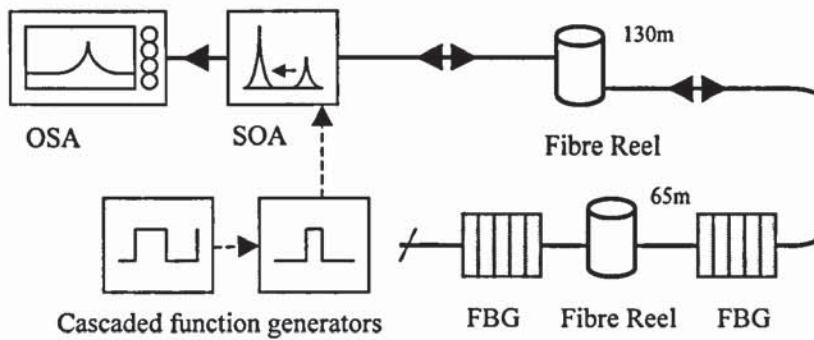
Figure 3.10 The equipment configuration that was used to access the SOA as an optical gate and a light source

3.6.2 Experimental results

Table 3.4 shows the optimum pulse repetition frequency for selection of each grating, while Figure 3.11 shows the combined recordings taken using the OSA for each of these settings. The peak optical signal power, the mean level of the background noise and the ratio of the two values were taken from the recordings and are shown in Table 3.5.

Fibre Bragg grating number	Central wavelength [nm]	Optical propagation period [μs]	Pulse repetition frequency [kHz]
1	1558.73	1.31	763.4
2	1559.63	1.97	507.6

Table 3.4 The optimum function generator settings for selection of the two FBGs
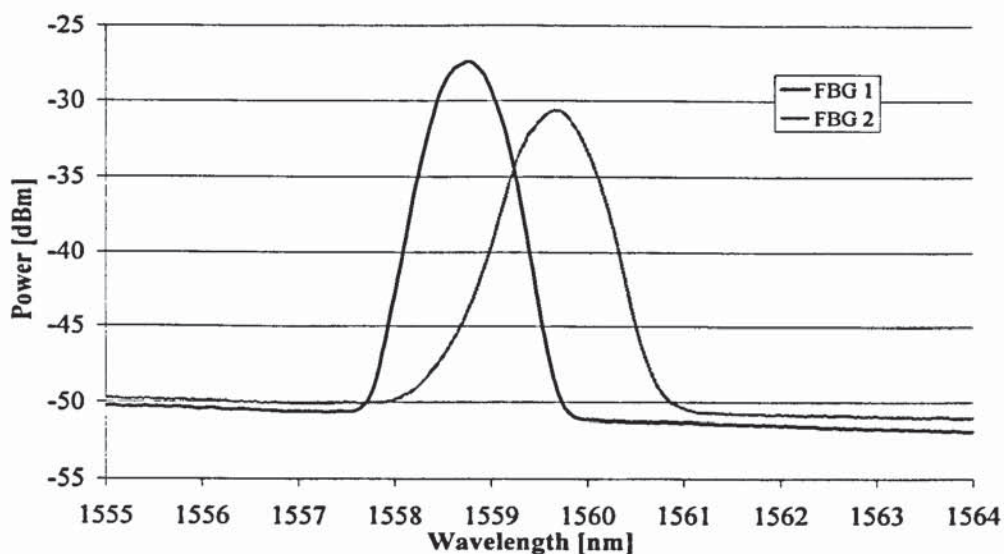
Figure 3.11 An overlay of OSA recordings taken of the signals received from each FBG when the SOA was used as both the gate and the light source

Fibre Bragg grating number	Peak optical signal power [dBm]	Mean background noise power [dBm]	Ratio of the values [dB]
1	-27.4	-51.3	23.9
2	-30.6	-50.8	20.2

Table 3.5 The parameters for the FBG signals (as taken from the OSA recordings)

3.6.3 Observations and conclusions

A clear observation from this experiment was that the removing of around 4m of optical path length (associated with the coupler and interconnecting patch cords) resulted in a higher optimum pulse repetition frequency setting for selection of each grating. Although this readjustment was predicted from the standard time-of-flight theory, it did highlight that whilst the TDM system was simple in concept, it would be potentially beneficial to invest time in developing a procedure or simple automation technique to reduce experimental adjustment time and make the optimisation more repeatable if further work were to be conducted in the future.

More directly this experiment proved that the SOA could be used as both the light source and the gate in a TDM sensor interrogation system. Removing the SLED and the coupler not only reduced the complexity of the optical circuit, it also demonstrated a reduction in cost, size and power consumption.

Reducing the 6dB optical circuit loss created by the coupler also showed an increase in the peak signal strength by >5dB and an improvement in the OSNR by >4dB, with little change in the signal shape. The small changes that occurred to the central wavelength were easily attributed to disturbance of the gratings during change of the experimental configuration.

Most importantly however, the thoughts and observations that occurred during this experiment led to the realisation that since ASE was emitted from both facets of the SOA there was probably no significant difference between the connections labelled 'input' and 'output' and that the SOA would likely operate connected in either direction. Experimentally connecting the SOA such that the ASE emitted from the 'output' facet illuminated the FBG sensors, and such that the gating and amplification of the resulting reflections occurred from 'output' to 'input' proved this hypothesis, as there was no significant difference in overall performance.

This realisation that the SOA was bi-directional led to the idea of adding a partial reflector to the optical circuit, between the SOA and the OSA, to attempt to return some of the signal normally delivered to the OSA, back into the SOA for re-circulation to the FBG sensors. The idea required the SOA to simultaneous amplify and gate in both directions, but if successful it was seen as a potential method of increasing the level of the signal used to illuminate the sensors.

3.7 Adding a broadband reflector to re-circulate the signal

This proposal of adding a partial reflector to re-circulate some of the signal back into the SOA was considered further and it was concluded that it should be possible to experimentally verify using a chirped FBG (CFBG) [7, 8, 9] as the reflector. It was decided that such a CFBG should be sufficiently broad to cover the operating wavelengths of the two sensor FBGs and have a reflectivity of at least 20%, but no more than about 95%. This was decided since lower reflectivity was likely to re-circulate little signal and a higher reflectivity would significantly limit the signal delivered to the OSA.

3.7.1 Circuit configuration and operation

The circuit configuration used is shown in Figure 3.12 and was similar to the previous experiment, except for the addition of a CFBG between the SOA and OSA. The actual grating used was broader and more reflective than was considered ideal, but this was the best that was available from the company spare stock. The parameters for this device are shown in Table 3.6.

Parameter	Typical value
Central wavelength	1544 nm
Bandwidth	45 nm
Reflectivity at central wavelength	≈95 %

Table 3.6 The parameters for the chirped FBG used as the broadband reflector in Figure 3.12
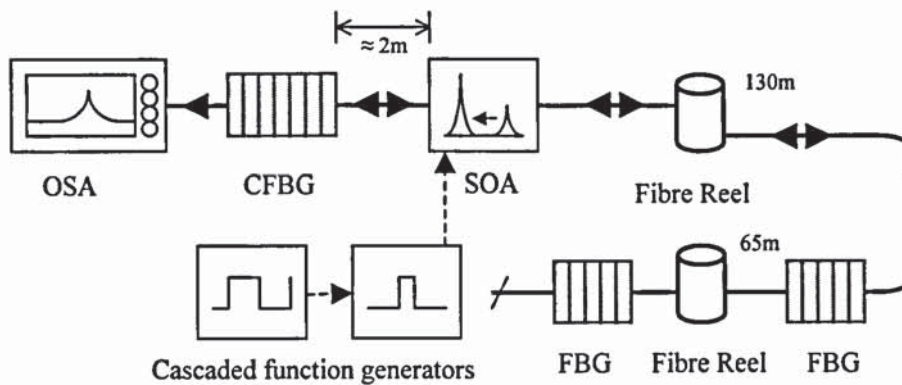
Figure 3.12 The equipment configuration that was used to access the effect of re-circulating some of the sensor signal

In this configuration any signal that was emitted from the SOA towards the OSA arrived at the CFBG broadband reflector. For wavelengths that were within the bandwidth of this grating, approximately 95% of signal was immediately reflected back towards the SOA, whilst the remaining 5% continued to propagate to the OSA. All wavelengths outside the bandwidth of the grating propagated directly into the OSA with minimal attenuation.

When considered starting from an idle state, the intended operating principle of the re-circulating circuit was as follows:

- An initial electrical pulse was output from the cascaded function generators and caused the turn 'on' of the SOA. This resulted in broadband optical emission of ASE from both facets of the device

- The ASE emitted from one facet (known as the front facet) immediately began propagation towards the FBG sensors via the 130m fibre reel

- The ASE emitted from the other (rear) facet began propagating towards the CFBG broadband reflector

- Around 10ns later, on reaching the reflector positioned 2m from the SOA, approximately 95% of the ASE with wavelength equal to bandwidth of the grating was reflected back towards the SOA, whilst the remainder continued towards the OSA

- A further 10ns later, the reflected signal that arrived back at the SOA was gated through and amplified. This occurred as the electrical drive pulse was ≈200ns long and so the SOA was still in the 'on' condition

- Now propagating from the front facet of SOA was a combination of the general ASE background and a raised stronger level of ASE equal to the bandwidth of the CFBG reflector

- This emission continued for ≈180ns until the SOA was returned to the 'off' condition at the end of the electrical drive pulse period

- A total optical pulse ≈40m in length therefore propagated towards, and was reflected from, each of the FBG sensors in a manner similar to that of previous experiments

- However, in contrast to previous experiments, when a reflection for a single sensor arrived back at the SOA (in synchronisation with the next electrical drive pulse), a different pattern of events occurred

- The signal was gated through the device and propagated towards the OSA, but around 95% of the signal, including the wavelengths equal to the sensor FBG profile were returned back to the SOA for further amplification

- The expected result was that the optical pulse that was then emitted from the front SOA facet would contain an even higher level of signal with wavelength equal to the single FBG sensor under interrogation and so provide an even stronger reflection during the next cycle

- The signal propagating through the reflector that arrived at the OSA would therefore contain a large portion of 'out-of-band' ASE beyond the lower and upper regions of the CFBG profile and a peaked signal equal to the profile of the grating under interrogation

- It was anticipated that by operating in this manner, using two passes of the SOA each time, an increasingly stronger level of sensor illumination would occur for each cycle of the system, until some maximum was reached

3.7.2 Experimental results

Figure 3.13 and Figure 3.14 show recordings taken with the OSA when the system was adjusted to deliver a signal from each of the FBGs. The peak optical signal power, the mean (non integrated) level of the background noise (within the bandwidth of the reflector) and the ratio of the two values were taken from these OSA recordings and are shown in Table 3.7.
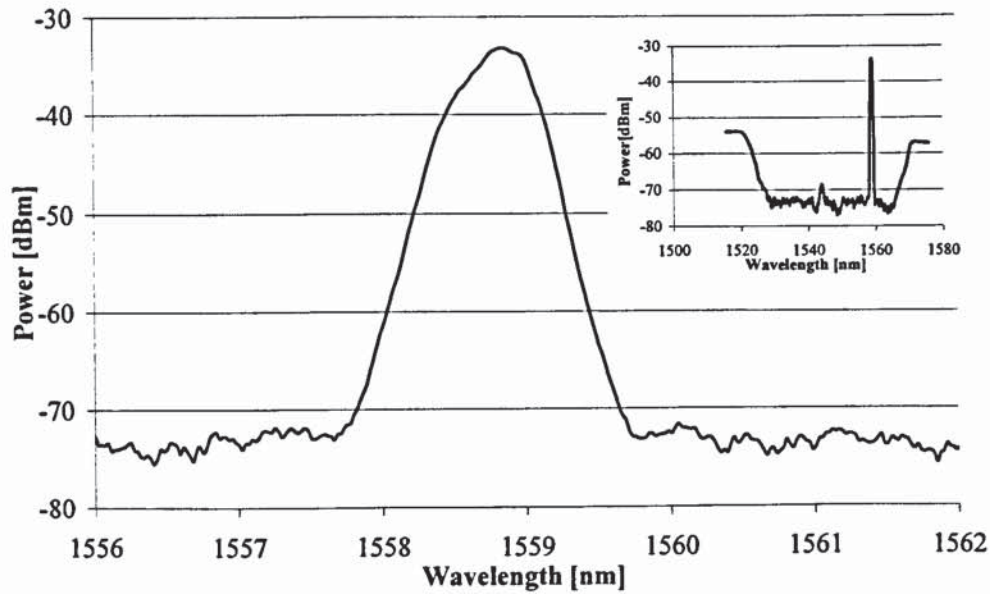
Figure 3.13 An OSA recording of the signal peak received when the re-circulating system was adjusted to FBG 1. The inset is a wider bandwidth view that also shows the effect of the CFBG reflector
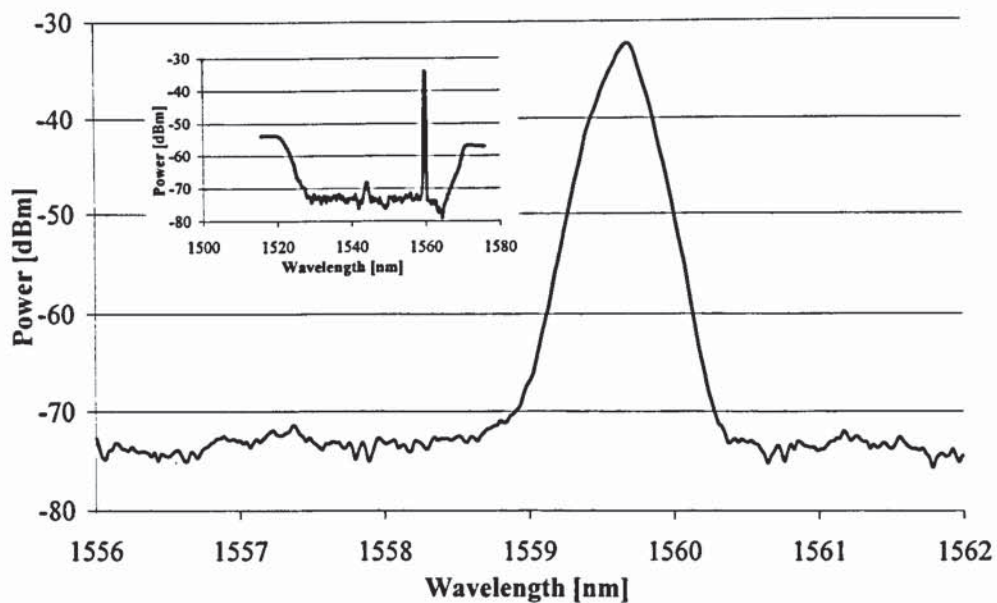
Figure 3.14 An OSA recording of the signal peak received when the re-circulating system was adjusted to FBG 2. The inset is a wider bandwidth view that also shows the effect of the reflector

Fibre Bragg grating number	Peak optical signal power [dBm]	Mean background noise power [dBm]	Ratio of the values [dB]
1	-33.1	-73.1	40.0
2	-32.5	-73.4	40.9

Table 3.7 The characteristics of the FBG signals (as taken from the OSA recordings)

Despite the high reflectivity, and therefore the effective high insertion loss, of the reflector the peak signal received by the OSA was still -33dBm, whilst the optical signal to background noise ratio (OSNR) had increased substantially to >40dB. This is an exceptionally high figure.

A further observation made whilst adjusting the system and taking these measurements was that the level of the 'out-of-band' ASE (i.e. the ASE beyond the bandwidth of the CFBG reflector) fell significantly when the pulse repetition period was successfully tuned to interrogate a sensor, but rose again when tuned to lie between sensors.

Figure 3.15 shows a plot of the variation in the level of 'out-of-band' ASE as a function of the repetition period, when the system was tuned around the optimum location for the first FBG sensor.
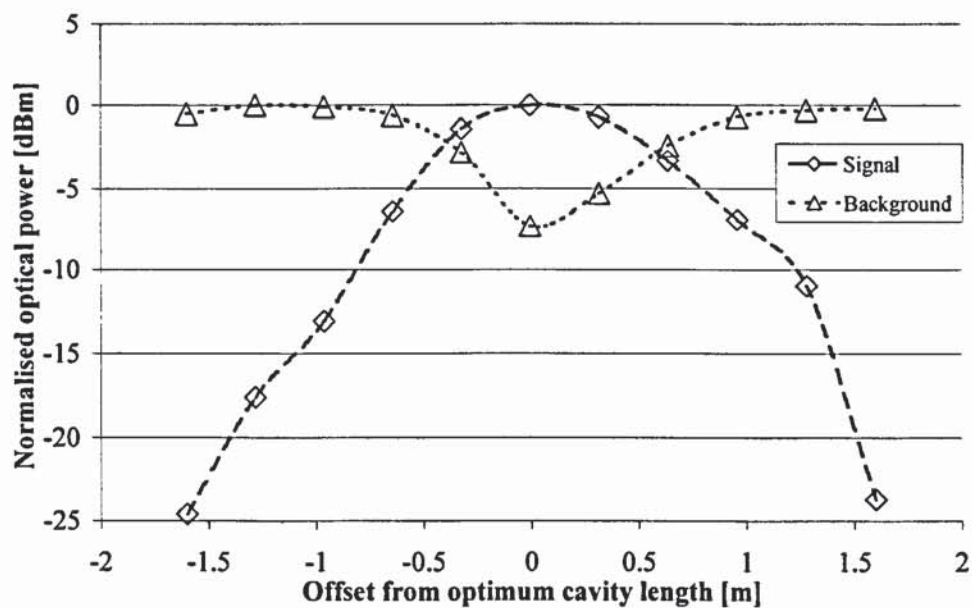
Figure 3.15 The variation in the 'out-of-band' ASE as the system was tuned around the optimum repetition period for FBG sensor 1

3.7.3 Conclusions

This experiment showed that adding a reflector to the optical circuit and using the SOA bi-directionally in a cyclic system provided an extremely significant increase in performance. Compared to the non-cyclic case the average signal power delivered to the OSA only decreased by ≈5dB, whilst the OSNR increased by >16dB. It was also expected that a more optimum (lower) level of reflectivity from the CFBG would

maintain the exceptional cyclic performance, whilst increasing the 'output' signal delivered to the OSA.

Another equally important conclusion was the beneficial effect of a reduction in the SOA generated ASE 'background' signal when the system was correctly tuned to a sensor. This was a result of the SOA power being focused into the amplification of the required sensor signal, so reducing the population inversion within the device and limiting the chance of spontaneous emission [6]. This characteristic of SOAs was therefore found to have an overall advantage of further increasing the OSNR performance.

Finally, in conclusion, though the experiment was very simple and conducted with only basic lab equipment and FBGs from spare stock it was clearly apparent that using a switched SOA in a cyclic configuration was a truly novel approach that provided a TDM interrogation technique with exceptional performance. This new configuration was therefore named the 'resonant cavity' architecture as it operated by creating a virtual laser-like cavity between the broadband (rear) CFBG reflector and (an easily selectable) FBG sensor via the switched SOA gain medium, such that the optical sensor signal could by considered to cycle or resonate.

3.8 Removing the 'out-of-band' ASE using a coupler

Despite the many extremely positive results of the first cyclic system experiment, a couple of disadvantages existed regarding extraction of the cavity signal 'through' the rear reflector. Though the total number of components was very low, the configuration resulted in the delivery of all out-of-band ASE into the measurement instrument (i.e. all wavelengths beyond the bandwidth of the CFBG reflector). Whilst this was of no consequence for correct identification of the sensor signal using the OSA, it did not allow the use of other wavelength detection instruments (such as the Burleigh wavemeter) or the possible use of passive (ratiometric) techniques [10, 11, 12, 13].

A further disadvantage of extracting the signal through the rear reflector was the requirement for a CFBG with an intermediate level of reflectivity and ideally a low level of ripple across the grating profile. Although it is not impossible to achieve this, the cost to manufacture such a device was known to be greater than that of manufacturing a device with a very high >98% reflectivity.

89

For these reasons an attempt was made to extract the cavity signal as it was reflected off, rather than through, the rear reflector.

3.8.1 Circuit configuration

The circuit configuration used is shown in Figure 3.16, with the details of the new higher reflectivity, narrower reflector shown in Table 3.8. The layout was similar to the previous experiment, but with the addition of the coupler between the reflector and SOA. The coupler was a fused fibre device with a transfer ratio of 10% / 90%. The position of the connection to the OSA was moved to receive the output that was extracted using the 10% tapping, in order to allow the majority of the signal (90%) to remain in the cavity. Otherwise, the principle of operation of the system was the same as for the previous experiment.

Note that the notation used to identify the tap ratio for each arm of the fibre coupler is in accordance with that typically used by coupler manufacturers and is labelled with respect to the signal propagating (bi-directionally) in the cavity.
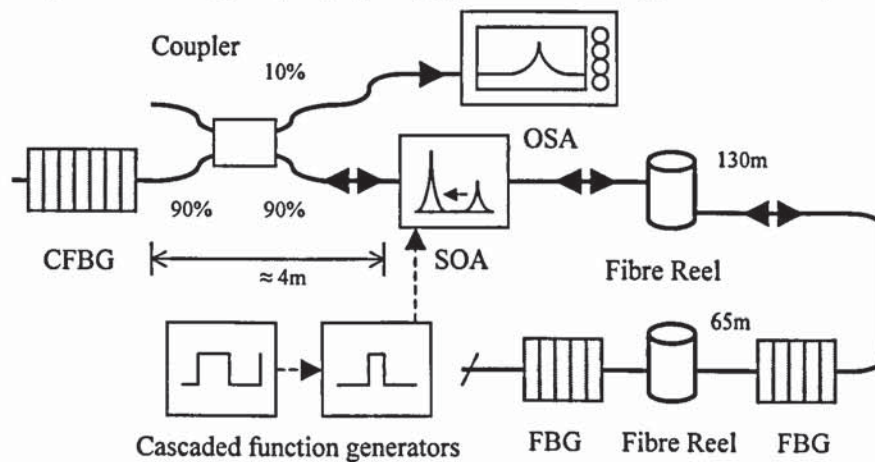
Figure 3.16 The equipment configuration that was used to access the removal of 'out-of-band' ASE by the addition of a fibre coupler

Parameter	Typical value
Central wavelength	1550.5 nm
Bandwidth	19 nm
Reflectivity at central wavelength	>99 %

Table 3.8 The parameters for the narrower, higher reflectivity CFBG used as the broadband reflector in Figure 3.16

3.8.2 Experimental results

Figure 3.17 shows a recording taken using the OSA when the pulse repetition period was adjusted to establish a virtual cavity between the rear reflector CFBG and the first FBG sensor. Table 3.9 shows the key characteristics of this signal.
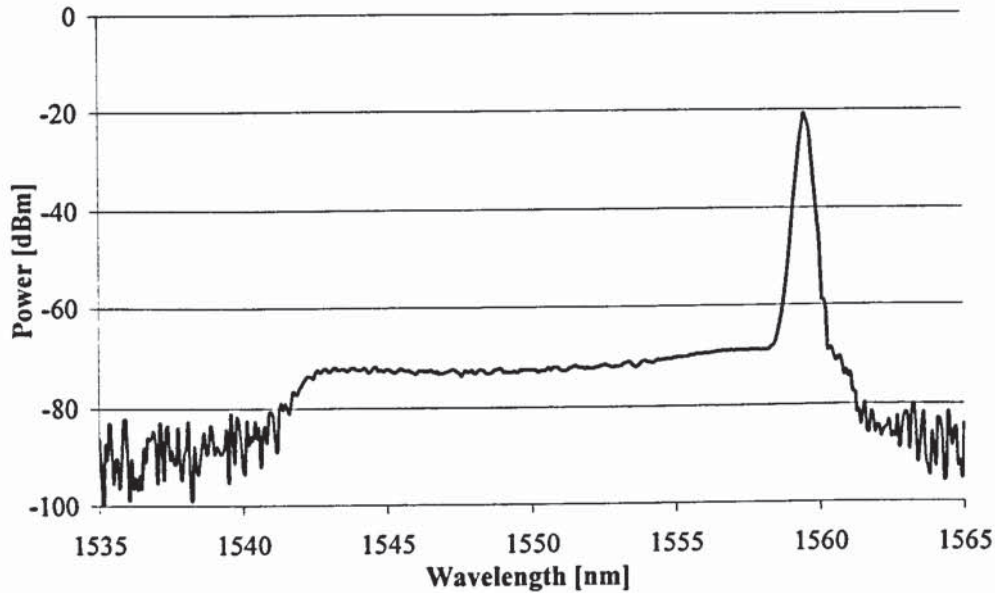
Figure 3.17 An OSA recording of the signal received from FBG 1 for the configuration that provided greatly reduced 'out-of-band' ASE. The OSA noise floor was −90dB

Bandwidth of background [nm]	Peak optical signal power [dBm]	Mean background noise power [dBm]	Ratio of the values [dB]
20	-20.7	-72.0	51.3

Table 3.9 The characteristics of the FBG signal (as taken from the OSA recording)

3.8.3 Observations and conclusions

The results proved that by extracting the cavity signal as it was reflected from the rear CFBG (using a coupler) the bandwidth of the ASE (noise) was limited to the bandwidth of the reflector. This factor alone provided an effective increase in total OSNR.

Most importantly however, by reducing the reflector width, the peak signal increased by a further 12dB, while the peak to background ratio increased to an extremely high value of 51.3dB. It was concluded that by limiting the background noise that the SOA was required to amplify the device could focus on amplification of the required peak and also reduce the unwanted ASE background that it generated.

91

It was deemed that these two results would be extremely significant if a situation arose where the resonant cavity architecture was used with a passive ratiometric detection scheme [10, 12].

This new optical circuit configuration also had the advantage that the level of signal extraction could be easily chosen by changing the coupler transfer ratio. Since no signal was extracted from beyond the rear reflector this component could be made $\approx$100% reflective, significantly easing the manufacture process and allowing an inherently lower reflection ripple. Unfortunately, there was a disadvantage with this configuration, which was the increase in optical path length from the SOA to the rear reflector due to insertion of the coupler. This increased length caused an increase in the 'dead time' and some consequential reduction in OSNR. The 'dead time' was the name given to the time period when the SOA was first turned 'on', when the signal emitted from its front facet contained only ASE and none of the amplified cycling signal. This was because the cycling signal was not emitted until the returning reflection had been gated through the SOA, had travelled to the rear reflector and returned to the SOA. Increasing the distance from the SOA to the reflector increased this transit time. The greater the ratio of the 'dead time' ASE noise compared to the total optical signal, the lower the effective OSNR.

In this experimental set-up the path length between the SOA and rear reflector was approximately 4 metres (due to the available patch cords and coupler), which resulted in an estimated 'dead time' of $\approx$40ns. This was insignificant in the experiment due to the large $\approx$200ns optical pulses that were used, but was thought to be inappropriate for a practical system that employed shorter pulses and closer spaced gratings. Fortunately however, it was considered that by fusion splicing all fibre joints the total path length from an SOA to a CFBG reflector via a fused fibre coupler could be less than 50cm, which was more acceptable.

3.9 Moving the coupler to the 'front' of the SOA

Extracting the cavity signal using a coupler placed at the front of the SOA was also investigated. It was anticipated that this would have the advantage of higher signal level (due to the extra amplification pass of the SOA), but would be disadvantaged by the presence of ASE noise across the full bandwidth of the device.

3.9.1 Circuit configuration and operation

The circuit configuration used is shown in Figure 3.18. This was similar to previous configurations, but with the coupler positioned at the front facet of the SOA. The principle of operation was the same as for the previous experiment.
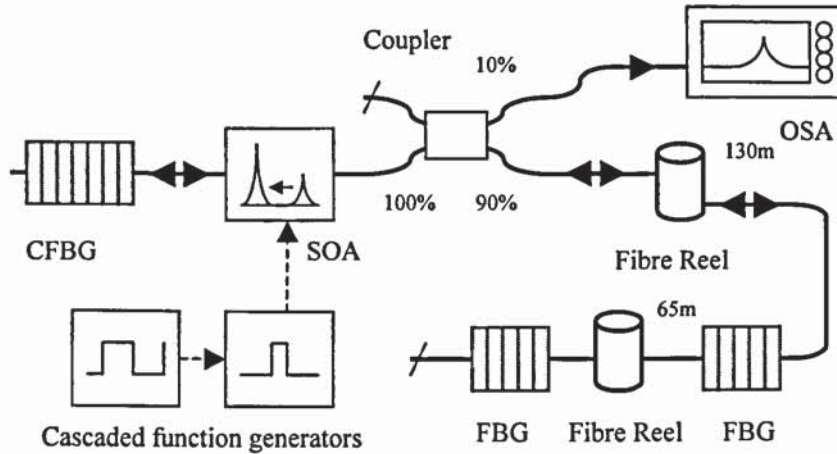
Figure 3.18 The equipment configuration that was used to extract the signal from the 'front' of the SOA

3.9.2 Experimental results

Figure 3.19 shows a recording taken using the OSA when a virtual cavity was established between the rear reflector CFBG and the first FBG sensor. Table 3.10 shows a comparison between the optical signals obtained with this configuration and those taken with the previous coupler position of Figure 3.16.
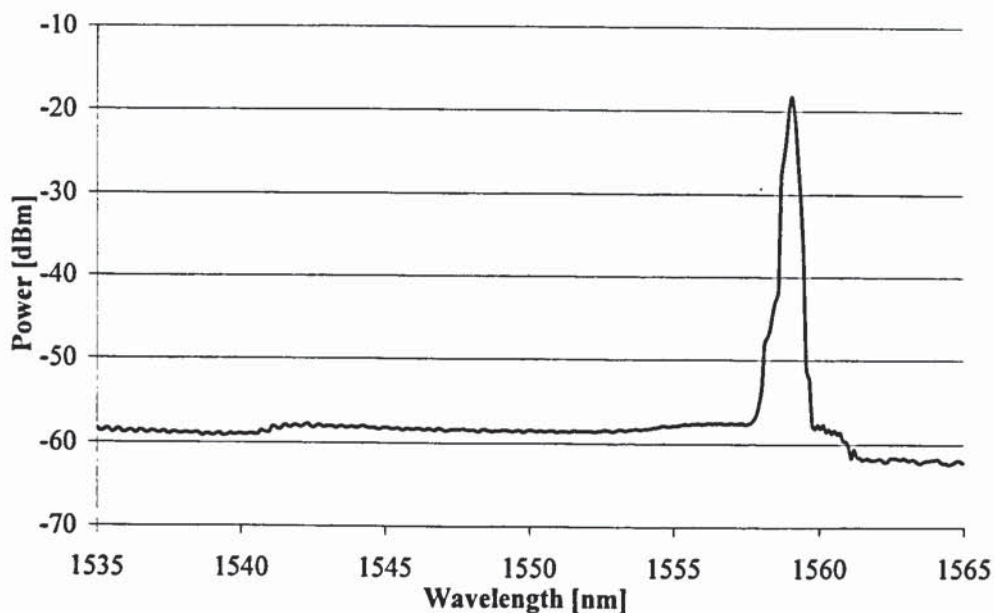
Figure 3.19 An OSA recording of the signal extracted from the 'front' of the SOA when the system was tuned for resonance with FBG 1

93

Optical configuration	Cavity signal is extracted from	ASE noise bandwidth	Mean ASE noise level	Peak signal level	OSNR near peak
Figure 3.16	Rear reflector	20 nm	-72.0 dBm	-20.7 dBm	51.3 dB
Figure 3.18	Front of SOA	>60nm	-58.0 dBm	-18.3 dBm	39.7 dB

Table 3.10 A comparison between the signals reflected from the rear reflector and the 'front' of the SOA

3.9.3 Observations and conclusions

As expected the results for this experiment showed that the peak signal level was higher and that the ASE noise extended for the full bandwidth of the SOA device. But the results also showed that the increase in ASE noise level was greater than the increase in signal level, causing a reduction in the (peak to background) OSNR, when compared to the cavity signal extracted in the previous circuit configuration.

Most importantly, if account was taken of the total integrated power of the signal and total integrated power of the ASE noise and the ratio of these values calculated, then the true OSNR was now significantly lower than for the previous configuration.

It was considered that as this new configuration provided a higher signal output power but greater ASE noise it was most suitable for use with spectrometer and scanning filter based wavelength detection schemes that are naturally bandwidth limited [14, 15, 16, 17, 18], while the previous arrangement was more suitable for ratiometric detection.

3.10 Extracting the signal reflected from the sensors

Finally, brief consideration was given to the benefit of rotating the coupler in the cavity (which was the same as effectively repositioning the OSA to the other coupler arm, since the coupler was reversible) so as to extract the signal as it was directly reflected from the sensors, rather than after it had passed through the SOA.

It was considered that, whilst this arrangement would effectively circumvent the optical gating effect of the SOA, a hypothesis was made that due to the resonant cavity architecture and the natural reduction in ASE generated by the SOA (in the presence of the strong cycling sensor signal) the interference of other sensors may not be too significant for, for example, a WDM based system that used the resonant cavity architecture as a method to extract a strong signal from a single sensor at a time.

3.10.1 Circuit configuration and operation

The circuit configuration used is shown in Figure 3.20. This had the same arrangement and mode of operation as the previous configuration except for the rotation of the coupler.
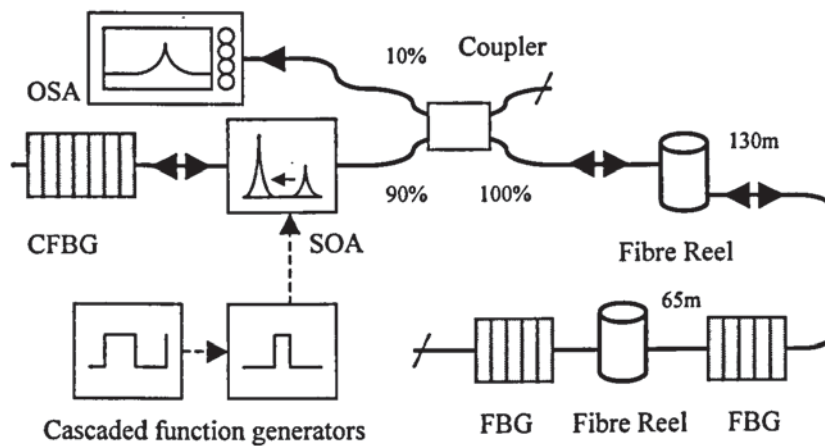
Figure 3.20 The equipment configuration that was used to extract the cavity signals as they were reflected directly from the sensors

3.10.2 Experimental results and observations

Figure 3.21 and Figure 3.22 show recordings taken with the OSA when a virtual cavity was established between the rear reflector and each of the sensor FBGs. Table 3.11 shows measurements (taken from these recordings) of the peak level of the required resonant cavity 'signal', the interfering 'noise' from the other sensor and the ratio of the two values.
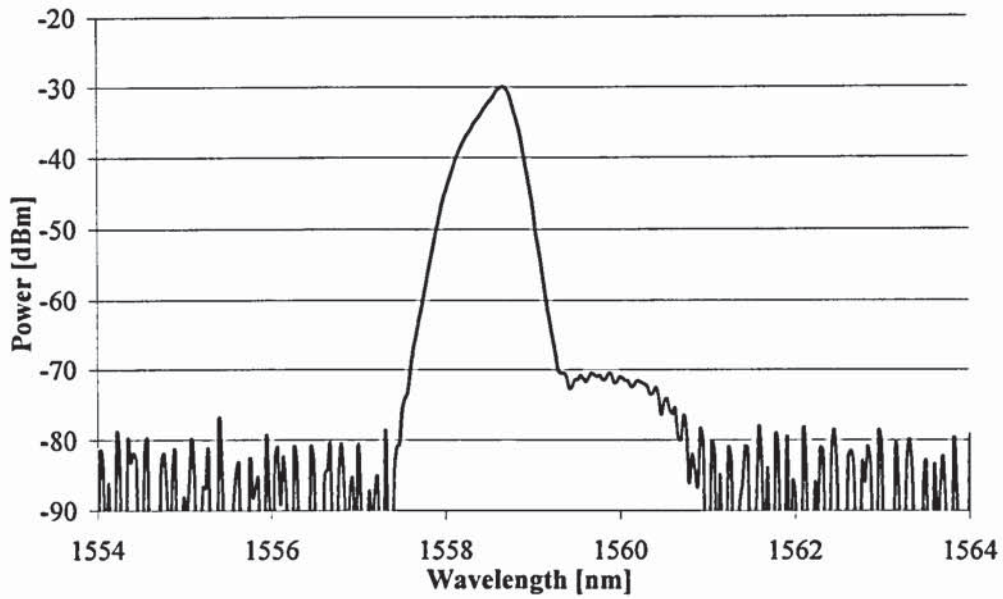
Figure 3.21 An OSA recording of the signal reflected directly from the sensors. The system was tuned for resonance with FBG 1, but interference from FBG 2 is visible
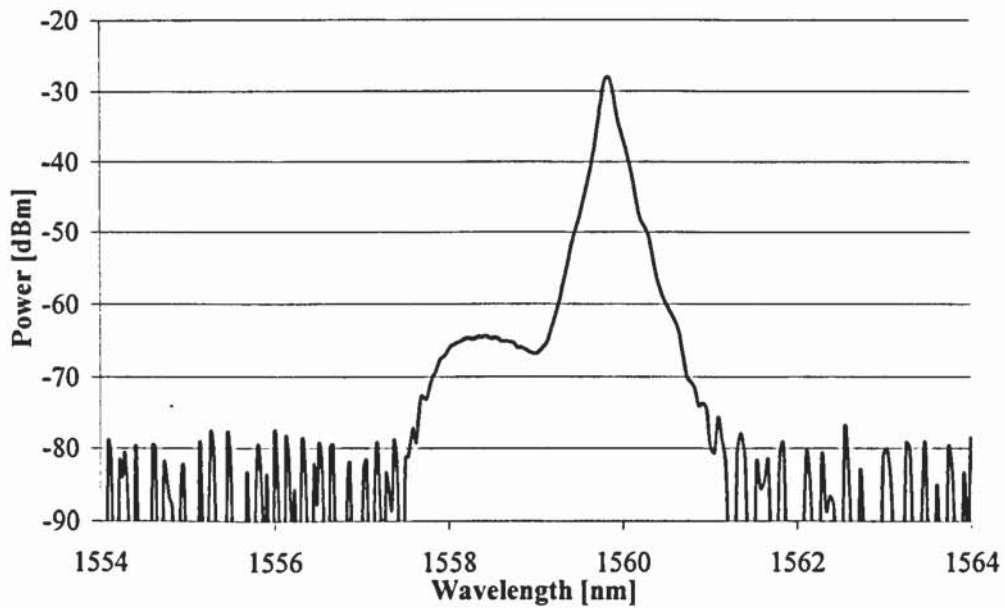
Figure 3.22 An OSA recording of the signal reflected directly from the sensors. The system was tuned for resonance with FBG 2, but interference from FBG 1 is visible

Virtual cavity created with sensor	Level of required sensor (signal)	Level of interfering sensor (noise)	Ratio of these values (OSNR)
1	-30 dBm	-70 dBm	40 dB
2	-28 dBm	-64 dBm	36 dB

Table 3.11 The level of the required and interfering signals, as measured from the OSA recordings

An observation from this experiment was that when the pulse repetition period was adjusted such that no virtual cavity was established (i.e. the period did not match the optimum value for either sensor) the ASE emitted by the SOA was broad and approximately flat, such that both sensors were equally illuminated. With this setting the configuration was essentially behaving as a standard WDM system [4].

3.10.3 Conclusions

It was concluded that this configuration could have significant practical application in a WDM interrogation system that used any wavelength detection scheme that was only able to operate with the reception of a single grating signal at a time. Using this variation of the resonant cavity architecture provided a method of extracting a strong signal from a single sensor, rather than equal (lower) strength signals from all sensors.

Additionally, whilst it was expected that the OSNR would decrease as additional sensors were added to the system, the results of Table 3.11 showed that the true integrated OSNR for a low sensor count system was far higher than for all previous optical circuit configurations. This was due to the removal of the majority of the ASE background noise; only the ASE within the bandwidth of the interfering sensor was present.

3.11 Practical TDM using low reflectivity sensors

Whilst the initial experiments established that the resonant cavity architecture provided the potential for optically gated TDM sensor interrogation, it was known that a practical system would require the use of low reflectivity, narrow bandwidth sensors if wavelength shadowing and 3-reflection crosstalk were to be kept at acceptable levels [19, 20, 21]. Therefore, two FBG sensors were manufactured with nominally equal wavelengths and lower reflectivity to quickly determine if the system would still operate.

Reducing the sensor reflectivity caused a reduction in the level of the reflection signal. This was expected to have a similar effect to that of increasing the optical loss in the virtual cavity. A variable attenuator was therefore also added to the configuration to allow controlled adjustment of the cavity loss to further evaluate performance.

3.11.1 Circuit configuration and operation

Prior to inserting the attenuator, the optical configuration used was similar to the previous arrangement of Figure 3.16. The configuration that included an Agilent 8156A variable optical attenuator is shown in Figure 3.23. In both configurations lower reflectivity sensor FBGs were used, the key properties of which are provided in Table 3.12.
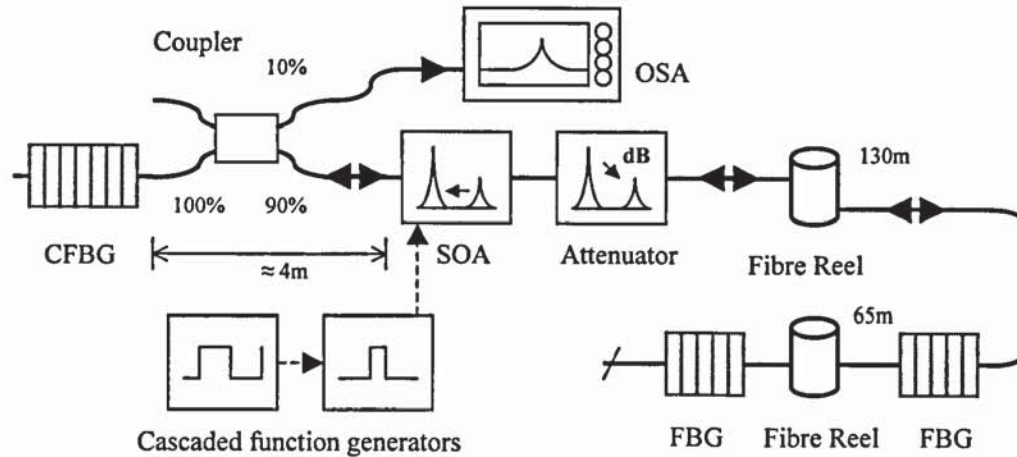
Figure 3.23 The equipment configuration that was used to access the feasibility of using low reflectivity FBG sensors in the resonant cavity architecture

Fibre Bragg grating number	Central wavelength [nm]	Reflectivity at central wavelength [%]	FWHM bandwidth [pm]
1	1553.6	4	180
2	1553.4	4	185

Table 3.12 The parameters for the lower reflectivity FBG sensors used in Figure 3.23

3.11.2 Experimental results

Figure 3.24 shows a recording taken with the OSA when a virtual cavity was established between the rear reflector and the first sensor, before the optical attenuator was inserted into the circuit. Figure 3.25 shows a plot of the change in peak signal, background ASE noise level and the ratio of these two values, before the attenuator was inserted (0dB value) and when the attenuator was inserted and adjusted through a range of values. The minimum level that could be created by the attenuator was calibrated using the SLED source and a power meter and was found to be 3.8dB.
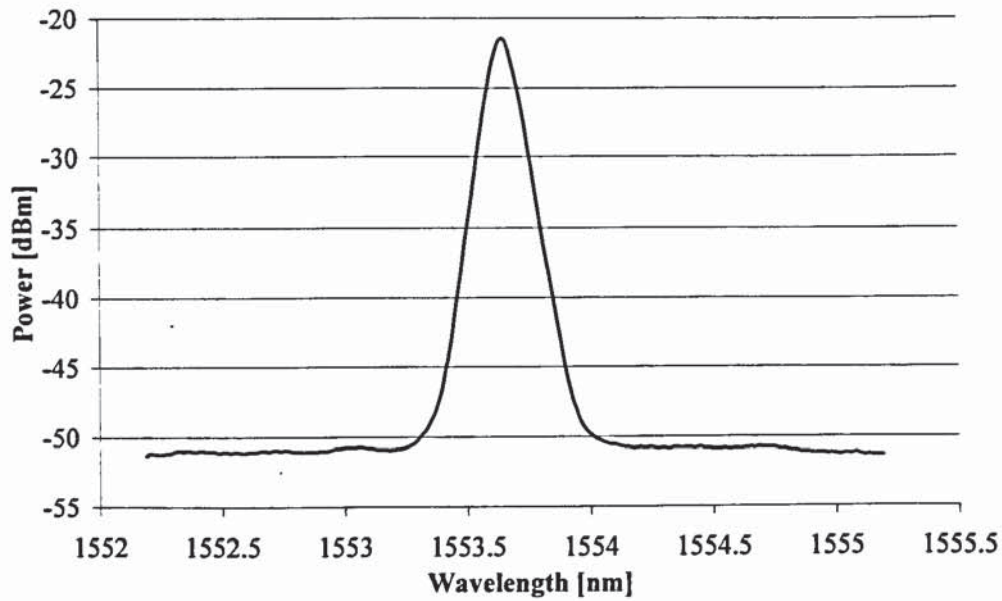
Figure 3.24 An OSA recording of the signal from FBG 1 without the attenuator in place
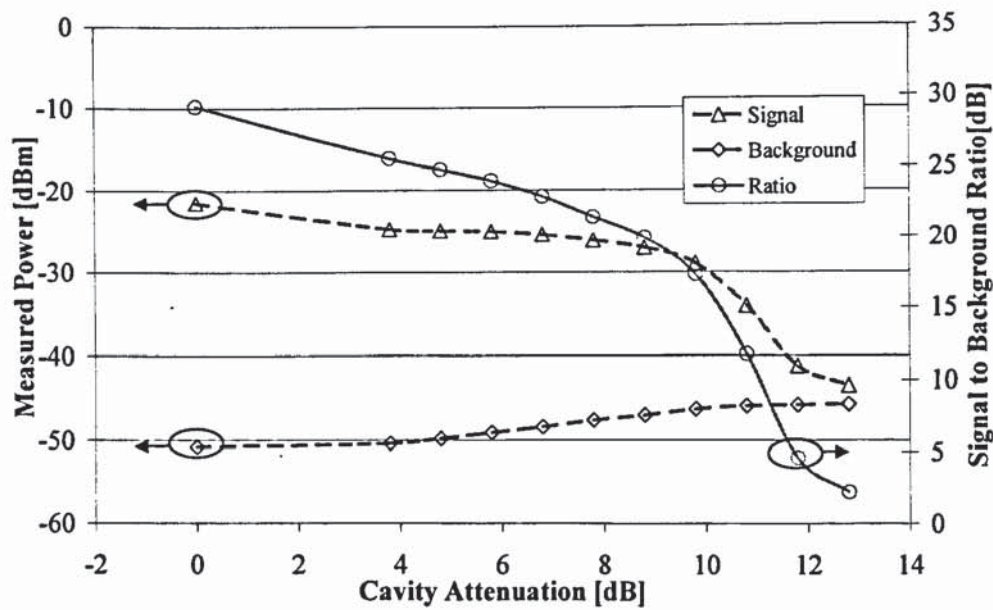
Figure 3.25 The change in the peak signal and the background ASE noise for low reflectivity FBG sensor 1 when varying levels of attenuation were added to the cavity

3.11.3 Conclusions

The results showed that although the peak level and the signal-to-ASE-background ratio were both significantly reduced as a result of using lower reflectivity sensors, a resonant cavity could still be achieved until the attenuator reached 13dB. As an attenuator setting of 3dB could be considered as creating a total cavity loss of 6dB (due to the bi-directional dual pass of the instrument) this was considered the equivalent of having a cavity with no added loss, but with a sensor grating reflectivity reduced by a

99

further factor of ~4. A value of 13dB therefore represented possible operation with very low reflectivity sensors (<<1%).

In conclusion, it was considered that the resonant cavity architecture appeared capable of providing optically-gated time-division-multiplexing of Bragg grating sensors that were of sufficiently low reflectivity that they should not suffer significant wavelength shadowing or 3-reflection crosstalk [19, 20, 21].

3.12 Basic evaluation of grating shadowing and crosstalk

Having proved that the resonant cavity architecture was compatible with low reflectivity sensors, a theoretical and experimental appreciation of the numerical level of wavelength-shadowing induced crosstalk was considered beneficial.

A basic mathematical model was developed, which assumed that the SOA acted as a pure, linear amplifier and that each of the FBGs in the architecture modified the optical cavity signal according to the ideal transmission and reflection profiles provided by the Optiwave IFO software package that was used to design them. Functions were added to the basic model to adjust the number of cavity cycles that the optical signal experienced, the system gain and loss and the reflectivity of each grating. An animation section was also developed to allow automatic plotting of the effect of varying the wavelength overlap between cavity sensors.

Although based on many assumptions and simplifications, the final software was considered valuable since it provided the ability to investigate the effect of using FBGs with different profiles or reflectivity and provided some appreciation of the likely shape and response of the cavity signal.

Having used the model to assess a range of possible sensor profiles some FBG arrays were then also produced to allow actual experimental measurement of the crosstalk.

3.12.1 Methodology

The basic mathematical model used to predict the form and level of wavelength-shadowing induced crosstalk was developed using National Instruments' LabVIEW and is shown in Figure 3.26. Operation of this software was as follows:

- First a standard grating design package (Optiwave IFO) was used to create data files of the theoretical transmission and reflection profiles of the sensors to be modelled. For this step the exact reflectivity of the profiles was largely unimportant

- These data files were then loaded into the LabVIEW model

- Modification of the effective reflectivity of the profiles used in the modelling was then possible using simple controls to allow easy evaluation of the effects of crosstalk from devices of different reflectivity

- System gain and loss were also modelled and adjusted in a similar manner

- The number of cycles of the signal in the cavity and the effect of the transmitted signal after each cycle was then also adjustable using various controls and could be plotted using visual charts

- Calculation of the peak and central wavelength of the cavity signal after each cycle was then carried out by the software to provide a plot of the cycling induced profile error

- Animation of these results (as the wavelength offset between sensors was adjusted) then produced plots of crosstalk as a function of both wavelength-separation and sensor bandwidth
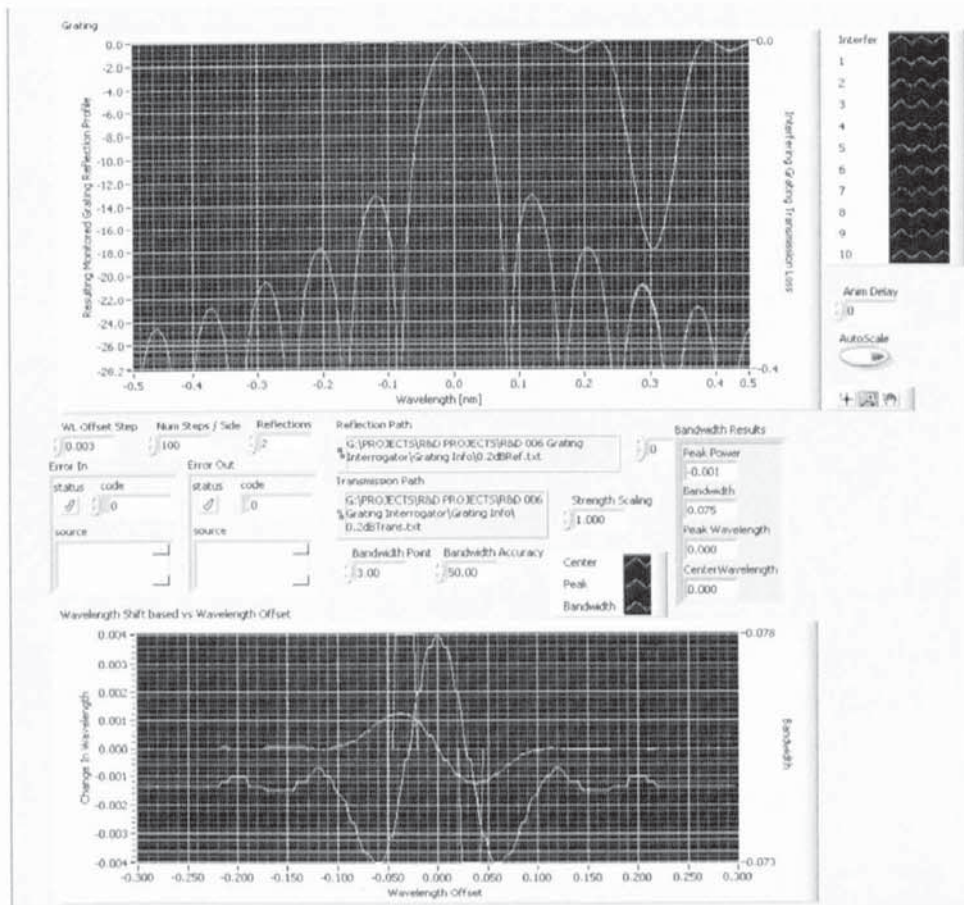
Figure 3.26 A screen snapshot of the animated model that was developed and used to predict the form and extent of wavelength-shadowing induced crosstalk

Figure 3.27 shows the optical circuit configuration that was used to experimentally determine the level of interaction that actually occurred between sensors. It can be seen that in this experiment an improved pulse generator was used. This device was able to deliver very short high-power SOA drive pulses that allowed the sensors to be spaced at just 2m intervals. The full design details for this circuit are discussed in chapter 4, but its principle of operation can be considered as being the same as for previous configurations.

To improve confidence in the results, two different FBG sensor arrays were evaluated; the first had sensors that were ~4% reflective with 300pm FWHM bandwidth, while those in the second array were also ~4%, but had only 75pm bandwidth. In each case the FBGs were temperature tuned by up to $60°C$ (with an accuracy of $\approx 1°C$) by thermo-electric coolers (TECs). To evaluate the crosstalk the wavelength of sensor 1 was tuned across the spectral range of sensor 2, whist the central wavelength of the resonant signal from each sensor was measured with the OSA and recorded.
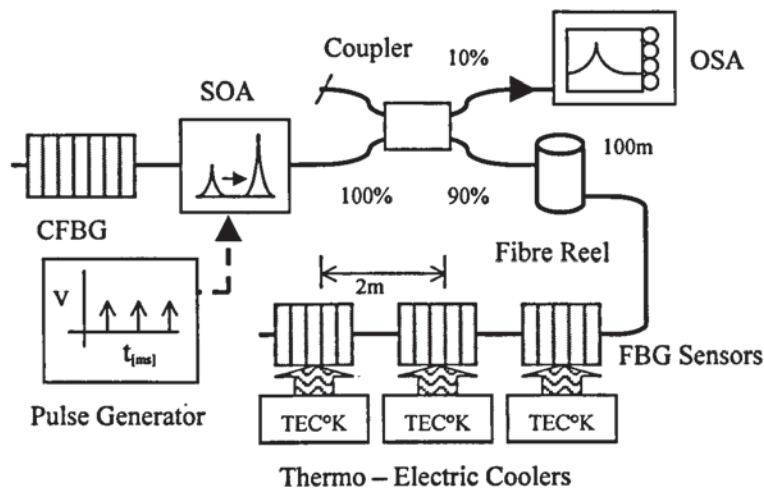
Figure 3.27 The equipment configuration that was used to experimentally measure the extent of wavelength-shadowing induced crosstalk

3.12.2 Results and observations

Figure 3.28 and Figure 3.29 show the experimentally obtained results for the 300pm and 75pm bandwidth FBGs respectively.
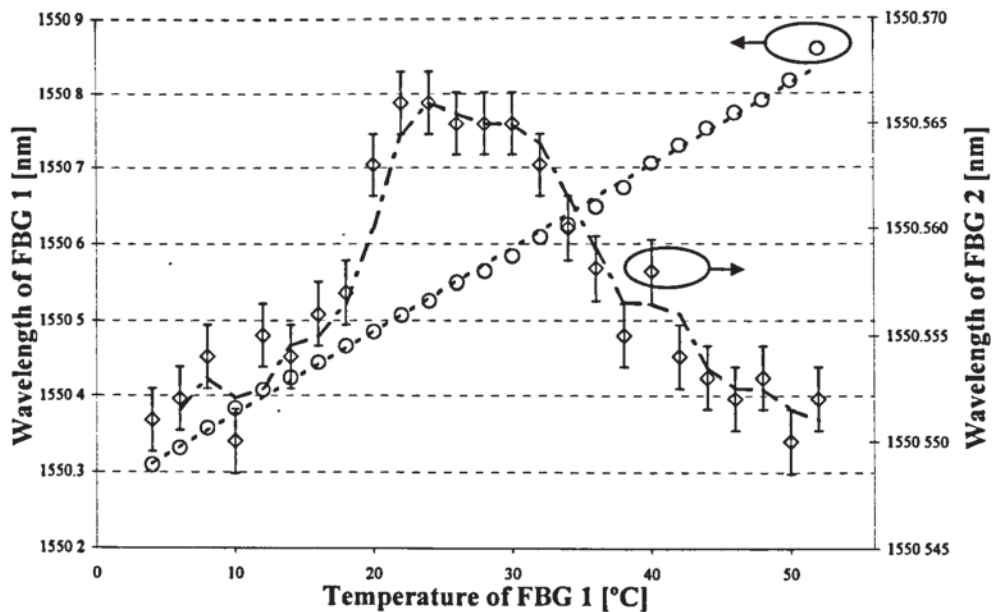
Figure 3.28 The results of experimental evaluation of wavelength-shadowing induced crosstalk for FBG sensors of 300pm bandwidth
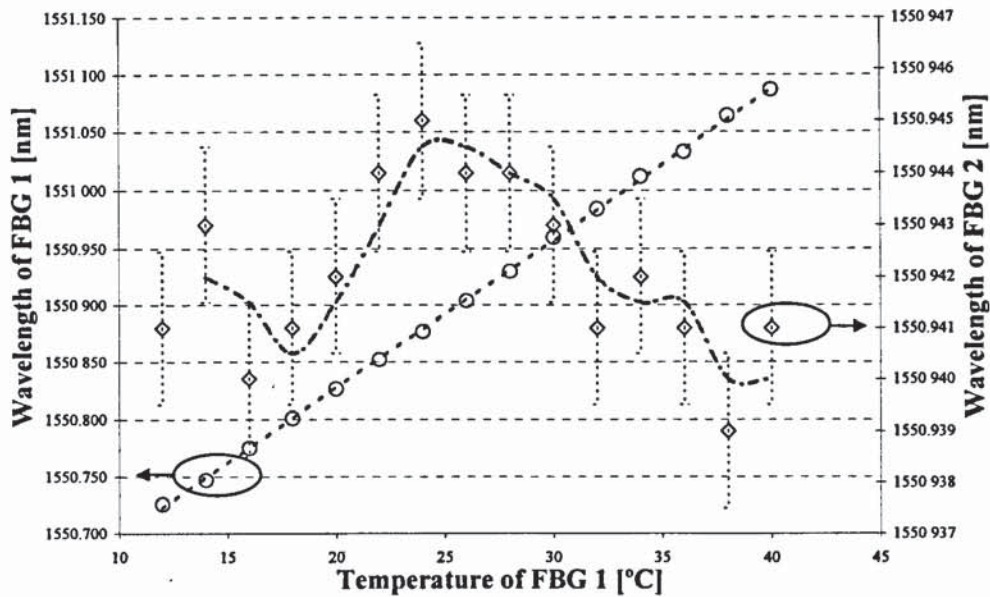
Figure 3.29 The results of experimental evaluation of wavelength-shadowing induced crosstalk for FBG sensors of 75pm bandwidth

The error-bars indicate that exact central wavelength measurement was difficult using the OSA due to its wide (50pm) filter window, while the limited range achieved by temperature tuning also reduced the full effectiveness of the experiment. For the broader gratings only the basic central peak could be recorded, but for the narrower gratings the tuning range was sufficient to suggest that the shape of the crosstalk-induced shift was approximately a 'sinc' like function.

This shape was favourable with the mathematical modelling of the two overlapping Gaussian FBG profiles, but the magnitude was found to be slightly larger than the basic modelling had predicted. Table 3.13 shows the experimental and modelled shifts and the error between them for both grating profiles.

Sensor grating 3dB bandwidth	Modelled peak-peak wavelength shift	Experimental peak-peak wavelength shift	Difference between values
75pm	3.8 pm	≈5 pm	1.2 pm
300pm	15.2 pm	≈16 pm	0.8 pm

Table 3.13 The experimental and modelled levels of wavelength-shadowing induced crosstalk for the two bandwidths of FBG sensor

An further observation from the experiment, which was in reasonable agreement with the modelling, was that the main reason for an effective shift in central wavelength was as a consequence of a change in the signal profile shape; rather than a complete shift in the profile, the shadowing caused a reduction in strength to one side of the signal only,

104

which created an asymmetry. Since this asymmetry was most apparent near the peak, but of less significance ~5dB down, it was concluded that using a curve fitting technique could remove the shadowing effect and reconstruct the original signal, and so reduce the total measured crosstalk.

3.12.3 Conclusions

The experimental results showed that although a small level of wavelength-shadowing induced crosstalk did occur when using low reflectivity sensors, the directly measured magnitude for the narrow sensors was acceptable for most practical systems; shadowing effects of <10pm for a system designed for a >10nm range equated to <0.1% error.

Additionally, due to asymmetric nature of the crosstalk, it was concluded that mathematical curve fit correction could probably be developed to reduce this measured magnitude still further, if required.

A further conclusion of the experiment was that as a small discrepancy did exist between the experimentally measured and mathematically modelled results, perhaps a greater understanding of the internal dynamics of the resonant architecture would be required if a better model was to be produced.

3.13 Basic evaluation of cavity signal evolution

After further consideration regarding the reason for some discrepancy between the basic modelled results and the experimentally measured system, a decision was taken investigate the evolution of the cavity signal from its initial phase as a flat broadband ASE pulse, through to a strong and narrow laser-like peak. A hypothesis was made that for each cycle of the system the signal would become stronger and narrower until equilibrium was reached. It was proposed that this evolution would be mathematically related to the repeated self-convolution of the sensor grating profile.

3.13.1 Experimental configuration

The experimental set up used is shown in Figure 3.30. The optical configuration included a single low reflectivity sensor and was similar to many previous arrangements. The pulse generator, however, was specially developed for this experiment. The detailed design of this device is discussed in chapter 4, but an outline

of its mode of operation is given in Figure 3.31 and its use in the experimental procedure was as follows:

- The pulse generator configuration was controlled from a PC via an Ethernet connection

- The pulse repetition period of the generator was initially configured to cause cyclic cavity resonance with the single FBG sensor in the usual way

- The generator configuration was then changed so that instead of delivering a continuous chain of pulses, it failed to deliver every other pulse.

- When a pulse was not delivered to the SOA the device remained in the 'off' condition and provided attenuation of >50dB. Any reflections that return to the SOA in this condition were therefore fully blocked and absorbed from the system

- In such a condition the OSA was used to record the cavity signal, which did not contain any cycling pulses

- The pulse generator was then re-adjusted to deliver two correctly timed pulses and to miss every third pulse

- Again, the OSA was used to record the cavity signal, which then contained pulses that had cycled once in the system

- The generator was repeatedly re-adjusted in this manner to deliver an incrementally greater number of cycling pulses before missing an output and stopping the cyclic action

- For each re-adjustment of the generator, the OSA was used to record the cavity signal

- The process was repeated until no significant change was seen in the OSA recordings

106
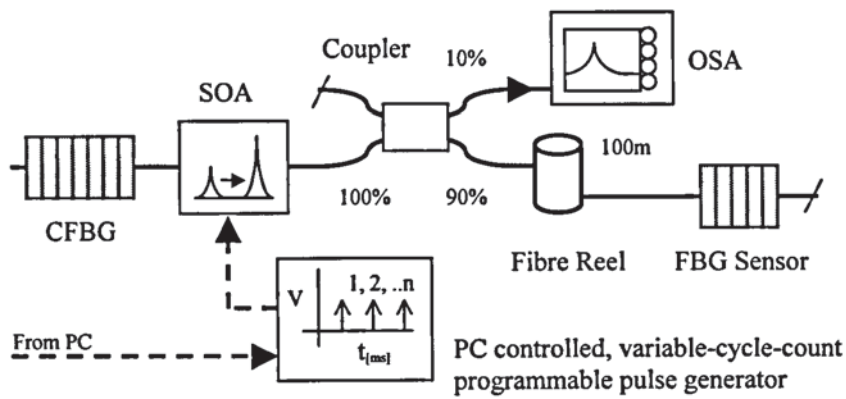
Figure 3.30 The equipment configuration used to assess the cavity signal evolution

Figure 3.31 An outline of the operation of the 'pulse counting' signal generator that was developed to assess the cavity signal evolution

3.13.2 Results

Figure 3.32 shows an overlay of the recordings taken with the OSA for increasing cavity cycles. Unexpectedly, little change of signal shape occurred, but the strength of the cavity signal did increased with each cycle until 11 pulses or 10 complete cavity cycles, after which no further significant change occurred.

Figure 3.33 shows an oscilloscope trace of the optical signal level that was measured in the cavity (using the amplified photodetector of Figure 3.5) when the system was set to cycle 9 times. This also shows that the signal level continued to increase until it reached an approximate equilibrium after 8 cycles.
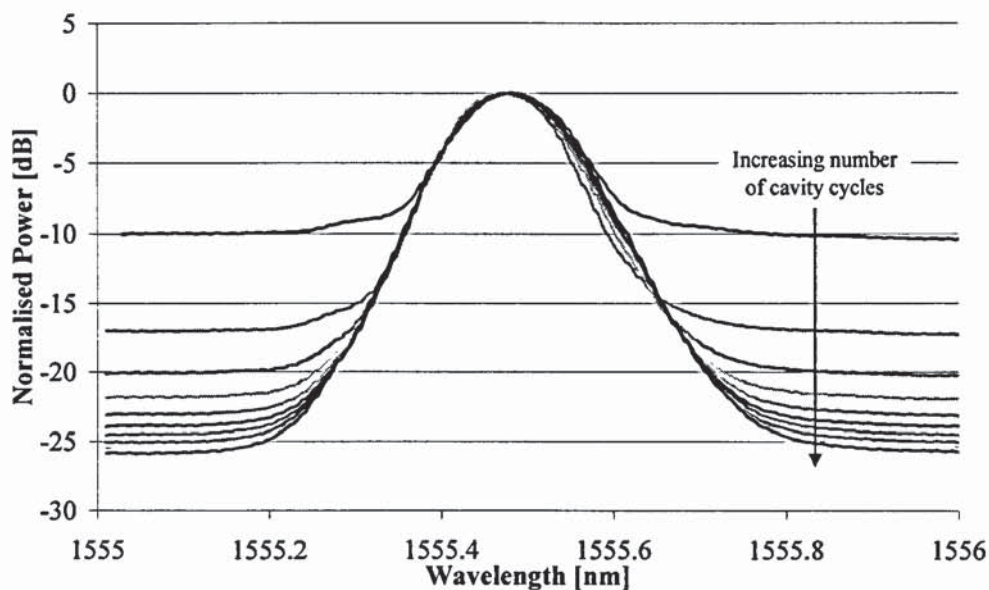
Figure 3.32 An overlay of OSA recordings taken of the cavity signal after an increasing number of cavity cycles
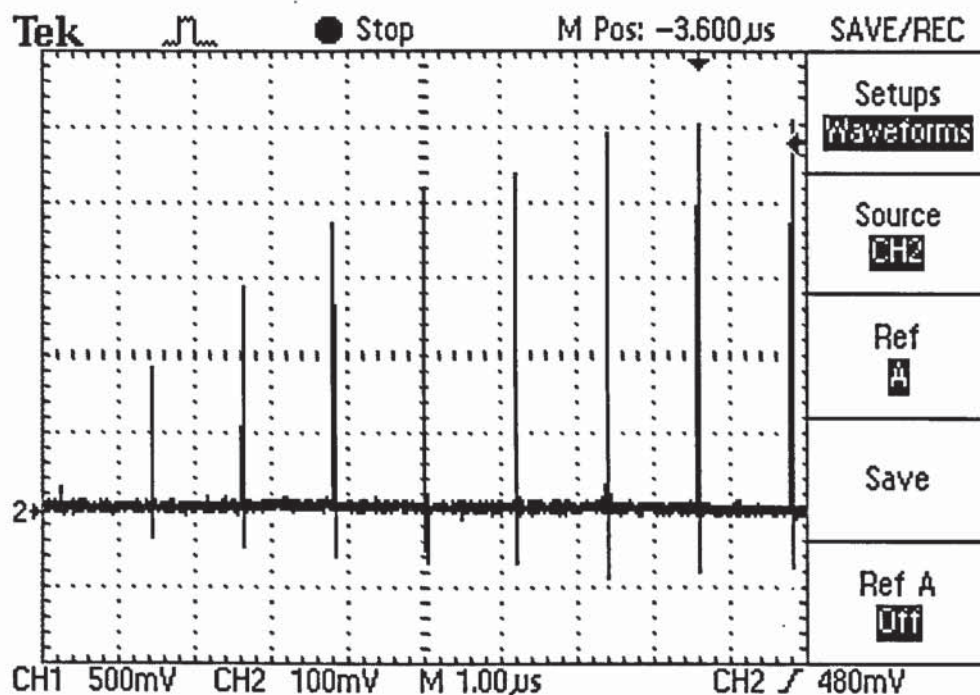
Figure 3.33 An oscilloscope trace of the cavity signal amplitude showing its evolution over a series of 9 cycles

3.13.3 Conclusions

The results of this experiment were considered to prove that whilst for each cycle of the cavity the optical signal was only modified once by the sensor profile, once by the rear reflector profile and the twice by the SOA gain characteristic, the signal did not remain

108

constant, but evolved in both strength and shape during repeated cycling until an equilibrium was achieved. It was felt that since (within the optical limits experienced by the system) the FBGs could be considered entirely passive and linear, the SOA was proven to exhibit a complex and highly non-linear optical characteristic, which although documented for standard telecommunications operation had not previously been considered or proven in this switched architecture.

It was concluded that the experiment had been sufficient to fully confirm that an evolution of the cavity signal did occur and that equilibrium was typically reached in less than 10 cycles, but unfortunately it was felt that creation of an accurate model of the system would require more effort and a better understanding of the complex operating regime of the SOA. Unfortunately, due to time and equipment constraints, no further work was carried out to take this model further.

3.14 Multiple rear reflectors for hybrid WDM/TDM operation

During experimental work an idea was proposed for a hybrid WDM / TDM system that would offer the potential to reduce the spacing required between adjacent FBG sensors. This was favoured since at that time (using the typical resonant cavity architecture) the minimum allowable sensor spacing was 1-2m and could not be reduced further due to a requirement for an optical pulse of sufficient length to operate the wavelength detector system.

The new idea was to use a series of rear reflectors, each operating in distinct wavelength regions (e.g. type 'A' covering a wavelength region 'A' and type 'B' covering region 'B') and to then interleave FBG sensors of different wavelengths (e.g. a type 'A' that operated in wavelength region 'A' and type 'B' that operated in region 'B'), such that sensors of similar wavelength (e.g. all type 'A') were at least 2m apart, but such that sensors of different wavelengths (i.e. a type 'A' and a type 'B') were spaced closer together. It was then proposed that by making further modifications to the programmable pulse generator, a dual pulse system would allow dynamic selection of an individual rear reflector, thus forcing cavity resonance with only a single sensor in any 2m sensing region (e.g. resonance between a type 'A' rear reflector and a type 'A' sensor FBG).

3.14.1 Experimental configuration

Figure 3.34 shows the experimental configuration that was used to evaluate the idea, whilst Table 3.14 shows the optical characteristics of the sensor and rear reflector FBGs. The full detailed design of the dual-pulse version of the programmable pulse generator used for this configuration is discussed in chapter 4, but an outline of its mode of operation is given in Figure 3.35.

The experimental procedure was as follows:

- The programmable pulse generator was adjusted so that the time between each of the pulses within a pulse pair (t_3-t_2) was equivalent to the propagation from the SOA to rear reflector type 'A' and back again

- The duration between separate pairs of pulses (t_1-t_2) was then adjusted to cause cavity resonance with the first sensor (i.e. FBG 1)

- An OSA recording was then taken of the cavity signal

- The period (t_3-t_2) was then changed (which naturally also changed the overall repetition duration of the periodic sequence) to favour the rear reflector of type 'B' and achieve resonance with the second of the sensors (i.e. FBG 2)

- A second OSA recording was then taken of the new cavity signal

- The procedure was then repeated for FBG sensors 3 and 4 by first adjusting the time period (t_3-t_2) to operate the resonant system in wavelength region 'A' (using rear reflector 'A'), but with a setting (t_1-t_2) suitable for sensor 3, then re-adjustment was made of period (t_3-t_2) to allow a new resonance with rear reflector type 'B', and hence with sensor 4

110
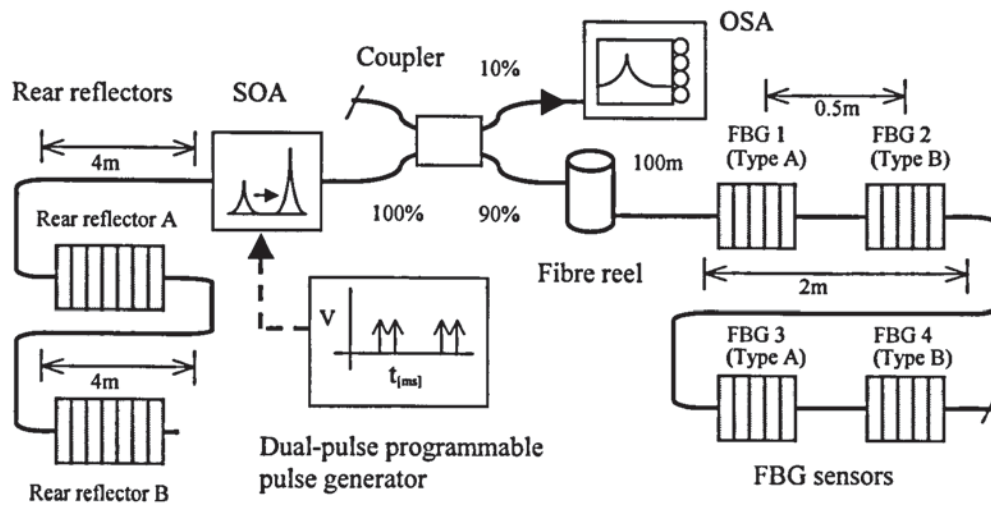
Figure 3.34 The equipment configuration used to assess the hybrid WDM/TDM dual-pulse resonant cavity architecture

Fibre Bragg grating	Central wavelength [nm]	Bandwidth [nm]	Reflectivity [%]
Rear reflector A	1552.0	6.6	>95
Rear reflector B	1565.1	6.0	>95
Sensors of type A	1553.9	0.3	≈4
Sensors of type B	1565.6	0.3	≈4

Table 3.14 The parameters for the rear reflector and sensor FBGs used in Figure 3.34

At time t_0 the SOA is turned on to produce the (required) broadband ASE pulse that propagates towards the rear reflectors (and an interfering pulse that propagates towards the sensors).

At time t_1 the SOA is turned on to gate through the reflection from one of the rear reflectors. This gated signal provides the required sensor illumination and propagates towards the sensors.

At time t_2 the SOA is turned on to gate the reflection from the required sensor and lower level interference from sensors nearby. These signals all propagate towards the series of rear reflectors.

At time t_3 the SOA turns on again to gate only the required sensor signal, since this has been preferentially reflected from a single rear reflector and therefore arrives in sync with the SOA. It is amplified and propagates out again towards the sensors to start the complete cycle over again, in a manner similar to the occurrence at time t_1.

Careful consideration of the required and interfering illumination and reflection signals shows that only a single sensor will be optimally cycled in the cavity.

This is because there will be only a few consecutive sensors located spatial within the array such that the propagation time from the SOA to the sensors and back is a close match to time duration between pulse pairs (i.e. time t_2-t_1), and also since of those few sensors, only one will have a wavelength that falls within the reflection bandwidth of the single rear reflector. This reflector is the (only) one that is spatially positioned at a propagation time (t_3-t_2) from the SOA.

By adjustment of the pulse generator durations (t_2-t_1) and (t_3-t_2), any single grating can be selected for cavity resonance, even though gratings may be closely spaced.

Figure 3.35 An overview of the mode of operation of the dual-pulse SOA drive used in the hybrid WDM/TDM resonant cavity architecture

3.14.2 Results and observations

Table 3.15 shows the peak optical signal power, the general background noise and level of interference for each of the four sensors.

Sensor	Peak power [dBm]	Background [dBm]	Largest interference [dB]
1	-22.4	-47.0	-42.1
2	-24.3	-46.8	No interference noted
3	-21.6	-48.3	-45.3
4	-23.7	-47.0	No interference noted

Table 3.15 The peak signal and interference levels experienced by each of the sensors in the dual-pulse system

3.14.3 Conclusions

The first experimental results of using multiple rear reflectors to closely space sensors by hybrid WDM / TDM successfully demonstrated the technique. The level of interference was low and the tuning between sensors could be quickly and easily achieved.

112

Therefore, although further work was not carried out on the technique at the time, additional work is very likely in the future. Such work will include trials with a standard telecommunications WDM splitter to allow the use of multiple, parallel arrays of FBG sensors, each operating in a different wavelength window, as defined by the splitter.

Other work using this hybrid system and a WDM splitter will include trials of a series of looped sensor configurations that are hoped to provide sensor redundancy and failure tolerance, for use in fire detection and harsh area sensor systems.

3.15 Summary of results

This chapter has included numerous proof-of-concept experiments that have each covered an entirely new optical sensing circuit configuration. Each of these configurations has been shown to provide a unique range of advantages, disadvantages and operational characteristics, which are likely to mean that one particular circuit variant would be favoured over another, depending on the requirements of a particular application. Therefore, to ease with reference and comparison when selecting between circuit configurations, Table 3.16 provides a brief summary of the results for many of the configurations detailed within this chapter. However it should be noted that as each of the experiments was carried out individually (over a period of several months), comparison between results should be considered only as an outline guide; before any decisions are taken a more detailed reference should be made to the appropriate sections of this chapter.

Optical circuit configuration and the associated reference section within this chapter	Optical signal level at peak (mean) [dBm]	Optical signal to noise ratio [dB]	Comments
None cycling pulses with SLED source, gated SOA and high reflectivity sensors (Section 3.5)	-33.5	19.5	Unidirectional gating only
None cycling pulses with SOA as source, amplifier and gate. High reflectivity sensors (Section 3.6)	-27.4	23.9	Unidirectional gating only
Resonant cavity. Signal extracted through rear reflector. High reflectivity sensors (Section 3.7)	-32.5	40.9	High out-of-band ASE noise
Resonant cavity. Signal extracted off rear reflector. High reflectivity sensors (Section 3.8)	-20.7	51.3	No out-of-band ASE noise
Resonant cavity. Signal extracted from front of SOA. High reflectivity sensors (Section 3.9)	-18.3	39.7	Higher out-of-band ASE noise
Resonant cavity. Signal extracted direct from sensors. High reflectivity sensors (Section 3.10)	-28.0	36.0	Integrated OSNR is very large
Resonant cavity. Signal extracted off rear reflector. Low reflectivity (4%) sensors (Section 3.11)	-22.0	29.0	Low crosstalk, low cost sensors

Table 3.16 A brief summary of the results taken for many of the optical circuit configurations detailed within this chapter

3.16 Chapter conclusion

3.16.1 The novel resonant cavity architecture

This chapter detailed the proof-of-concept experiments designed primarily to prove the original hypothesis; that it was possible to time-division-multiplex FBG sensors using the optical gating characteristics of an SOA. The successful outcome of these experiments not only proved the hypothesis but also led to the conception of a novel and entirely unique method of TDM sensor interrogation. The resonant cavity

114

architecture developed was shown to provide a real solution to optical gated TDM, using only low reflectivity sensors and a few solid-state components to generate large OSNR, high peak signal power and minimum crosstalk. As such this novel architecture represented a significant milestone in TDM sensor interrogator research.

Previously reported WDM interrogation systems suffered from a number of drawbacks; due to the finite optical bandwidth of the source and detector components they supported only a limited number of sensors with a limited measurement range. They also required expensive bespoke array design using high reflectivity sensors at different wavelengths and produced installed solutions that were difficult to extend at a later time. These factors therefore made most WDM variants of limited commercial value. The few previously reported TDM systems were also shown to be commercially unattractive, either due to requirements for large sensor spacing and inherent problems with noise and poor OSNR, or as a result of the requirement for numerous expensive, bulky, fragile and power inefficient components.

By contrast, the limiting factors of previously reported systems were eliminated in the novel resonant cavity architecture and so it was concluded that commercial opportunity existed for this new technology. An extensive series of patent protection applications were therefore filed and significant company focus was directed to identifying the revenue potential. A market study investigated both new and existing optical sensing applications to quantify the limitations imposed by other interrogation technology and identify the potential improvements offered by a new approach. Three primary market areas were identified, offering a large revenue potential for a TDM system that could be produced in volume and that delivered a low cost, high sensor count, solid-state solution. The fundamental optical specification for such a system largely dictated the interrogation of tens of low reflectivity sensors, spaced a minimum of 2m apart. However, also highlighted was the fact that existing systems suffered from limited environmental performance and flexibility, and as such the development of a range of power supply and connectivity options and extended environmental operation and lifetime, was also considered essential.

3.16.2 Key sub-systems

Following the decision to develop a commercial TDM sensor interrogation around the resonant cavity architecture, a modular and iterative research and development process was initiated. Figure 3.36 shows the key sub-systems that were identified and

evaluated to determine their fundamental significance to the project and the risk of failure they may contribute. Those that represented the greatest level of risk were assigned the highest priority and were generally developed first.
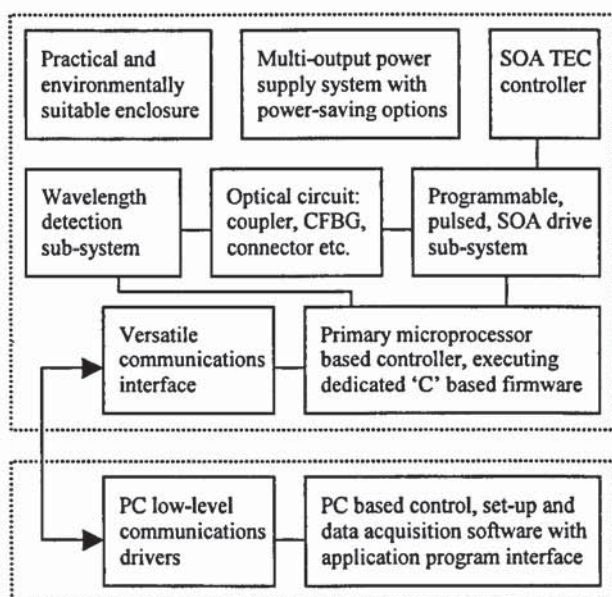
Figure 3.36 The key sub-systems that were originally envisaged for a commercial fibre sensor interrogator based on the resonant cavity architecture

- *Configurable pulsed SOA drive system*

In contrast with the original proof-of-concept arrangement, a requirement of the final commercial SOA drive system was that it occupied a minimal PCB footprint, had total volume no greater than a matchbox and was capable of gating the reflection signal from sensors spaced only 2m apart, anywhere within many thousands of metres of fibre. Successful development of a configurable drive system capable of switching the SOA with nanosecond speed and accuracy over a large range, whilst ensuring a stable operating current and temperature, was considered the most crucial and difficult part of the project. Failure to produce a solution with sufficient versatility was expected to render the final system commercially unviable.

- *Wavelength measurement system*

Assuming that a commercially viable level of optical multiplexing could be established from the SOA drive, wavelength measurement was considered to be the next most important sub-system. The valuable proof-of-concept experiments demonstrated a number of circuit configurations for extraction of the cavity signal, each having different optical characteristics. Coupled with other results, which showed only a single dominant sensor signal existed in the cavity at any time, it was concluded that a

116

range of techniques for the wavelength measurement sub-system could be employed within the resulting TDM interrogation system.

- *The power, connectivity and control systems*

It was concluded that the power supply, connectivity and control sub-systems were of significantly lower risk, since although challenging, they were thought likely to be development-only tasks and were not expected to require significant new research.

Although the key sub-systems were initially identified as isolated units, it was anticipated that overlapping and interrelated development would occur between systems. In particular it was concluded that progress should be made in a series of incremental steps (rather than directly aiming for the final system specification) as this was expected to allow the greatest freedom for the natural cycle of 'research-leading development-allowing further research'. Therefore, for clarity, the following chapters provide separate detailed discussion of each of the key sub-systems; though it should be remembered that often work was actually carried out concurrently amongst systems.

1   I. Bennion, J. A. R. Williams, L. Zhang, K. Sugden and N. J. Doran 'UV-written in-fibre Bragg gratings', *Optical and Quantum Electronics*, **28**, 1996, pp.93-113

2   K. O. Hill and G. Meltz 'Fiber Bragg grating technology fundamentals and overview', *J. Lightwave Technol.*, **15**, 1997, pp.1263-1276

3   C. R. Giles, 'Lightwave applications of fiber Bragg gratings', *J. Lightwave Technol.*, **15**, 1997, pp.1391-1404

4   A. D. Kersey, M. A. Devis, H. J. Patrick, M. LeBlanc, K. P. Koo, C. G. Askins, M. A. Putnam and E. J. Friebele, 'Fiber grating sensors', *J. Lightwave Technol.*, **15**, 1997, pp.1442-1463

5   Y. J. Rao, 'Recent progress in applications of in-fibre Bragg grating sensors', *Optics and Lasers in Eng.*, **31**, 1999, pp.297-324

6   J. Mørk, M. L. Nielsen, T. W. Berg, 'The dynamics of Semiconductor Optical Amplifiers: Modelling and applications', Opt. Photon. News, **14**, 2003, pp.42-48

7   J. Martin, F. Ouellette, 'Novel writing technique of long and highly reflective in-fibre gratings', *Electron. Lett.*, **30**, (10), 1994, pp.811-812

8   R. Kashyap, P. F. McKee, R. J. Campbell, D. L. Williams, 'Novel method of producing all fibre photoinduced chirped gratings', *Electron. Lett.*, **30**, 1994, pp.996-997

9   K. C. Byron, H. N. Rourke, 'Fabrication of chirped fibre grating by novel stretch and write technique', *Electron. Lett.*, **31**, 1995, pp.60-61

10　S. M. Melle, K. Liu, R. M. Measures, 'A passive wavelength demodulation system for guided-wave Bragg grating sensors', *Photon. Technol. Lett.*, **4**, 1992, pp.516-518

11　S. M. Melle, K. Lui, R. M. Measures, 'Practical fibre-optic Bragg grating strain gauge system', *Appl. Opt.*, **32**, 1993, pp.3601-3609

12　M. A. Davis, A. D. Kersey, 'All-fiber Bragg grating strain-sensor demodulation technique using a wavelength division coupler' *Electron. Lett.*, **30**, 1994, pp.75–77

13　K. Sugden, I. Bennion, 'Chirped gratings produced in photosensitive optical fibers by fiber deformation during exposure', *Electron. Lett.*, **30**, 1994, pp.440

14　A. D. Kersey, T. A. Kerkoff, W. W. Morey, 'Multiplexed fiber Bragg grating strain-sensor system with a fiber Fabry-Perot wavelength filter', *Opt. Lett.*, **18**, 1993, pp.1370-1372

15　H. Geiger, M. G. Xu, N. C. Eaton, J. P. Dakin, 'Electronic tracking system for multiplexed fiber grating sensors', *Electron. Lett.*, **31**, 1995, pp.1006-1007

16　C. G. Askins, M. A. Putnam, 'Instrumentation for interrogating many-element fiber Bragg grating arrays embedded in fiber/resin composites', *Proc. SPIE Smart Sensing, Processing and Instrumentation*, 1995, **2444**, pp.257

17　C. Jáuregui, A. Quintela, J. M. L. Higuera, 'Interrogation unit for fibre Bragg grating sensors that uses a slanted fiber grating', *Opt. Lett.*, **29**, 2004, pp.676-678

18　K. Zhou, A. G. Simpson, X. Chen, L. Zhang, I. Bennion, 'Fiber Bragg Grating Sensor Interrogation System Using a CCD Side Detection Method With Superimposed Blazed Gratings', *Photon. Technol. Lett.*, **16**, 2004, pp.1549-1551

19　A. D. Kersey, 'Analysis of intrinsic crosstalk in tapped serial and Fabry-Perot interferometric fiber sensor arrays', Proc. SPIE Fiber Optic Laser Sensors VI, **985**, 1988, pp.113-116

20　C. G. Askins, M. A. Putnam, 'Instrumentation for interrogating many-element fiber Bragg grating arrays embedded in fiber/resin composites', *Proc. SPIE Smart Sensing, Processing and Instrumentation*, 1995, **2444**, pp.257

21　C. C. Chan, Y. J. Gao, K. T. Lau, H. L. Ho, L. M. Zhou, W. Jin, 'Characterisation of crosstalk of a TDM FBG sensor array using a laser source', *Optics and Laser Technol.*, **33**, 2001, pp.299-304

4 CONFIGURABLE SEMICONDUCTOR OPTICAL AMPLIFIER DRIVE SYSTEM

4.1 Chapter overview

In the previous chapter the results of a market research study concluded that a commercial interrogation system based on the resonant cavity architecture would require a minimum fibre Bragg grating (FBG) sensor spacing of 2m. Achieving this goal was largely dependant on an ability to control a semiconductor optical amplifier (SOA) in such a manner so as to perform the function of an optical gate with nanosecond switching speed and timing accuracy.

However, attaining a goal that was nearly two orders of magnitude greater than had been demonstrated in the proof of concept experiments depended on the successful design of a dedicated SOA drive sub-system. Therefore, this chapter focuses on the research and development that occurred on this, the single most essential part of the resonant cavity fibre sensor interrogator.

Details are given of the steps taken in a cycle of 'research driving development, allowing further research' that concluded with the final commercial system design. Included in the discussion is the requirement for and development of a variable gain control system that was found to be essential for correct device operation in variable loss environments, as well as details of a range of test harnesses, auxiliary functions and SOA drive variants, which were also produced to support parallel research on the wavelength detection and micro-controller sub-systems.

The chapter concludes with a comparison between the initial requirements of the sub-system and the specification of the final commercial design and then reflects on the academic and commercial importance of this successful result.

Although the majority of the experimental work described in this chapter is new and does not repeat existing work, it does build on a wealth of knowledge gained by previous researchers working in fibre Bragg grating based optical sensing and electronics. Since many excellent review articles [1, 2] and books have covered earlier work it is not the intention of this chapter to repeat this information. The reader is, however, encouraged to refer to chapter 2 for an overview of the theory.

4.2 The implications for operation with 2m spaced sensors

In chapter 2 it was shown that in wavelength-division-multiplexed (WDM) systems the minimum sensor spacing is only limited by FBG fabrication and so is typically a few centimetres for modern manufacturing methods. The actual WDM interrogation technique does not dictate any spatial limitations as all FBG sensors operate in distinct wavelength windows. It was also explained that this is not the case for TDM, since all FBGs occupy the same wavelength window and so sensor spacing is directly dictated by the optical gating speed that can be achieved at the interrogator.

For a typical single mode optical fibre having an effective refractive index (n_{eff}) of 1.48, reflections from FBG sensors spaced at 2m intervals were shown to arrive just 19.4ns apart. This result highlighted the first criterion for any optical gating system designed to operate with closely spaced FBG sensors:

- For sensor spacing of 2m, the optical gate must open, allow the required reflection to pass through, and then to close again within 19.4ns

In reality, it was realised that since 19.4ns specifies the total period available for the gate to open, allow the signal through and close again, the actual time available for the gate to switch between the open and close states must be minimised, such to maximise the total integrated signal delivered to the wavelength detector during the gate open phase.

Two further criteria were therefore also considered essential for an optical gating system designed to operate with sensors only 2m apart:

- The time taken to switch between the open and closed states must be as fast as possible and in every case must be in a time significantly less than 19.4ns

- The time resolution required to determine when the optical gate should open and when it should closes must also be accurate to within a fraction of 19.4ns

However, it was also considered that there would be applications where it was possible to space FBG sensors at distances greater than 2m. Therefore, it was preferable to also provide a facility for variable optical gate timing, to optimise the total received signal power and improve total optical signal to noise ratio (OSNR) in those applications employing widely spaced sensors.

Table 4.1 shows the target timing specification for the SOA drive sub-system, as it was perceived when design of a commercially viable interrogator first began.

Parameter	Descriptive target	Numerical target
Time taken to open optical gate	Fraction of 19.4ns	2ns
Time taken to close optical gate	Fraction of 19.4ns	2ns
Time gate open for 2m spaced sensors	Large part of 19.4ns	15ns
Time gate open for variably spaced sensors		15ns-75ns

Table 4.1 The target timing specification for the SOA drive sub-system

4.3 The proof of concept SOA drive system

Having established some of the target specifications for the final system, focus turned to evaluating the performance of the drive system used in the early proof of concept experiments. An appreciation of the performance of the original solution was favoured in order to provide a foundation for incremental improvement and allow charting of progress towards the final solution.

4.3.1 The original drive arrangement

Figure 4.1 and Figure 4.2 review the original drive components and their behaviour and also show a connection to an amplified photodetector and oscilloscope that was sometimes used to monitor the optical output signal.
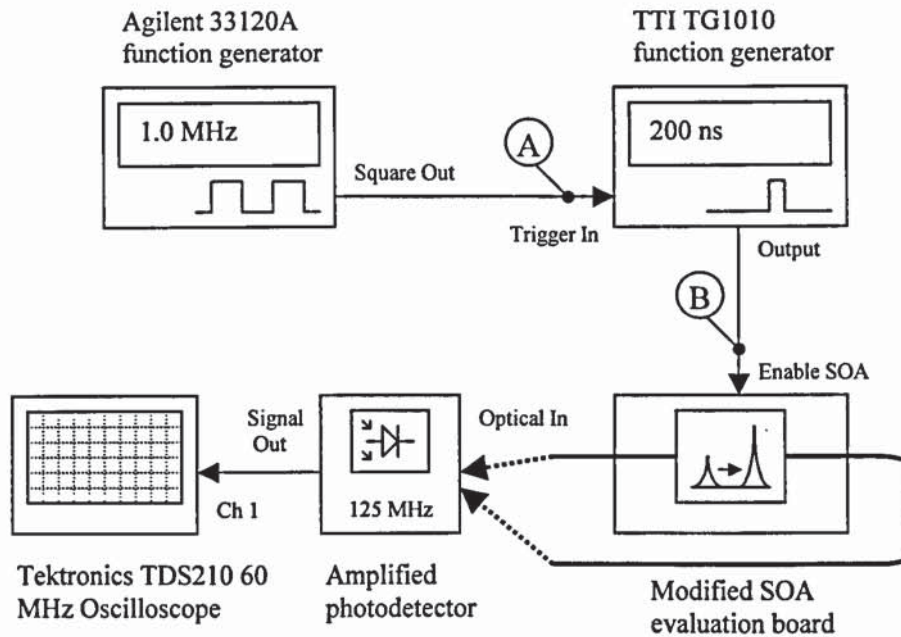
Figure 4.1 The pulse generator and SOA drive components that were used to conduct the early proof of concept experiments
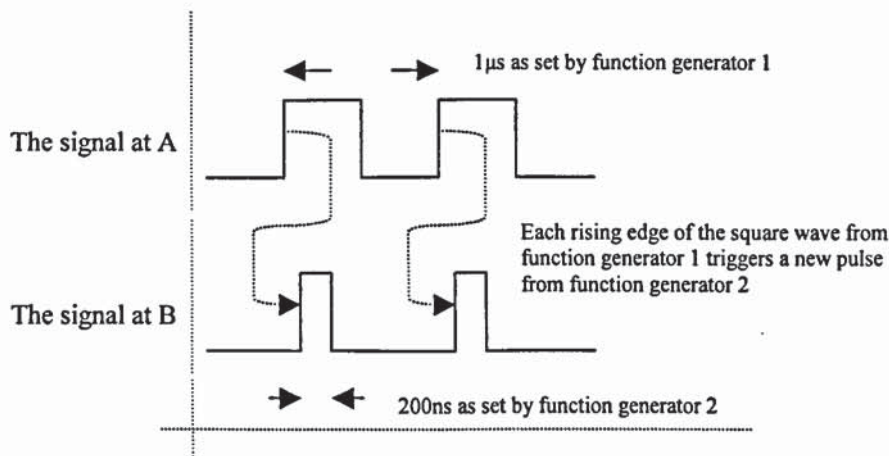
Figure 4.2 An idealised representation of the signals at locations A and B in Figure 4.1

4.3.2 The disadvantages

This original arrangement had proved simple and inexpensive to construct in the laboratory and had been sufficient for early proof of the resonant cavity architecture, but it was found to have limitations that made it unsuitable for a commercial system. These included:

- The use of two laboratory instruments, which were bulky, power inefficient and expensive

- A limitation of the Agilent instrument that meant that the matching of the cavity round-trip time was only possible by adjustment of the signal repetition rate in the frequency domain rather than the time domain

- A limitation of the Agilent instrument, manifesting from it utilising direct digital synthesis, which meant that it suffered from reduced tuning resolution at higher frequencies, so resulting in sensors further from the SOA being tuned with greater ease than those closer to the SOA

- A limitation of the TTI instrument (which was also DDS based) that meant it suffered from a limited pulse length resolution of only 50ns and a shortest pulse of 50ns

- A further limitation (that also appeared to be due to the digital nature of the TTI instrument) resulted in variable triggering latency of between 25 and 50ns. This caused jittering in the pulse positioning and hampered accurate tuning of the instrument when matching the resonant cavity round-trip time

- Finally, measurements taken using the photodetector and oscilloscope indicated that electrical pulses of 100ns duration resulted in the SOA generating optical pulses with durations of up to 300ns

4.4 Logic-gate-delay based pulse generator

Having considered all of the limitations of the previously described system it was felt that although the use of the Agilent square wave frequency source (as a method of adjusting the pulse repetition rate) was not ideal, it was not as limiting as the poor performance of the TTI function generator used to set the SOA 'on' time.

A simpler, but more reliable replacement for the pulse generator was therefore required to allow research into the cause of the large discrepancy between the length of the electrical drive pulses to the SOA and the duration of the optical signal so produced, as discussed in chapter 3.

4.4.1 The design requirements

The design requirements for this replacement pulse generator were as follows:

- Simple

- Internal experimental use only

123

- Quick to construct from common components (less than 1 day)

- Low cost (preferably less than £100)

- Need not be elegant, but should be reliable (required for a few weeks)

- Need not provide accurate timing, but should have short-term repeatability (over a period of 10 minutes)

The functionality required was as follows:

- Preferably TTL compatible, but anything up to 10V could be accommodated

- Should be edge triggered from a square wave source (10kHz to 2MHz)

- Should produce a square pulse with duration of between 20 and 100ns

- May have a constant latency between trigger and output if necessary, but any variation in latency should be less than 20ns

4.4.2 The solution

The final solution designed and constructed to meet these requirements is shown in Figure 4.3. Figure 4.4 shows its response at points A-E for a complete square wave cycle, as input from a function generator to point A.
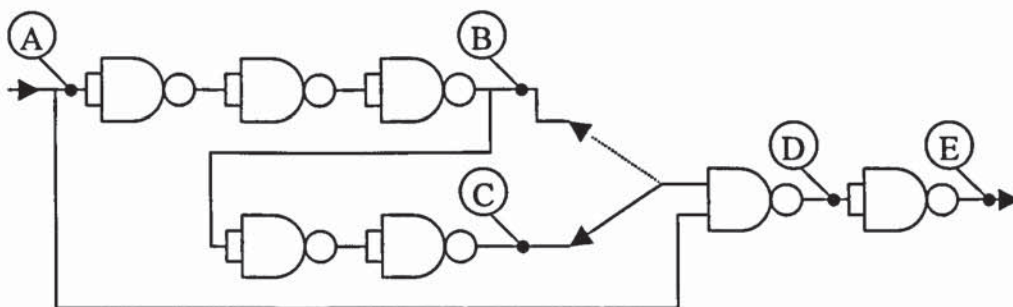
Figure 4.3 The final design of the logic-gate-delay based pulse generator

124
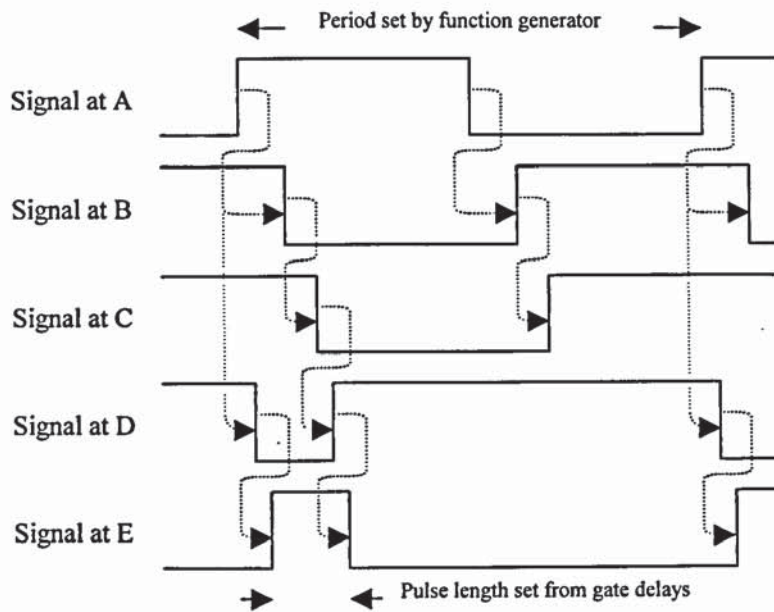
Figure 4.4 The response of the logic-gate-delay based pulse generator to a square wave input, highlighting the signals marked A-E in Figure 4.3

The design was based around two 'quad 2-input NAND' gates interconnected to utilise logic-gate input-to-output propagation delays [3, 4]. A switch was provided to select between 3 or 5 gate delays and had the potential to produce pulses in the range 15ns to 500ns depending on the logic family chosen [5]. Construction of the design required careful consideration of RF techniques to minimise stray coupling and provide effective switching performance; minimising lead length and tracking distance was a primary focus [6].

The completed solution worked well and was sufficiently short-term stable and repeatable that it caused no significant measurement error in a laboratory environment. However, it was very crude and was not intended for use in a production design due to the unpredictable variation that occurred between individual gates. These differences were known to be strongly dependent on operating temperature, the silicon batch, device manufacturer and their method of fabrication.

4.5 Measurement of SOA switching times

4.5.1 Circuit configuration

Using the logic-gate-delay based pulse generator the experiment shown in Figure 4.5 was conducted to determine the cause of the discrepancy that appeared to exist between the length of the electrical drive pulse delivered to the SOA and length of the optical pulse so generated.

125
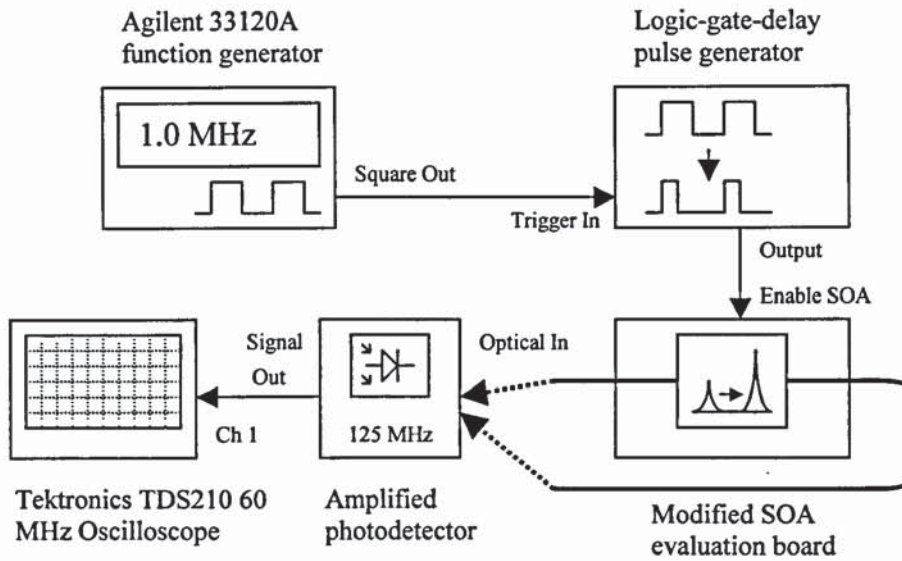
Figure 4.5 The experimental configuration that was used to determine the cause of discrepancy between the length of the electrical and optical pulses

The input electrical pulse duration was adjusted in steps based on selection of either 3 or 5 gate delays and with a range of different logic gates from different logic families. The actual duration of the electrical drive pulse delivered to the SOA and optical signal it provided were then measured and recorded using the two channels of the oscilloscope.

The experiment was repeated twice, first with the SOA in isolation and then with an Agilent 8164A tuneable laser source adjusted to provide a narrow signal of 0dBm power and 1550nm wavelength to act as an optical input signal.

4.5.2 Experimental results and observations

Table 4.2 shows the relationship between the duration of the electrical drive signal and the resulting optical output when the tuneable laser was disabled and SOA was driven in the absence of an optical input signal. It can be seen that the duration of the optical output was partially related to the duration of the input signal, but in all cases was significantly longer.

126

Duration of electrical drive signal into the SOA [ns]	Duration of the resulting optical output signal from the SOA [ns]
30	220
50	270
110	300

Table 4.2 The relationship between the length of the electrical and optical pulses when the SOA was operated in absence of an optical input signal

In contrast, Table 4.3 shows that the duration of the optical output could be significantly reduced if the tuneable laser was enabled and the SOA was required to amplify and deliver a large optical output.

Duration of electrical drive signal into the SOA [ns]	Duration of the resulting optical output signal from the SOA [ns]
30	90
50	120
110	180

Table 4.3 The relationship between the length of the electrical and optical pulses when the SOA was operated with a large optical input signal

4.5.3 Conclusion

It was concluded that the significant increase in the duration of the optical output (relative to the electrical drive) when the SOA was operated in the absence of an optical input signal might relate to saturated population inversion occurring within the device.

It was considered that when the electrical drive to the SOA was enabled, a population inversion would always begin to build, which in the presence of an optical input would be equally quickly depleted as stimulated emission occurred and a high power amplified optical output was produced. In this mode, when the electrical drive ended, the stimulated emission would quickly deplete the population inversion and the optical output would cease almost instantaneously.

In contrast, in the absence of an optical input signal, the population inversion would build until saturation was reached, as spontaneous emission would be the only significant depletion mechanism; some stimulated emission could occur, but it would be the result of spontaneous output in other parts of the device only. Therefore, beyond

the end of the electrical drive signal, an additional time would exist when spontaneous emission could continue to be produced, as the population inversion would be depleted less rapidly.

4.6 Trials with a dedicated laser-diode driver component

Having evaluated the performance of the original SOA drive circuit and determined that the optical pulse duration was potentially partially dependant on the presence of an optical input signal, attention was focused on alternative methods of controlling an SOA to provide some improvement on the switching performance.

One potential solution considered was the use of an iCHaus iC-HK dedicated laser-diode driver component designed for applications within telecommunication systems and laser printers. The small semiconductor device was promoted as having a fast switching speed, good compatibility with standard logic signals and being capable of advanced current control with feedback; so offering the potential for a variable-current mode of operation.

It was considered that by tailoring the current delivered to the SOA throughout each pulse period it might be possible to improve the overall switching performance. Unfortunately, since the datasheets and other manufacturer documentation was sparse, it was not possible to accurately determine upfront if the device would be suitable for operating an SOA in such a switched mode and so samples were ordered and a basic evaluation was conducted.

4.6.1 The experimental configuration

Figure 4.6 shows an abstract schematic of the circuit used to evaluate the device. The basic circuit was taken from an application example in the manufacturers literature, but with the SOA in place of the laser diode. The component values were calculated to provide a mid-range SOA current of around 100mA, with the length and repetition rate of the electrical drive pulses chosen to be similar to those of the previous experiment.

128
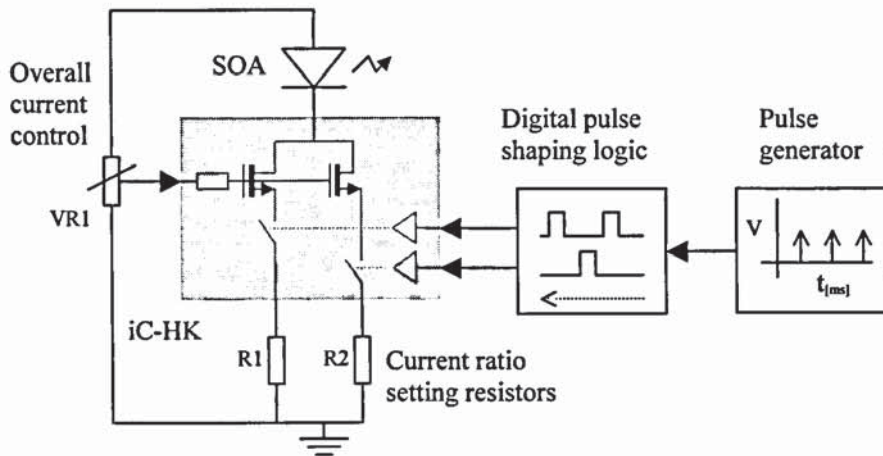
Figure 4.6 An abstract schematic of the electrical circuit that was constructed to assess the use of a laser diode driver device for high speed switching of the SOA

4.6.2 Results and conclusion

Initial results of the evaluation showed some improvement in switching performance, but pulse expansion of around 30ns still occurred. Most dramatically however, despite operating the device within its specified limits, catastrophic failure occurred after several minutes. Later exploration indicated that the output stage of the laser-diode driver had failed and fused short-circuit, so delivering an excessive level of current to the SOA and resulting in permanent damage to both components.

4.7 Totem pole (complementary) output drive for an increase in SOA switching speed

As a result of the costly destruction of an SOA a decision was taken to abandon the use of the laser-diode driver and attention turned to other alternative drive methods. It was clear that the SOA turned on quickly using only the simple open-collector transistor and current limiting resistor circuit design used in the proof of concept experiments. This was due to charge quickly flowing into the device when the transistor was turned on. However, it was also clear that as an open collector design, any charge contained within the SOA when the transistor was switched off would remain and would only decay naturally as a result of ASE generation.

By taking the view that the SOA could be modelled as a parallel capacitor and resistor combination it was then proposed that a totem pole or dual complementary transistor output drive arrangement might improve the rate of switch-off decay since charge could be actively removed from the SOA junction [7, 8].

129

4.7.1 The experimental configuration

An abstract schematic for the simple experimental circuit that was used to test the totem-pole arrangement is shown in Figure 4.7. It can be seen that the final output consists of NPN and PNP complementary pair transistors connected in open-collector configuration (Q2 and Q3) and then driven by a single pre-driver transistor (Q1). This design was constructed using standard components without a specially design PCB, but attention was given to minimising lead and track lengths to reduce stray coupling and thus improve RF performance. Using the gate-delay pulse generator, the amplified photodiode and the oscilloscope, the SOA switching behaviour was recorded and its speed measured.
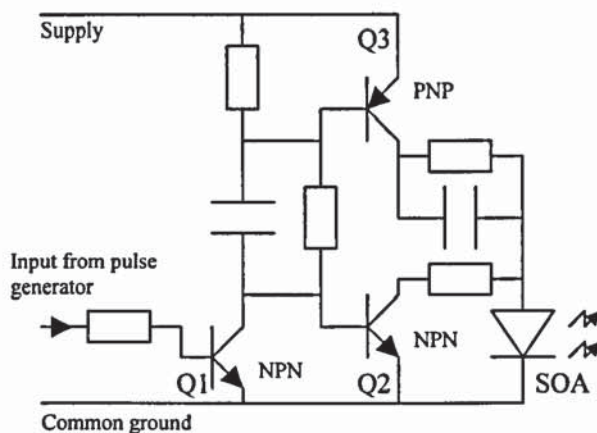
Figure 4.7 An abstract schematic of the electrical circuit constructed to assess using a totem-pole (complementary) output stage for high speed switching of the SOA

4.7.2 Results and conclusion

Figure 4.8 shows an example recording of the optical pulses generated by the SOA using this experimental totem pole driver. It can be seen that the optical pulses were significantly shorter than had been achieved using previous driver designs and so continued optimisation of component values and the addition of extra coupling and decoupling capacitance was tested. The result was that switching times were reduced yet further.

130

```
Tek      ⎍      ● Stop      M Pos: 13.00ns      CH1

                                                Coupling
                                                  DC

                                                BW Limit
                                                  OFF
                                                60MHz

                                                Volts/Div
                                                 Coarse

                                                Probe
                                                 10X

CH1  2.00V    CH2  100V    M 10.0ns      CH2 ∕ 172V
RefA 100V 10.0ns
```
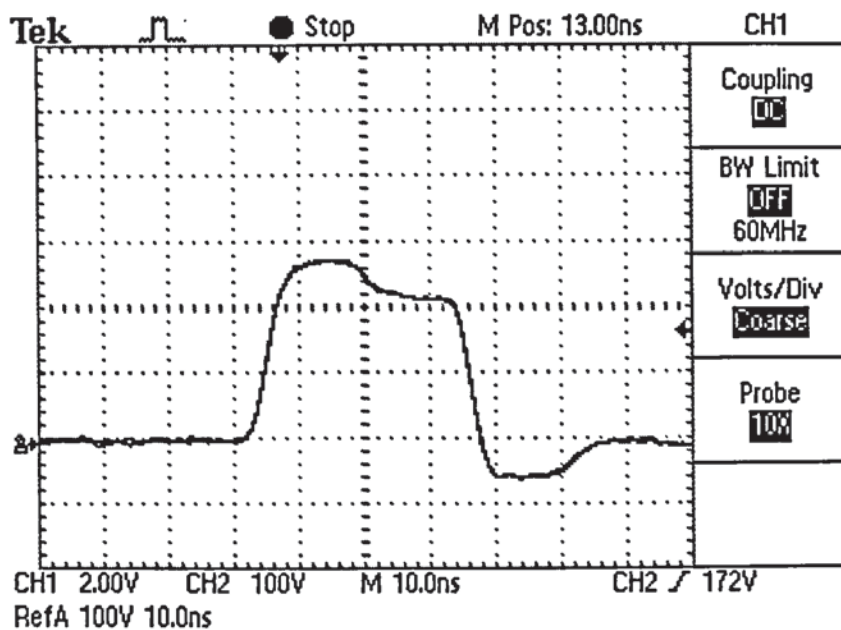
Figure 4.8 An example recording of the optical pulses generated by the SOA when it was driven using a totem-pole (complementary) output stage

4.8 *Integrated circuit totem-pole driver*

Following the improvements in switching speed attained by the use of a totem pole (complementary) output drive, other associated circuit arrangements were also designed and tested. During these tests it was found that when working towards the fast switching speed and high drive current criteria (of up to 250mA) needed for the final commercial design, discrete transistor driver arrangements were not the most effective solution. Discrete designs required numerous components, were larger, more expensive, had tighter PCB track layout constraints (for reduced stray coupling) and were more likely to generate significant electromagnetic interference than other integrated circuit alternatives.

4.8.1 74AC series parallel-connected gates

Therefore, the final chosen solution was based around parallel-connected 74AC series logic gates. These provided combined characteristics of high switching speed, a large, complementary drive, symmetric output current (25mA per gate), a low component count (due to 4 gates being contained in a single component), an ease of availability (through manufacture by multiple semiconductor fabricators) and a low cost of <$1 per component.

Table 4.4 shows the measured switching performance of the final 74AC based design.

131

Pulsed SOA drive current (max) [mA]	Switch on time (0-90%) [ns]	Switch off time (100-10%) [ns]
250	~3	~3

Table 4.4 The optically measured switching performance of the SOA when driven from the 74AC based logic gate based drive circuit

4.9 Direct digital synthesis based programmable pulse generator

Having successfully developed the high switching speed SOA drive circuit, effort returned to replacing the combination of the bench-top function generator and gate-delay pulse generator with a bespoke software controllable solution. Not only was software configuration of the pulse repetition period and duration an essential requirement for the final commercial system, it was also desirable early in the development cycle to reduce the repetitive manual instrument adjustment that was frequently required when conducting research experiments. However, although continual adjustment of pulse repetition period was essential to tune the resonant cavity between FBG sensors, pulse duration often remained constant for longer and so early software control of this variable was a lower priority. Replacing the Agilent bench-top laboratory function generator with a dedicated programmable oscillator was considered first.

4.9.1 Analog Devices AD9852

An evaluation board for the Analog Devices AD9852 300MHz integrated direct digital synthesis (DDS) component was purchased and trials were carried out. DDS had the distinct advantage of providing a direct relationship between the reference oscillator, the position of FBG sensors in the fibre and the reload value of the phase counter. Unfortunately however, despite attempts to operate the AD9852 device in numerous configurations both with and without additional components, the triggering performance suffered from jitter, while the power consumption and the quantity of support components required to implement this form of DDS in a final system were all considered disadvantageous.

4.10 Programmable counter-based pulse generator

Despite its limited performance, trials with the DDS system did provide the new idea of using a purely counter-based method for the pulse period adjustment. However, rather

than use an adder for phase accumulation (as in DDS), an arithmetic comparator and a reset-able counter [3] were proposed that would simply track time of flight directly.

The idea, which is depicted in Figure 4.9, retained the programmability of the DDS, but removed the requirement to convert to the analogue domain for generation of the output trigger pulse. This entirely digital design removed causes of jitter, had a greatly reduced component count and had PCB layout constraints that were considerably less stringent.
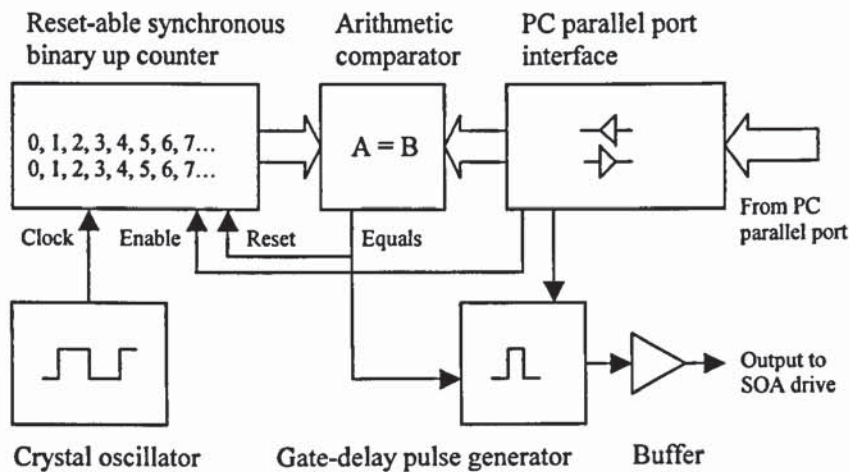
Figure 4.9 The basic counter based programmable pulse generator design

The method operation was as follows:

- An application written in C++ was executed on a Windows based PC to provide control via the computer parallel port. This control included an 8-bit numerical value

- The value was fed via the interface electronics to one input of an arithmetic comparator

- The second input to the comparator was provided by an 8-bit reset-able synchronous binary up-counter

- When the value of the counter matched that provided by the PC an 'Equals' signal was asserted

- The assertion of the 'Equals' condition triggered both the gate-delay pulse generator and the resetting of the counter back to zero

133

- Adjustment of the value provided by the PC resulted in direct control of the time between the counter reset cycles and therefore allowed control of the pulse repetition period

- As the counter was clocked from a highly stable and frequency accurate crystal oscillator, a direct relationship existed between the counter match value, the pulse repetition period and the FBG sensor position within the fibre

- Later expansion of the PC application also allowed rapid switching of the pulse repetition period to provide fast sequential cycling between multiple sensors

4.10.1 Implementation using Xilinx CoolRunner XC95108

The first version of this design was implemented using a Xilinx (formally Philips) CoolRunner complex programmable logic device (CPLD). This device was chosen on the basis of ease of component sourcing, availability of free Windows based software design tools and simple programming hardware requirements.

Initially the design was operated from a 40 MHz crystal oscillator, but this was later changed to 66 MHz and then 80 MHz. The maximum cavity length and the spatial tuning resolution achieved for each frequency variant is shown in Table 4.5. In each of these cases the spatial tuning resolution was a direct function of the reciprocal of the oscillator frequency (i.e. repetition pulse repetition period), the speed of light in the fibre ($\sim 2 \times 10^8 \, ms^{-1}$) and the fact that the reflection signals were required to travel both to and from each sensor, so covering twice the basic separation between the sensor and the rear reflector, as explained in section 2.5.1. As a consequence of this, the maximum cavity length that could be supported for each of the frequency variants was limited to 255 times the spatial tuning resolution. This was because the highest achievable value that could be accommodated by the 8-bit synchronous binary counter was 255 (i.e. a count of all 1's).

Crystal oscillator frequency [MHz]	Maximum cavity length supported [m]	Spatial tuning resolution along fibre [m]
40	640	2.5
66	385	1.5
80	320	1.25

Table 4.5 The cavity length and spatial tuning characteristics of the XC95108 implementation of the counter based programmable pulse generator

4.11 The requirement for greater spatial tuning resolution

As research continued it became necessary to improve the spatial tuning resolution of the pulse generator to better than 1.25m, whilst at the same time maintaining a maximum cavity length of at least 300m. Unfortunately, though crystal oscillators were readily available up to 125MHz, the propagation delay of the CoolRunner CPLD series meant that frequencies beyond 80MHz could not be used and so faster programmable logic devices and more advanced pulse generator designs were required.

4.11.1 The Lattice Semiconductor MACH4000 series

Extensive research into propagation delay characteristics and the internal logic block architecture for all major logic manufacturers and devices highlighted the Lattice Semiconductor MACH4000 series as the most appropriate solution. In particular the devices were chosen for their very wide input terms, which allowed reduction of the counter logic to unity depth.

Initial trials using sample parts and an extended version of the original logic description resulted in successful demonstration of operation at 125MHz with an 11-bit counter and comparator.

4.11.2 Counter dithering for resolution virtual sub-division

A novel idea was also conceived to improve the resolution of the pulse generator without necessarily needing to increase the counter oscillator frequency and without the previously associated reduction in maximum possible resonant cavity (reach) length. This new technique was termed 'dithering' due to its unstable appearance on an oscilloscope and consisted of repeated adjustment of the pulse repetition period between two adjacent integer count values to create a new virtual sub-division. Figure 4.10 gives a graphical example of this idea, where adjustment between counter values of 6 and 7 can be seen to produce virtual periods of 6.00, 6.25, 6.50 and 6.75.
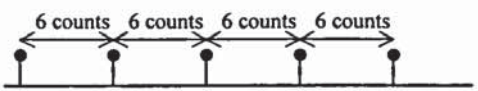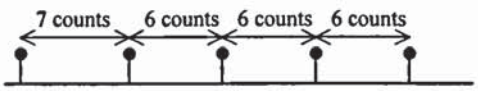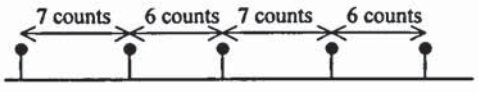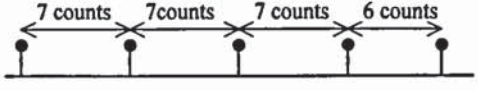
The pattern of pulses generated to form a virtual sub-division of the period	Total number counts over 4 pulse periods	Average counts per pulse period
6 counts 6 counts 6 counts 6 counts	6 + 6 + 6 + 6 = 24	24 / 4 = 6.00
7 counts 6 counts 6 counts 6 counts	7 + 6 + 6 + 6 = 25	25 / 4 = 6.25
7 counts 6 counts 7 counts 6 counts	7 + 6 + 7 + 6 = 26	26 / 4 = 6.50
7 counts 7counts 7 counts 6 counts	7 + 7 + 7 + 6 = 27	27 / 4 = 6.75

Figure 4.10 An example of using counter 'dithering' to create resolution virtual sub-division

It was hypothesised that although the level of sub-division could theoretically be extended beyond a factor of four, there was likely to be little significant improvement since actual pulse repetition period would always be integer based.

4.11.3 Basic implementation of sub-division 'dithering'

The block diagram of the first version of this sub-division 'dithering' implementation is shown in Figure 4.11. This was a direct hardware implementation of Figure 4.10 and was limited to an 8-bit counter due to the logic complexity, logic depth and the associated propagation delay. It was however, sufficient to experimentally test the concept and investigate its performance within the resonant cavity architecture.

The principle of operation of this implementation of sub-division 'dithering' was as follows:

- An application written in C++ was executed on a Windows based PC to provide control via the computer parallel port. This allowed storage of both an 8-bit numerical value for the basic pulse repetition period (B) and a 2-bit 'dither' factor (i.e. '0 / 4', '1 / 4', '2 / 4' or '3 / 4'), within the registers of the parallel port interface

- The arithmetic adder was then used to calculate the associated value of 'B+1' by adding a constant of '1' to the 'B' value stored in the parallel port interface

136

- The synchronous counter was then allowed to count incrementally though up to 8-bits, whilst its output was continuously compared to 'B' and 'B+1' match values, using the two arithmetic comparators

- The two 'equals' conditions from the arithmetic comparators was then gated via separate AND-OR logic, as controlled by the 'dither control logic' to determine which of the two match conditions was used to reset the counter

- Dependant on the 'dither' factor stored in the parallel port interface the 'dither control logic' could therefore cycle alternately between match conditions of 'B' or 'B+1' counts of the counter, as required to create the intended virtual sub-division spatial tuning value
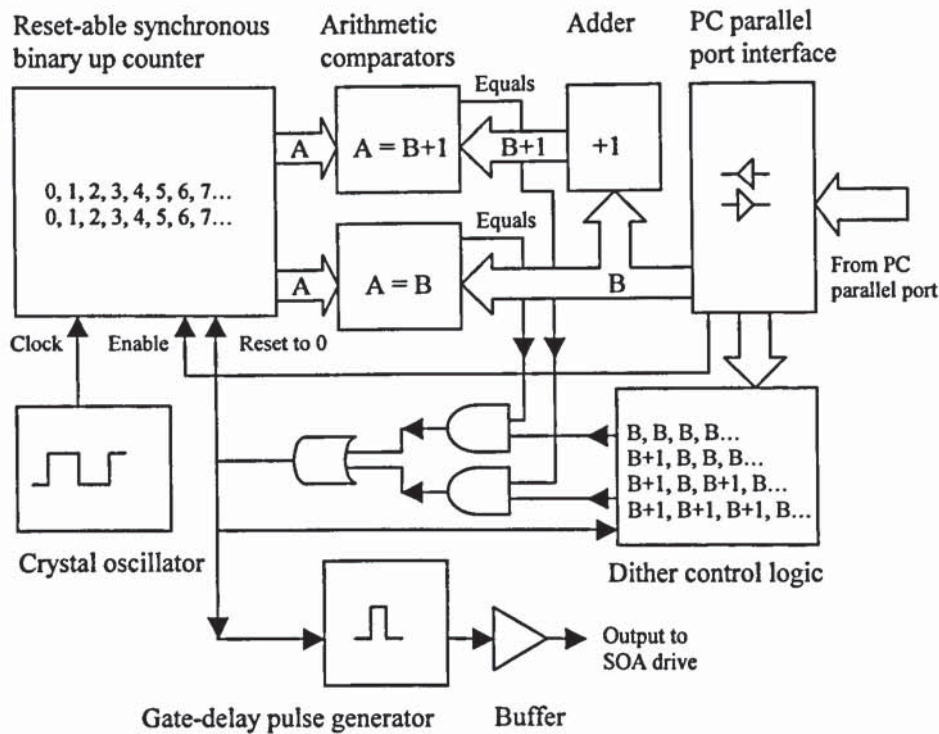
Figure 4.11 The basic implementation of 'dithering' based resolution virtual sub-division

4.11.4 Optimised implementation of sub-division 'dithering'

The primary reason for the high logic complexity in the basic implementation was the requirement for two full-width arithmetic comparators and two full-width adders (one for the synchronous counter and one for the generation of 'B+1' term).

Fortunately, with further consideration a simple but novel reversal of the count process was conceived that dramatically reduced the logic complexity. This subtle optimisation is shown in Figure 4.12, where it can be seen that in contrast to the previous design that

137

used two arithmetic comparators to compare the count to 'B' or 'B+1', the counter was now always compared to a single integer count 'B'. Instead on equality, the counter was now selectively reset to either '0' or '1', with 0 and 1 being simple logic variations affecting only the lowest binary bit of the counter. By selecting to reset the counter to 0 the resulting next pulse repetition period became equal to a count of 'B' as normal, whereas when reset to 1 the full pulse period became 'B–1'. Reversal of the dither control logic from using 'B' and 'B+1' to 'B–1' and 'B', then ensured that the original dither technique was maintained, but the logic depth and complexity was greatly reduced.
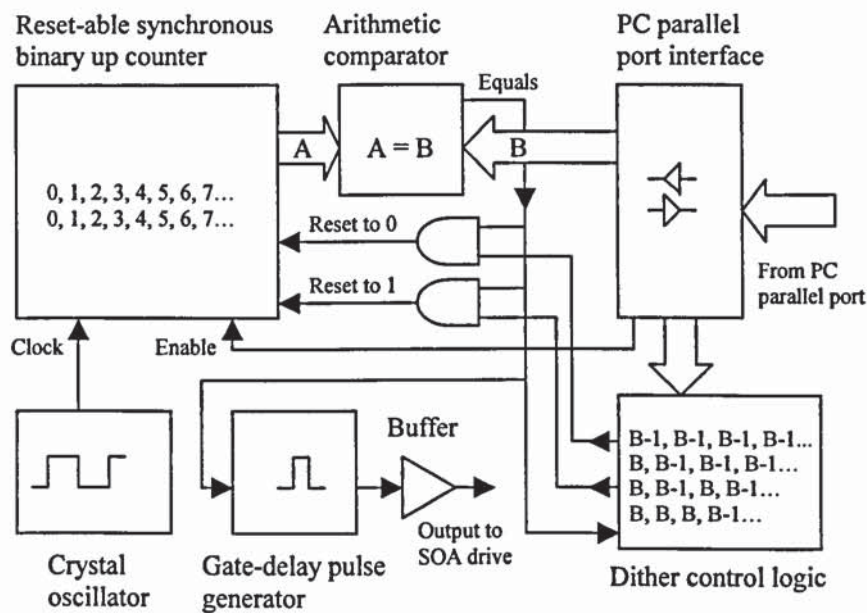
Figure 4.12 An optimised implementation of 'dithering' based resolution virtual sub-division

The final result was the successful implementation of a programmable pulse generator with a full 16-bit period selection (from 14 full bits plus a factor 4 of dither) and a total propagation delay of <3ns.

4.11.5 Increase of the reference oscillator to beyond 125MHz

As a result of research on the wavelength discrimination system, the requirement for still finer tuning resolution became apparent. However, as experimental analysis of the dither technique indicated that greater than factor-four sub-division would not provide improvement a 'real' increase in resolution was required. This implied an increase in the reference oscillator frequency, but as crystal oscillators above 125MHz were not generally available a frequency multiplier was needed. Research was conducted, two potential devices were sourced and experimental trials carried out.

138

The first device tested was a Semtech SK12429LV that offered programmable output in 1MHz steps up to 400MHz for use in PC motherboards. However, despite successful demonstration to over 300MHz, the device was not chosen for the final system since it required >600mW of power.

The second device was a XRT8020 from Exar, which although nominally used to generate clocks of 624MHz and 312MHz for use in SONET telecommunications systems, was made to deliver 320MHz and 640MHz by change of the reference crystal to 20MHz. Some difficulties with handling and soldering of the tiny 4mm x 4mm leadless package were experienced during early experiments, while level conversion from low voltage differential signalling (LVDS) to single ended 2.5v (for the CPLD) was also disadvantageous. However, the low power device proved to be reliable and was therefore chosen for the final solution.

Figure 4.13 and Table 4.6 show details of this fully programmable pulse generator solution. This version also included fully programmable pulse length adjustment since with the increased reference oscillator frequency this was simple to implement using a second short counter.
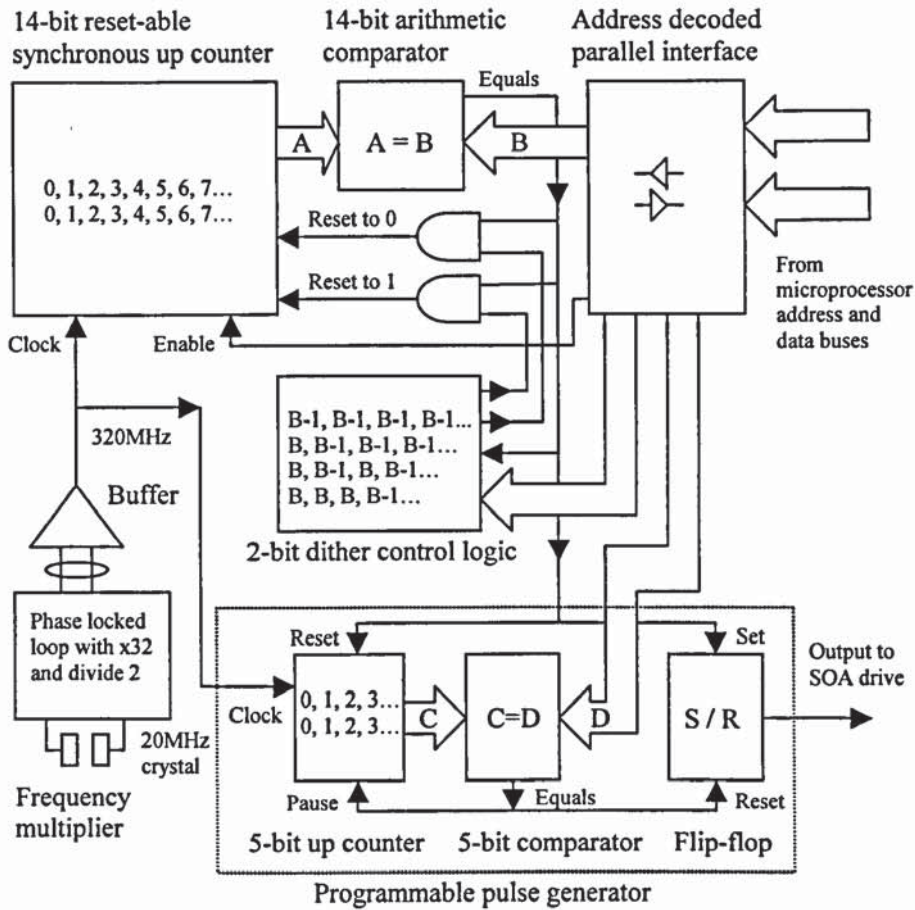
Figure 4.13 The fully programmable pulse generator, which was implemented using a frequency multiplier to create a 320MHz reference clock and an additional counter to provide a programmable pulse length facility

Parameter	Value
Oscillator frequency [MHz]	320
Maximum resonant cavity length supported [m]	10,240
Actual spatial tuning resolution [m]	0.31
Dithered effective spatial tuning resolution [m]	0.08
Maximum programmable pulse output duration [ns]	96
Resolution of programmable pulse duration [ns]	3.1

Table 4.6 The operating details and performance of the fully programmable pulse generator of Figure 4.13

4.12 Cavity-cycle-counting and dual-pulse variants

Although not required for the final system design, two further modifications were made to the programmable pulse generator to assist with some areas of the experimental research.

140

4.12.1 The cavity-cycle counting extension

The cavity-cycle counting pulse generator that was discussed in section 3.13 allowed experimental measurement of the cyclic evolution of the optical pulses in the resonant cavity through selective gating of the SOA drive.

The logic extension used to generate a specific number of equally spaced pulses (to specify the required number of cavity cycles), but to then miss a complete pulse (to terminate the cycling behaviour) is shown in Figure 4.14. This addition was implemented within the same CPLD as the original generator such that the old output was routed through the new logic. The extra counter and arithmetic comparator were triggered from the old output and used to selectively gate its signal.
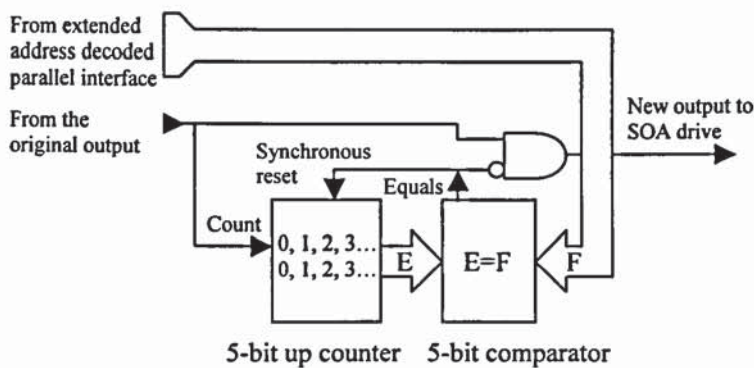
Figure 4.14 The logic extension to the programmable pulse generator, which was used to experimentally assess the cavity cycling behaviour of the optical pulses

4.12.2 Dual pulse variant

The second variant was the dual pulse programmable generator that was discussed in section 3.14. This allowed experimental verification of the hybrid WDM and TDM resonant cavity architecture by adaptive selection of multiple rear reflectors.

The logic extension that was required to achieve this behaviour consisted of an additional arithmetic comparator and a single OR gate, as shown in the complete schematic of Figure 4.15. It can also be seen that due to limited resources within the CPLD it was not possible to implement the dual pulse behaviour and maintain a counter length of 14-bits. This was, however, of no consequence for the experimental research since 8-bits were sufficient and it was also concluded that with the constant improvement in semiconductor density and speed, the ability to upgrade to a device capable of 14-bits with dual pulse functionality would likely be forthcoming.

141
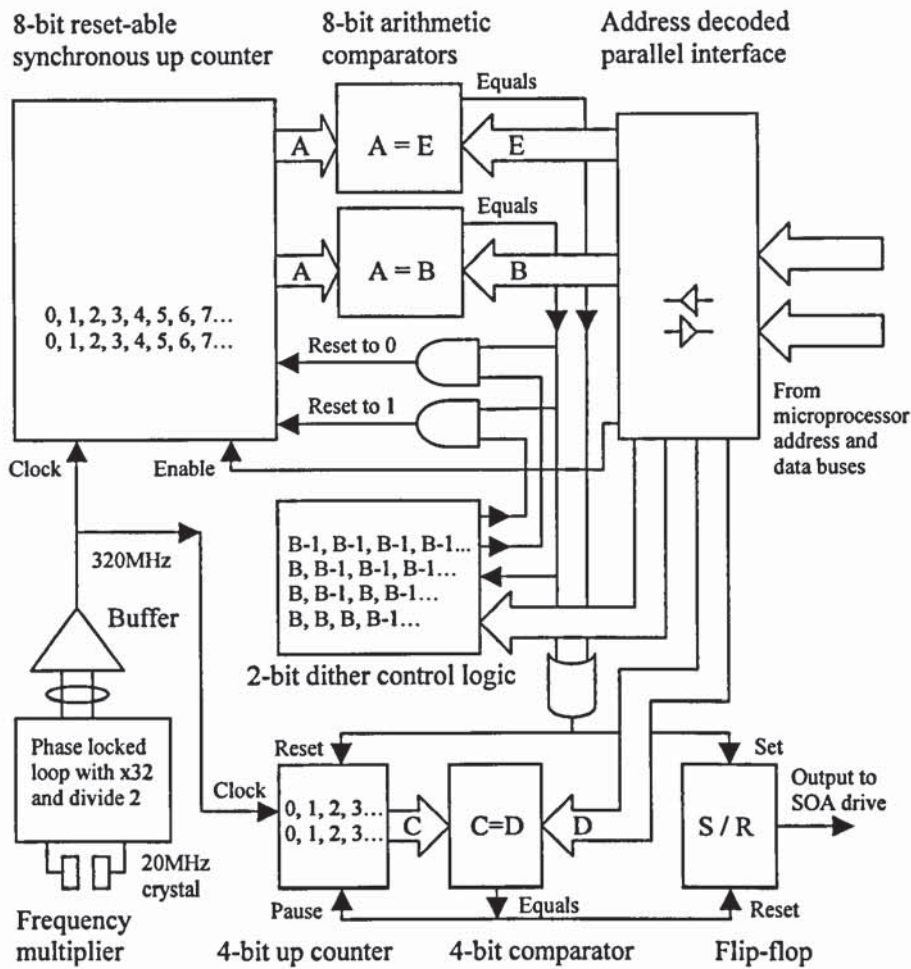
Figure 4.15 The complete schematic of the programmable pulse generator, including the logic extension that was required to provide dual-pulse behaviour

4.13 Variable gain control

In addition, research on the wavelength discrimination system showed that slight variations in FBG sensor reflectivity, cavity loss and tolerances in individual SOA performance parameters often resulted in significant variation in the cavity peak optical signal. This in turn caused differences in the power delivered to the wavelength detection system that meant that it was not sufficient to simply operate the SOA with a constant level of drive current for all devices with all possible sensor arrays. Instead it was essential that the operating conditions of the SOA could be tailored on a per sensor basis to ensure delivery of a constant signal level to the detection system and so optimise its performance.

Reference to typical SOA operating parameters, such as shown in Figure 4.16 and Figure 4.17, indicated that the peak optical power and gain (for both TE and TM primary orthogonal states of optical signal polarisation) were closely related to the operating drive current. Dynamic adjustment of the current was therefore deemed the

best method of controlling the SOA device performance in order to provide a match to variable cavity and sensor conditions.
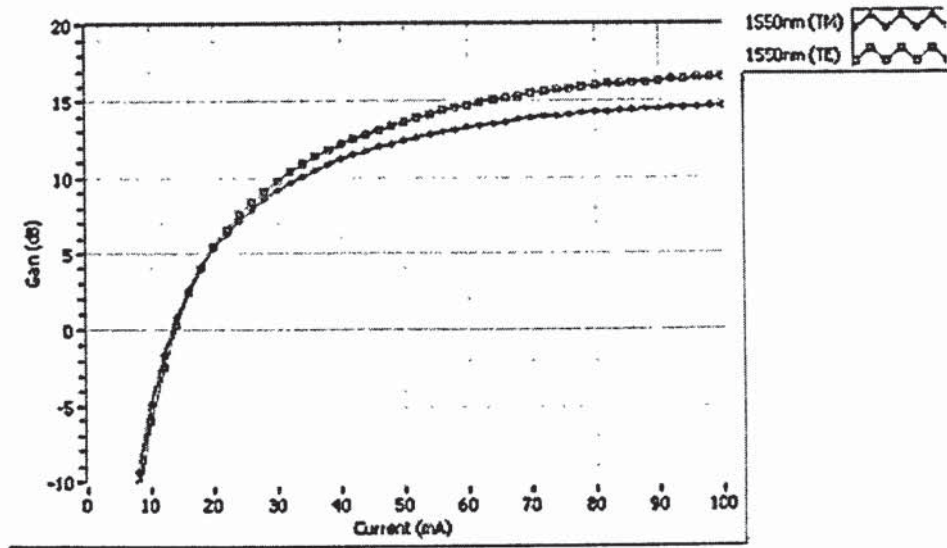
Figure 4.16 Typical SOA gain plotted as a function of forward drive current
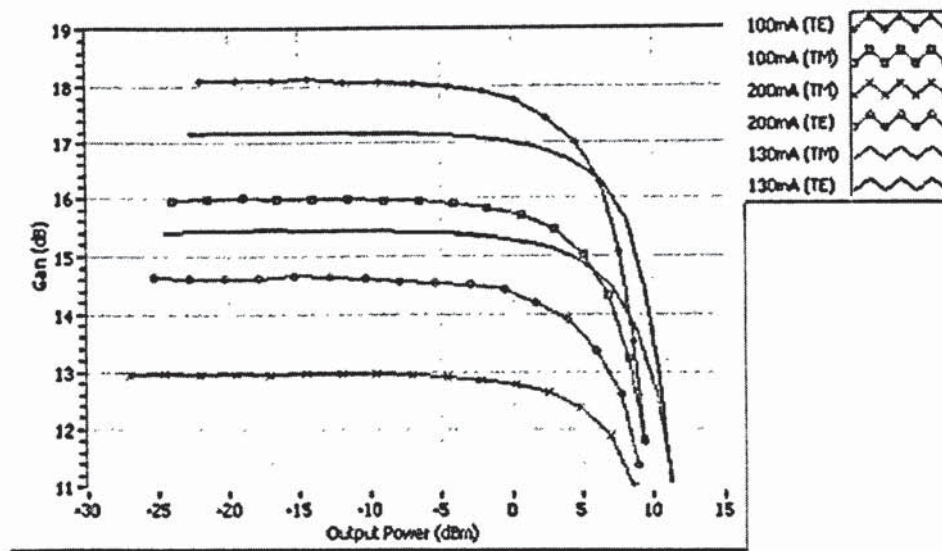
Figure 4.17 Typical SOA gain plotted a function of optical output power when operated with different levels of forward drive current

Figure 4.18 shows an overview of the final dynamic gain control system, which was based around an 8-bit digital to analogue converter and a high current amplifier. The design operated by providing microprocessor control of the supply voltage to the high speed SOA driver and hence allowed indirect adjustment of the SOA drive current without deterioration of switching performance.

143
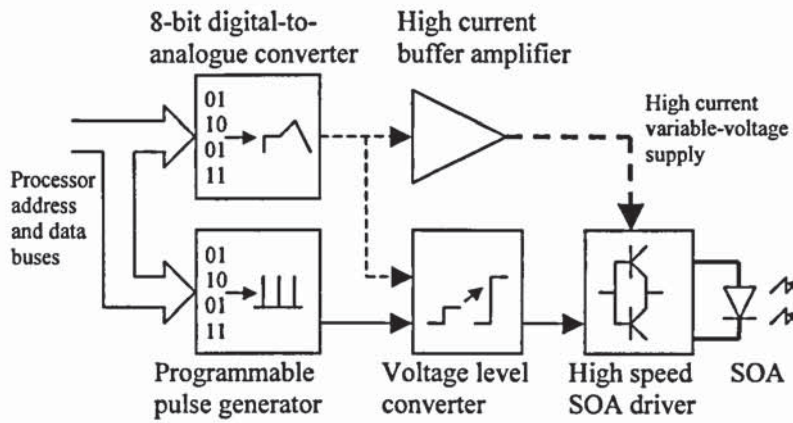
Figure 4.18 An abstract schematic of the SOA dynamic gain control system and its connection to the high speed SOA driver. (Dotted lines are analogue signals)

4.14 Chapter conclusion

A semiconductor optical amplifier drive sub-system was developed, enabling an SOA to generate highly defined, short optical pulses suitable for use in a TDM sensing system. Table 4.7 provides detail of the original target specification (driven by commercial requirements) compared against the resulting sub-system performance.

Parameter	Original target	Final performance
Maximum cavity length supported [m]	-	10,240
Resolution of gate switch timing [ns]	<19.4	3.1
Effective spatial tuning resolution [m]	<2	0.08
Minimum pulse output duration [ns]	15	~10
Maximum pulse output duration [ns]	75	96
Resolution of pulse output duration [ns]	-	3.1
Power consumption [mW]	-	<300
PCB footprint [cm^2]	-	8
Weight [g]	-	<50
Approximate cost [£]	-	25

Table 4.7 The full specification of the SOA drive sub-system that was used in the final commercial interrogator, including a comparison with the original design targets.

The final achieved specification was shown to exceed initial expectations, as the resultant sub-system had a footprint of only 8cm^2 and was capable of switching an SOA with sufficient speed and timing accuracy to allow high speed interrogation of sensors just 1m apart, thus proving its suitability for application within an interrogation system based on a resonant cavity architecture.

1   A. D. Kersey, M. A. Devis, H. J. Patrick, M. LeBlanc, K. P. Koo, C. G. Askins, M. A. Putnam and E. J. Friebele, 'Fiber grating sensors', *J. Lightwave Technol.*, **15**, 1997, pp.1442-1463

2   Y. J. Rao, 'Recent progress in applications of in-fibre Bragg grating sensors', *Optics and Lasers in Eng.*, **31**, 1999, pp.297-324

3   J. Millman, A. Grabel, 'Microelectronics' (2nd Edition), McGraw-Hill, New York (1987)

4   R. J. Smith, 'Circuits, Devices, and Systems' (3rd Edition), Wiley, New York (1976)

5   M. Tooley, 'Everyday Electronics Databook', Wimbourne Publishing Ltd, Wimbourne (1990)

6   M. O'Hara, 'EMC at component and PCB level', Newnes, Oxford (2003)

7   G. J. Ritchie, 'Transistor Circuit Techniques' (2nd Edition), Van Nostrand Reinhold, London (1987)

8   D. A. Neamen, 'Semiconductor Physics and Devices', Irwin, Boston (1992)

5 THE WAVELENGTH MEASUREMENT SUB-SYSTEM

5.1 Chapter overview

The previous two chapters have discussed the experimental proof of the resonant cavity architecture and the cycle of research and development that was conducted to produce a commercially viable implementation of the architecture, capable of operation with closely spaced, low reflectivity, commodity sensors.

This chapter continues this record of interrelated research and development by discussing the design, implementation and analysis of the other fundamental component required for a complete optical sensor interrogation solution; the wavelength measurement sub-system.

Beginning with a recap of the nature of the optical signals delivered by the resonant cavity time-division-multiplexing (TDM) architecture, the chapter first discusses the most compatible wavelength detection and measurement techniques that were available for design consideration. Details are then provided of the research and development conducted to implement the first sub-system design, which was based on the cost effective ratiometric measurement technique. Included are details of the decisions and compromises that were required as a result of fundamental limitations of the technique, as well as the measured performance of the final system.

The chapter then discusses the research and development conducted to produce a second, more robust and higher performance, but also more costly wavelength measurement sub-system, based on a diffraction element spectrometer. Experimentally measured results show that this design provided significantly improved performance and far fewer limitations.

5.2 Potential wavelength measurement techniques

Selection of the most appropriate wavelength measurement technique on which to base commercial development required a review of the nature of the optical sensor signals delivered by the novel resonant cavity architecture.

The proof of concept experiments of chapter 3 showed that unlike many wavelength-division-multiplexing (WDM) techniques that delivered broadband continuous-wave

146

optical signals from all sensors simultaneously, the resonant cavity approach was TDM based and therefore delivered pulsed optical signals of narrower bandwidth. Additionally, in contrast to electrically gated TDM techniques that required fast, noise-burdened signal processing electronics (for separation of weak sensor signals), the resonant cavity design was an optically gated approach that delivered strong, stable optical signals from each sensor individually.

Experimental results of sections 3.8 and 3.9 also demonstrated flexibility in the resonant cavity optical circuit design that allowed production of signals with different key characteristics. Figure 5.1 and Figure 5.2 review the options of having a very high peak signal power with a broadband background noise or a slightly lower peak signal power with a narrower background and a consequentially greater integrated OSNR.
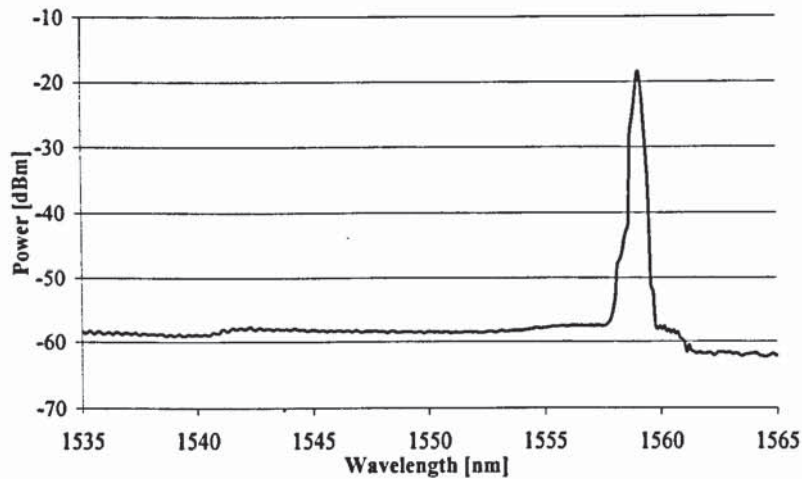
Figure 5.1 An OSA recording of the resonant cavity signal as extracted from the 'front' of the SOA
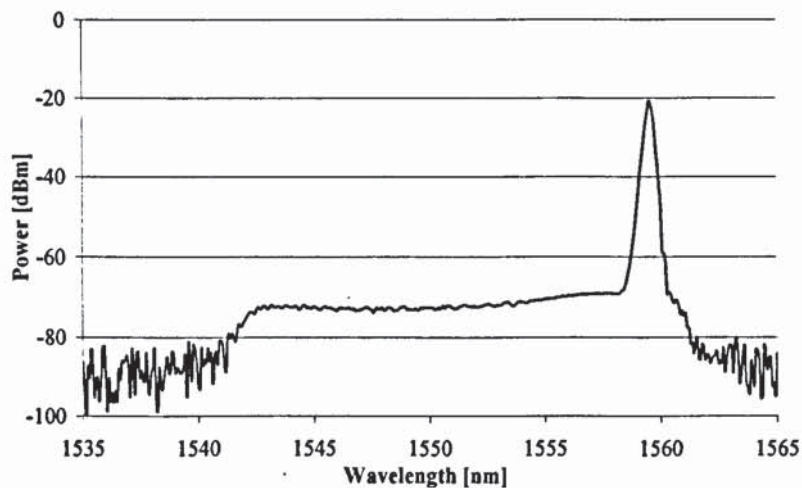
Figure 5.2 An OSA recording of the resonant cavity signal as extracted from the rear reflector

147

By comparing the nature of these optical signals with the requirements of the primary wavelength measurement methods three techniques were selected for further consideration. These were the scanning Fabry-Perot tuneable filter [1, 2], the passive ratiometric technique [3, 4] and the diffractive element spectrometer [5, 6, 7]. Table 5.1 highlights the primary characteristics that were known about each of these methods when commercial development on the interrogator first began.

	Scanning Fabry-Perot filter	Ratiometric technique	Diffractive element spectrometer
Complexity	High	Low	High
Product maturity	High	Low	Low
Speed	Low	High	Moderate
Wavelength range	Moderate - High	Low	Moderate - High
Physical stability	Moderate	High	Moderate - High
Spectral detail	High	Very low	Moderate - High
Cost	High	Low	Moderate - High

Table 5.1 The primary characteristics of the three wavelength measurement approaches that were considered for the commercial interrogator design

Of these methods, the scanning filter approach was the most commercially advanced, provided the highest spectral detail and was available in an easy-to-integrate component form. Being composed of a narrowband adjustable filter also meant that this approach was not detrimentally influenced by broadband ASE background noise. This factor enabled compatibility with either the very high peak power output configuration or the ASE-bandwidth-limited variant of the resonant cavity architecture. Unfortunately however, the low scanning speed, the inherent moving-part mechanical design and high cost of these devices meant that they were deemed inappropriate for further consideration.

The diffractive element spectrometer approach also had the advantage of providing a high level of spectral detail, but was also moderately fast and fundamentally solid-state. Unfortunately however, few commercial components were available and they were of moderately high cost and not directly compatible with the pulsed nature of the resonant cavity signal; factors that meant this approach was only considered as a secondary option.

The disadvantages of the ratiometric approach were an inherent low level of spectral detail and the fact that commercial maturity of devices capable of measuring >1nm was low. This limited maturity resulted from most devices being used in wavelength-locking feedback loops of laser diode driver systems, where a narrow wavelength range was sufficient. Additionally, the requirement for a large integrated optical signal-to-noise ratio (OSNR) signal for these devices dictated the use of the amplified spontaneous emission (ASE) bandwidth-limited output variant of the resonant cavity architecture; the higher peak power variant could not be employed, as the broadband ASE noise would have swamped the required signal. However, despite these limitations the advantages of the ratiometric approach were that it offered the potential for a small, very low cost, all solid-state solution that could operate at high speed from the pulsed resonant cavity signal. For these reasons the technique was given highest priority for further research and development.

5.3 Development of the ratiometric wavelength measurement sub-system

Having chosen to develop a wavelength measurement system employing the ratiometric technique it was decided that commercial sub-components would be used where possible, to reduce research and development costs and product time-to-market. A study was therefore conducted into the commercial availability of environmentally qualified components that incorporated both the wavelength detection opto-electronics and the signal processing electronics in a single hybrid module. Unfortunately no such modules were found, but a variant of a laser diode wavelength locker element was discovered that had the potential to provide the environmentally qualified opto-electronic front-end, if custom designed processing electronics could be developed to support it.

5.3.1 The Santec OWL-10 Wavetracer

The OWL-10 Wavetracer component from Santec, Japan was a prototype derivative of their standard wavelength locker component with a significantly wider operating wavelength range. The schematic of this component is shown in Figure 5.3. Externally the device was a hermetically sealed can of dimensions 40x15x8mm with a single-mode fibre pigtail for the optical input and a 6 pin single-in-line electrical termination for the output. Internally the device consisted of an optical micro-bench containing an optical beam splitter, a thin-film edge-filter, two photodiodes and a temperature sensor. The primary difference between this prototype Wavetracer variant and the standard

component was the width and profile of the edge filter, which was >12nm for the Wavetracer and <1nm for the standard component.
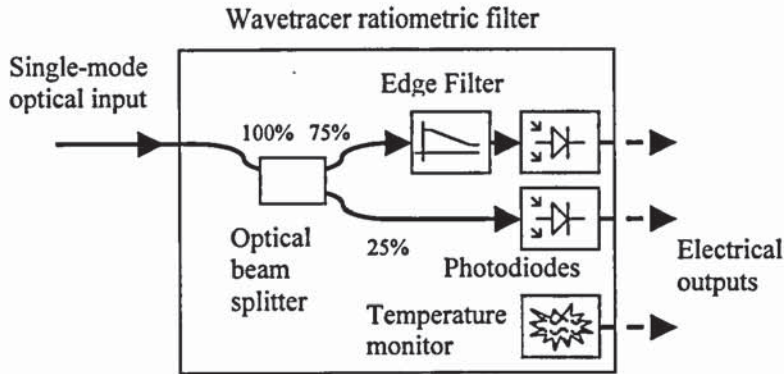
Figure 5.3 Schematic of the OWL-10 Wavetracer combined ratiometric filter and photo-detectors component from Santec, Japan

The mode of operation of the Wavetracer was similar to other ratiometric techniques, as follows:

- The narrow bandwidth optical signal under measurement entered the device via the standard single-mode fibre pigtail

- It was then split into two paths via the optical beam splitter in a ratio of approximately 25%:75%

- The 25% signal was then immediately incident on a standard photodiode to provide a reference measurement of the total incident optical power

- While the 75% signal was passed through a thin-film edge filter, the profile of which meant that the level of optical transmission was dependant on the wavelength of the incident signal

- The transmitted portion of the signal was then targeted onto a second photodiode to provide a measurement of its intensity

- Taking the mathematical ratio of the two photodiode measurements therefore provided an assessment of the wavelength of the incident signal

- Finally, a temperature sensor was also available to provide any fine calibration and adjustment to cater for environmental effects

150

5.4 Initial evaluation of the Wavetracer

As the Wavetracer was a prototype device, the manufacturer supplied performance data was limited (to a few discrete values) and so an internal evaluation was conducted. Figure 5.4 shows the experimental set up used, which included the construction of two simple trans-impedance photodiode amplifiers (connected to a National Instruments PC based DAQ data acquisition card) for measurement of the output response and an Agilent 8164A tuneable laser for provision of a variable wavelength optical input.
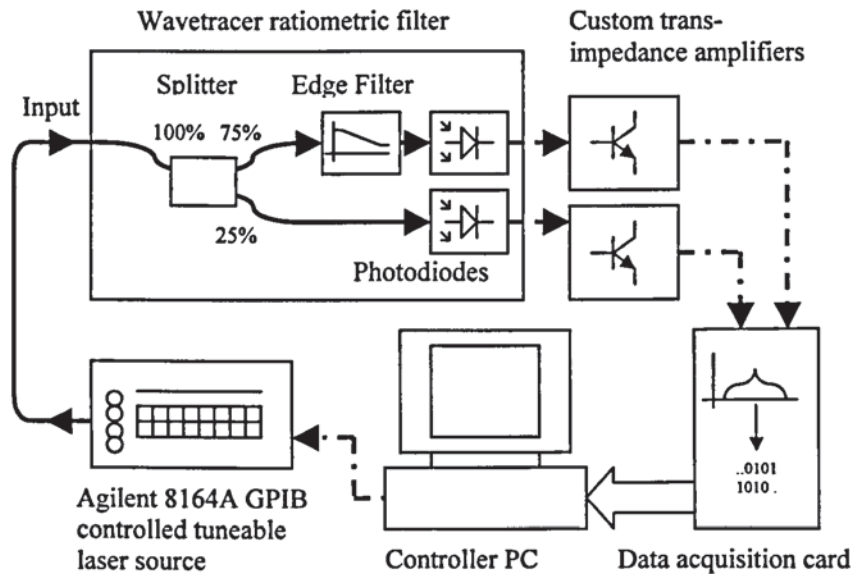
Figure 5.4 The experimental set up used to evaluate the performance of the prototype Wavetracer ratiometric filter

Figure 5.5 shows the measured response of the two Wavetracer photodiodes and the mathematical ratio of these signals when the tuneable laser was software stepped across the full operating wavelength range of the device.

151
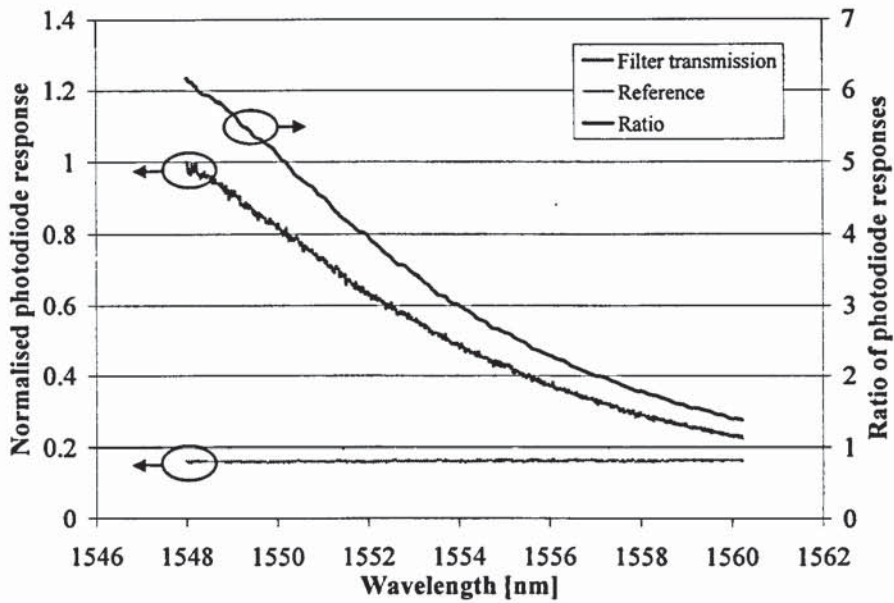
Figure 5.5 The response of the two Wavetracer photodiodes to a tuneable laser optical input stepped across the full operating wavelength range of the device

The general shape of the photodiode response was a curve that correlated well with the manufacture supplied discrete measurement values, but closer inspection of any small range of the response highlighted numerous flat regions. These occurred with approximately equal periodicity, as shown in Figure 5.6, and were detrimental to obtaining sensor wavelength measurement information with consistently high resolution across the full operating range.
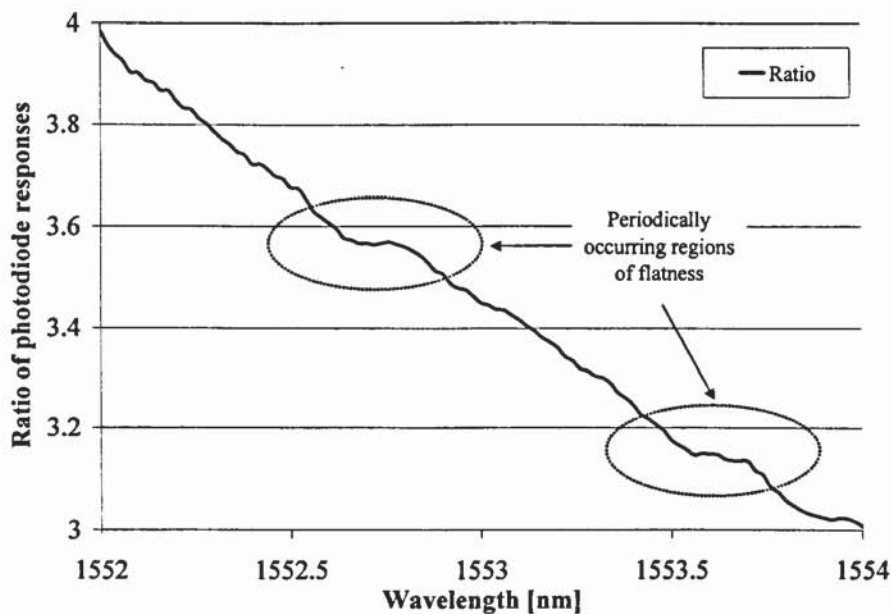
Figure 5.6 Closer inspection of a small section of the photodiode ratio response profile showing periodic regions of flatness

Fortunately further inspection by the manufacturer into the cause of this periodic flatness confirmed its existence and provided proof that it was the result of a Fabry-Perot cavity effect manifesting between the optical beam splitter and the edge filter. A corrective measure to the design, which consisted of adjusting the angles of incidence of these elements, was found to significantly reduce the back reflection effect and remove the periodic flatness from all later devices, as shown in Figure 5.7.
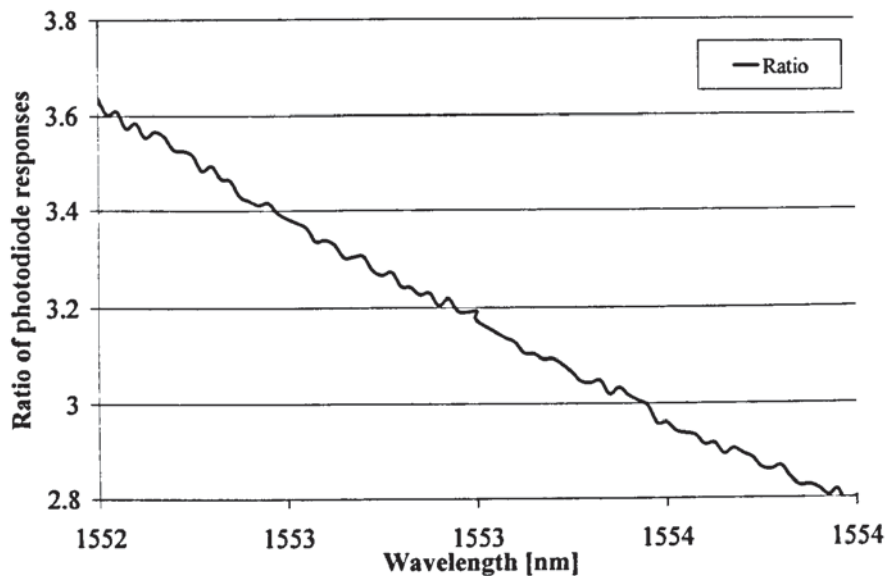
Figure 5.7 Closer inspection of the photodiode ratio response of a corrected ratiometric filter showing that no significant regions of flatness are present

5.5 Trials of the ratiometric filter using the output from the resonant cavity architecture

Following initial assessment using the tuneable laser, trials of the ratiometric filter were then conducted using the resonant cavity optical circuit. Figure 5.8 shows the optical circuit used, which included two low reflectivity FBG sensors, one of which was temperature tuned using a thermoelectric cooler, and two fused fibre couplers. The first coupler had 80:20 splitting ratio to extract the resonant cavity signal from the rear reflector (to reduce the out-of-band ASE, as explained in chapter 3), whilst the second had a 50:50 ratio to equally split this extracted signal between the OSA and the ratiometric filter. Some slight manual adjustment of the trans-impedance gain of the photodiode amplifiers was then carried out to optimise the dynamic range of the electrical signals delivered to the PC data acquisition card, as a result of the change from the tuneable laser to the resonant cavity signal.
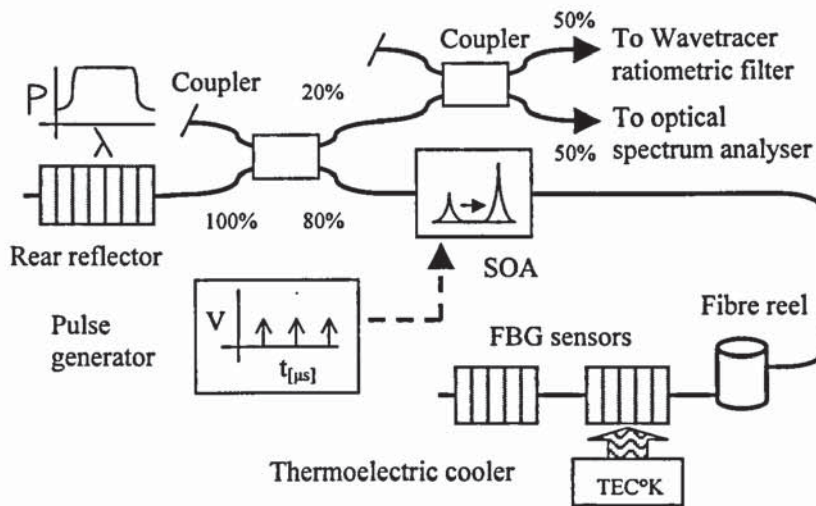
Figure 5.8 The optical circuit used to experimentally verify the response of the Wavetracer ratiometric filter to the resonant cavity optical signal

By temperature tuning the FBG sensor and recording both the wavelength of the cavity signal on the OSA and the response of the ratiometric filter using the PC, the graph shown in Figure 5.9 was produced. Figure 5.10 was then produced to show the residual error in the photodiode response with respect to a linear regression best-fit line. It can be seen that over the narrow wavelength range that was possible using temperature tuning, the response of the filter was largely linear with only minor profile ripples that equated to <20pm of effective measurement error.
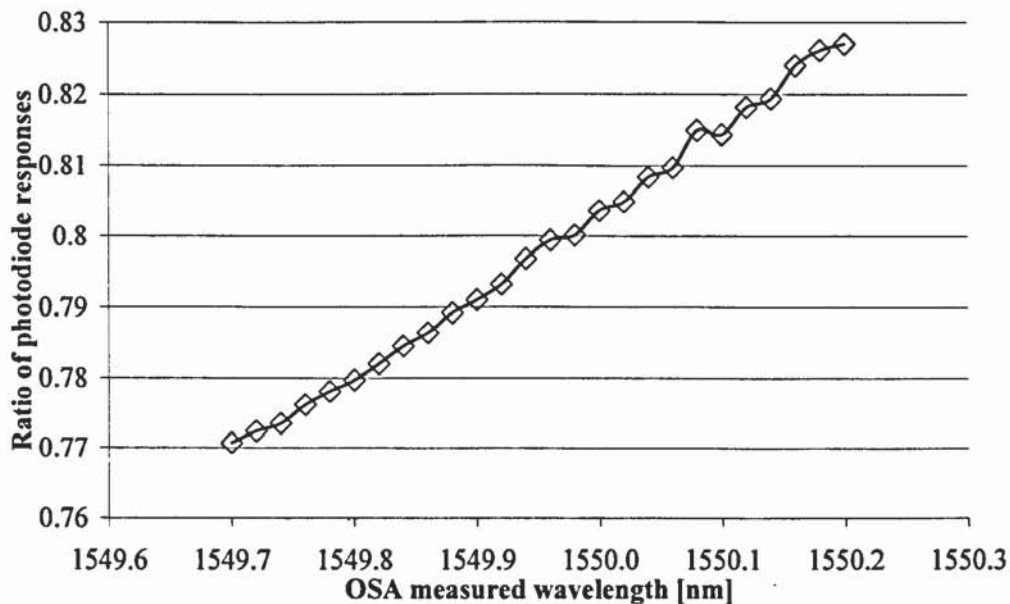
Figure 5.9 The response of the Wavetracer ratiometric filter to a temperature tuned resonant cavity signal
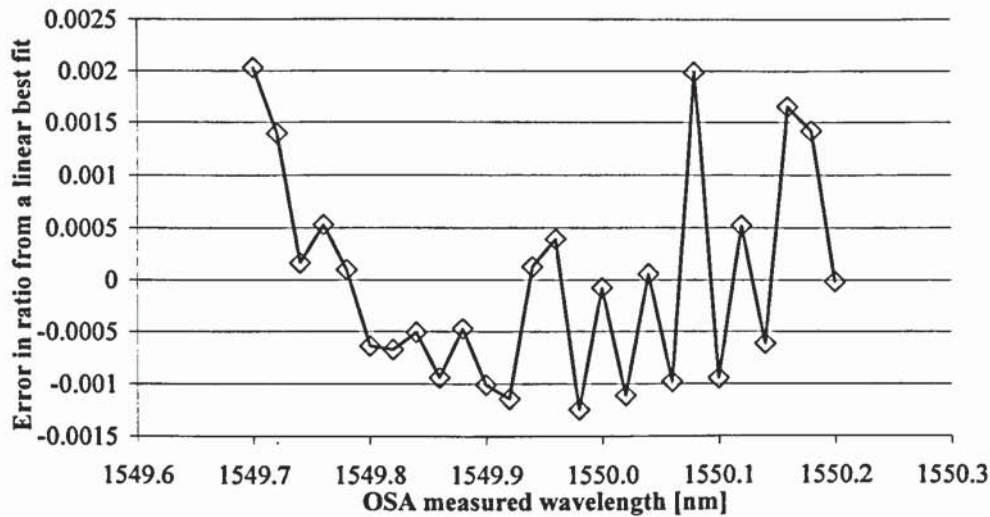
Figure 5.10 The residual error in the ratiometric filter photodiode response of Figure 5.9 when compared to a linear regression best-fit line

5.6 The design requirements for the signal processing electronics

Verification of compatibility between the resonant cavity architecture and the ratiometric filter was of fundamental importance, but the experimental evaluation also highlighted that the basic trans-impedance amplifiers and data acquisition hardware required significant improvement. The basic trans-impedance amplifiers were designed with a very low signal bandwidth such that the pulsed nature of the optical signal was fully smoothed prior to measurement by the DAQ hardware. This ensured that no synchronisation was required between the sample acquisition phase and the incoming optical pulses and that any delays between the measurements from each photodiode would not affect the accuracy of the final ratio result. However, having a signal bandwidth of <5Hz also meant that several seconds were required between adjustment of the optical input signal and its subsequent measurement. This was in contrast to the final commercial system requirements that dictated that measurements be taken in significantly less than 2ms in order to provide a performance of 500 samples per second.

Creating trans-impedance amplifiers and an analogue-to-digital converter that were highly linear and of low noise, but with sufficient bandwidth to process signals in <2ms required a number of compromises. These included:

- The fixing of the gain of each photodiode amplifier for all input signal levels, since it was not possible to maintain the required level of total linearity with multiple levels of gain

155

- Having a different set level of gain for each photodiode amplifier to match the signal range expected

- The use of a dual sample-and-hold ADC that could take a sample from each of the photodiodes simultaneously, but then perform the conversion sequentially, to eliminate timing and temperature fluctuations

- The synchronising of the acquisition phase of the ADC to the pulsing of the optical input such that signal droop in the amplifiers was constant for all samples

The linearity of the system was limited to the current state-of-the-art ADC components, which provided up to 16 bits of resolution. Taken simplistically such ADCs could be expected to provide a maximum measurement resolution of 1 in 2^{16} or 1.52×10^{-5}, which when equated directly to a wavelength measurement range of 12nm, would give an optical wavelength resolution of approximately 0.25pm. Referring to section 2.2.3, this would suggest a temperature measurement resolution of ~0.25°C or strain resolution of ~0.2με. In reality however, it was realised that the real resolution would be significantly worse for the following reasons:

- The ratiometric edge filter did not have a linear relationship between transmitted power and wavelength. This curved relationship would reduce resolution at higher wavelengths

- Localised imperfections in the filter profile would reduce resolution

- The optical input may not match the full working range of the ADC; thus weak signals would only occupy 13 or 14 bits of significance

- The combination of optical noise, electrical noise and imperfections in the ADC would reduce resolution by several bits

- Any non-linearity in the photodiodes, amplifiers, the ADC and the coupling components could also reduce performance

Following consideration for these factors it was concluded that full-band resolution could be as poor as 10pm, but that research and development based on the ratiometric

filter should still continue on the basis of cost. Focus was however given to reducing the impact of these limiting factors, where possible.

In particular, attention was given to ensuring a highly linear amplifier response, a minimisation of power-supply-borne electrical noise and the development of an optical gain control system to counter the lack of gain switching that was available from the electrical amplifiers.

The earliest variant of this optical gain control system consisted of a simple potentiometer for adjustment of the SOA drive current, such that all sensors were affected together. In contrast, the final dynamic optical gain control system allowed full independent software adjustment of the SOA drive current for each sensor individually. This later system allowed optimisation of the optical input signal level delivered to the ratiometric filter on a sensor-by-sensor basis and helped to ensure maximum coverage of the ADC measurement range; as described in detail in section 4.13.

5.7 Performance evaluation of the ratiometric wavelength measurement system

Following the first phase of development, the signal processing electronics were integrated with the optical and opto-electronic elements and a series of experiments were conducted to evaluate the performance and commercial viability of the design.

5.7.1 Short-range linearity and resolution measurement

Short-range linearity and resolution measurements were conducted by temperature tuning an array of four low reflectivity FBG sensors using the optical configuration of Figure 5.11.

157
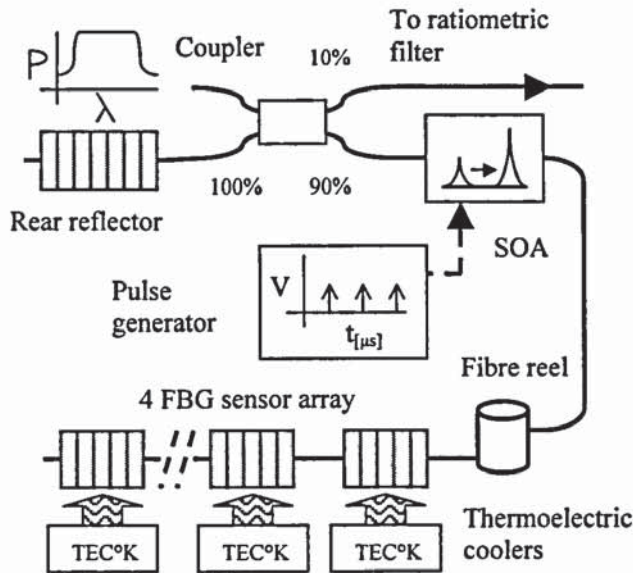
Figure 5.11 The optical configuration used to measure the linearity and resolution of the ratiometric measurement system

Figure 5.12 shows the response of each of the four sensors when their temperature was adjusted between 2°C to 50°C in steps of 3°. It can be seen that the ratiometric response from each sensor exhibited a strong linear relationship with temperature, but that the exact gradient varied slightly between sensors.
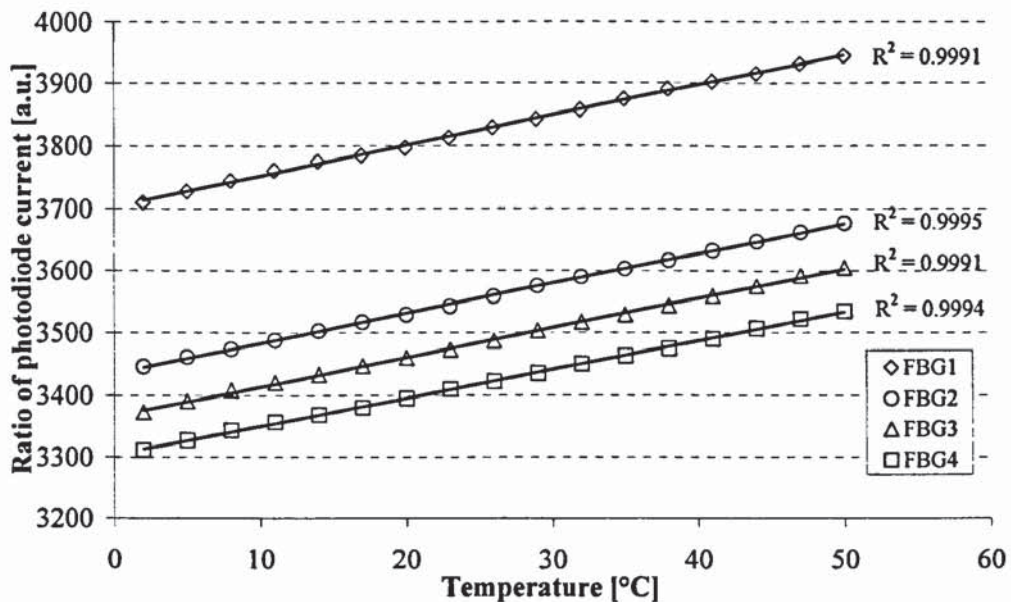
Figure 5.12 The ratiometric response of four low reflectivity FBG sensors when individually temperature tuned using thermoelectric coolers

Table 5.2 lists the gradients of a least-squares regression fit for each of the four sensors and the variation in each when normalised to that of sensor 1. The indicated difference of up to 4.7% was considered to arise from two primary sources:

158

- Variations in the optical profile and OSNR of the cavity signal produced by each sensor
- Marginal differences in the zero-strain wavelength of sensors that meant their operation was on slightly different sections of the filter curve, with consequential differences in localised linearity

Fibre Bragg grating sensor number	Gradient of ratiometric response to temperature	Gradient normalised to that of sensor 1 [%]
1	4.815	100.0
2	4.820	100.1
3	4.743	98.5
4	4.587	95.3

Table 5.2 The gradient of least-squares regression linear fit for each of the sensors shown in Figure 5.12 and their normalisation against that of sensor 1

The initial conclusion from these findings was that the ratiometric filter provided a highly linear response over a small measurement range with only a slight variation between sensors. Therefore, for the many applications that only required a general detection of strain change and not high precision measurements, it was decided that sufficient accuracy would result from the use of a single calibration curve for all sensors. However, these results also highlighted that for those applications that dictated greater absolute accuracy, with a strong sensor-to-sensor repeatability, a 4.7% variation was unacceptable and so on-site calibration of individual sensors would be required. The cost and difficulty in providing such calibration was expected to vary between applications and would occasionally reduce the marketability of the system, but this was not considered a fundamentally limiting factor to overall commercial success.

Resolution assessment was also conducted using the experimental configuration of Figure 5.11, but in this case finer temperature tuning was carried out over just 1°C in steps of 0.1°. To reduce the effect of measurement noise and improve the accuracy of the result, mean averaging was performed over 32 samples prior to the production of Figure 5.13. Independent OSA measurements also showed that the total 1°C temperature change created only 10.2pm of wavelength shift; a result that implied a very impressive resolution of around 1pm (with 32 times averaging) for the ratiometric system.
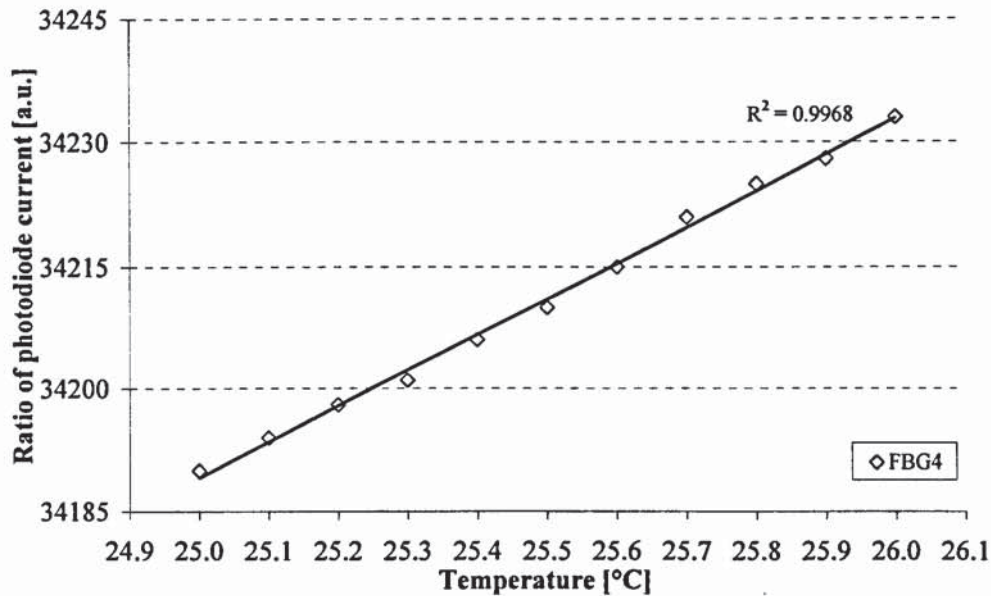
Figure 5.13 The results of resolution evaluation by temperature tuning sensor 4

5.7.2 High-speed strain measurement

Using the sensor calibration data collected during the temperature tuning experiments, high-speed strain measurement performance was then assessed using the experimental configuration of Figure 5.14. This first high-speed trial consisted of three 2m spaced, 4% reflective FBG sensors bonded to a composite cantilever beam using cyanoacrylate. Momentary application of load to the free end of the beam was used to induce oscillations, which were then detected as strain changes by the three sensors.
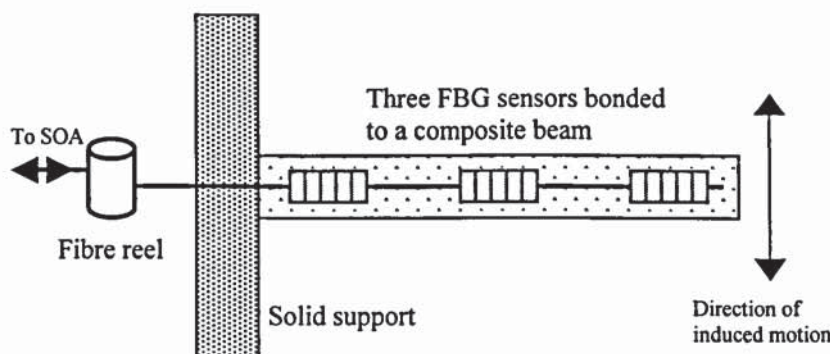
Figure 5.14 The experimental composite beam used to assess the high-speed strain measurement performance of the ratiometric wavelength measurement system

Figure 5.15 shows the strain induced in the beam from a single impulse when interrogated at 35Hz per sensor. This was achieved by cycling at a rate of 105Hz between each of the sensors in turn without applying any averaging. The wavelengths were mathematically offset for clarity during graphing and the inset was provided to give a detailed view of sensor 1. The results clearly demonstrated the damped

160

sinusoidal oscillations of the beam, as well as the expected diminishing level of strain as function of distance from the supported end.
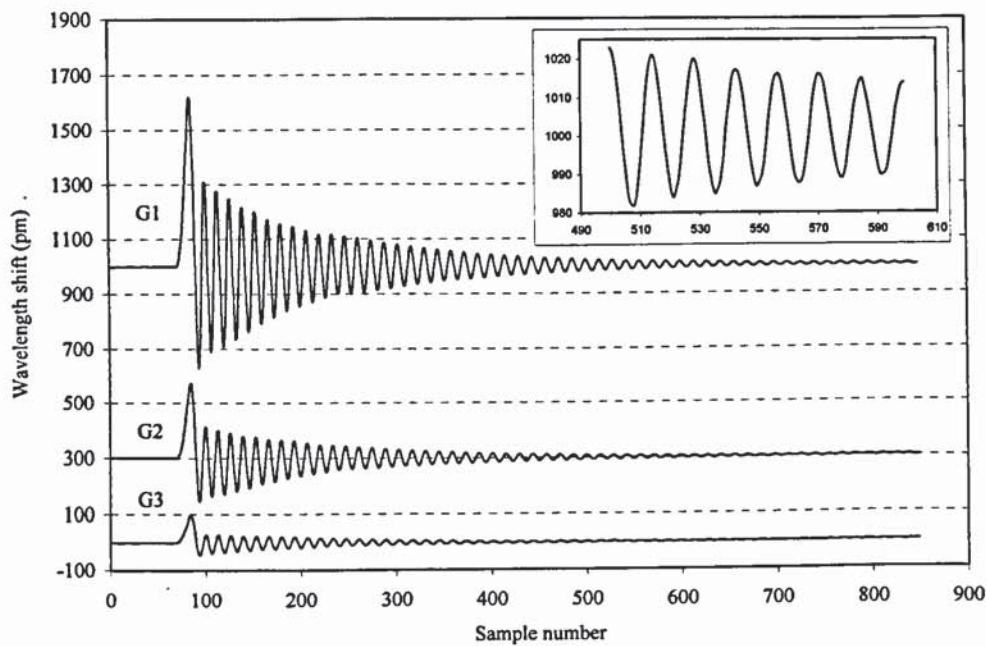
Figure 5.15 The measured strain induced in a beam after a single impulse, when interrogated at 35Hz per sensor. The inset provides a detailed view of sensor 1

Most significantly, the experiment highlighted a unique characteristic of the ratiometric TDM system. This was the potential for dynamic selection of the interrogation configuration in response to the changing application environment.

> When a general overview of a complete structure was required the system could be configured to interrogate all sensors at a modest rate, but on response to an event at a single sensor, the configuration could dynamically change to provide a far higher interrogation rate that was focused on just those sensors adjacent to the trigger.

This property of the resonant cavity architecture was considered highly significant for applications in online structural condition monitoring and vibration analysis, since it could not be achieved with the commercial WDM systems that employed standard scanning filter technology. With this notion, a slight, temporary change was made to the bandwidth of the trans-impedance amplifiers to allow the interrogation of a vibrating steel beam. This steel structure was similar in design to the composite beam, but had a significantly higher natural frequency of oscillation and therefore required a

161

greater rate of interrogation. Only a single low reflectivity FBG sensor was used for this experimental trial, but it was intended that a true system would employ numerous sensors, as previously described.

The results and post-analysis of interrogating the sensor at 4.4kHz are shown in Figure 5.16; included are a Fourier analysis of the signal and a detailed view of an oscillation peak. It can be seen that the natural resonant frequency of the structure was around 40Hz, but that the oscillations were not purely sinusoidal. The slight asymmetry in the oscillatory pattern, which was clearly apparent at this data capture rate, was a true feature of the vibration that resulted from the beam mounting arrangement.
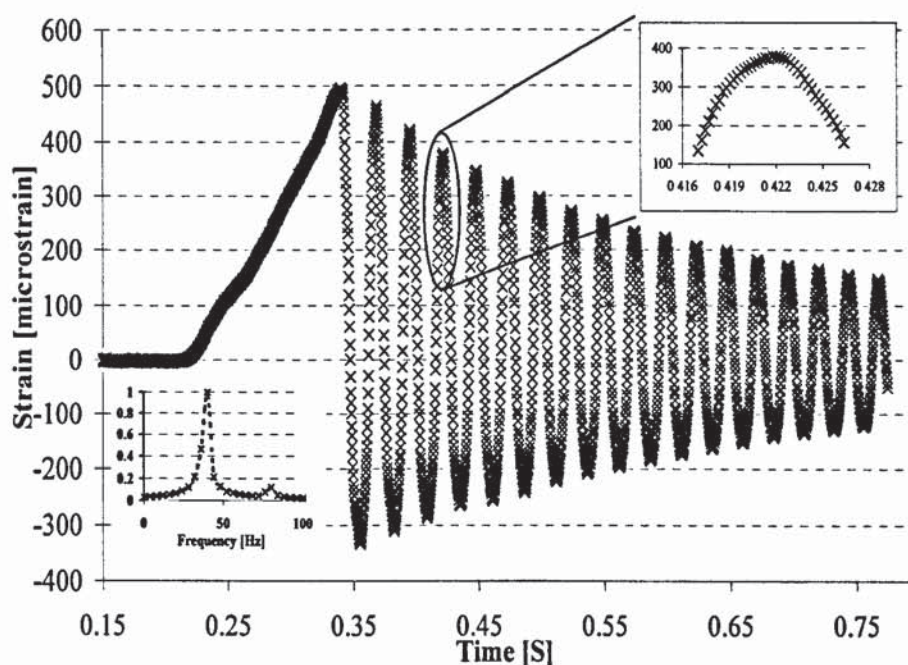
Figure 5.16 The measured strain induced in a plucked steel structure when interrogated at 4.4kHz. Inset 1 shows a Fourier analysis of the signal. Inset 2 shows a detailed view of a single oscillation peak

5.7.3 Polarisation dependency of measurements

Having assessed the response of the system to actual changes in temperature and strain, experiments were conducted to determine the level of error induced by changes in optical polarisation. It was known that physical disturbance of the fibre circuit, temperature effects and long-term drift were all contributory factors to changes in optical polarisation, and so assessment of the impact of these changes on the accuracy of the final measured signal was critically important.

162

Figure 5.17 shows the experimental configuration used to evaluate these effects. A HP 11896A polarisation controller was inserted into the sensor array to adjust the cavity signal polarisation, whilst assurance of full coverage of all polarisation states and a measurement of the degree of polarisation was achieved using a Profile PAT9000B polarisation analyser connected to the end of the array. The actual error was found by recording the maximum excursions of the ratiometric detector output when the system was set to monitor a strain-relieved, temperature stabilised FBG sensor.
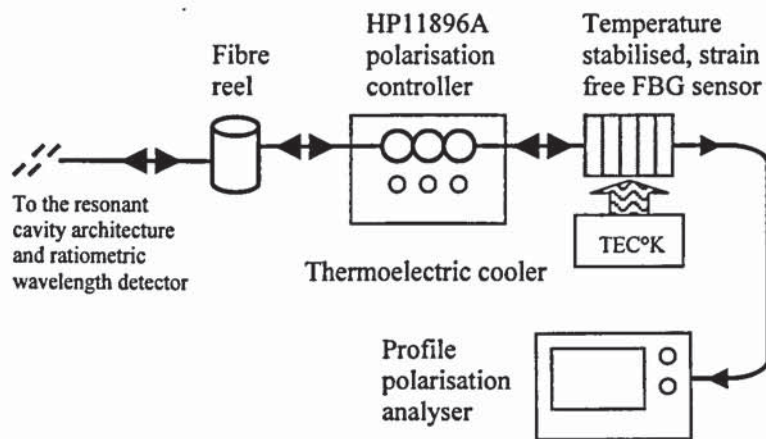
Figure 5.17 The experimental optical configuration used to assess the level of polarisation dependant error in the ratiometric wavelength measurement system

Figure 5.18 and Table 5.3 show the measured results when the experiment was repeated with the sensor held at four different temperatures. It can be seen that under worst-case conditions the polarisation induced wavelength error was 30pm. This equated to an approximate equivalent error of 3°C in temperature or 25µε in strain.
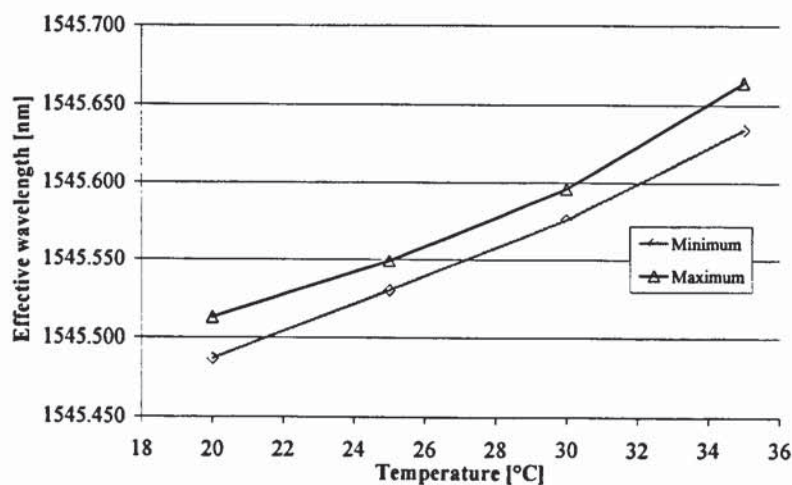
Figure 5.18 Graphical results of polarisation evaluation for the ratiometric wavelength measurement system

Temperature of sensor [°C]	Minimum effective wavelength [nm]	Maximum effective wavelength [nm]	Variation in wavelength [pm]
20	1545.487	1545.513	26
25	1545.530	1545.549	19
30	1545.576	1545.596	20
35	1545.634	1545.664	30

Table 5.3 Tabular results of polarisation evaluation for the ratiometric wavelength measurement system

Since the level of polarisation induced measurement error was higher than was preferred for some commercial applications research began into ways of reducing it. Careful examination of the results from the previous experiment highlighted that measurement extremities usually occurred when the cavity signal was in a high degree of polarisation and so attempts were made to depolarise the signal. Ideally an electronic (active) polarisation scrambler would have been used to verify this idea, but as no such equipment was available, research was conducted using three different passive depolarisers from Phoenix Photonics. Unfortunately however, due to the narrow bandwidth of the cavity signal, insufficient depolarisation occurred using these devices. A commercial decision was therefore taken to cease this work on the basis that the likely cost of depolarising the signal would outweigh the benefits.

5.7.4 Cavity attenuation dependency

Discussions with system vendors and end-users regarding deployment of fibre sensing solutions indicated that for many installations system optical loss was carefully controlled and could be made stable and repeatable. However, a few applications were highlighted where losses arising from connectors, fibre patch cords and splicing could not be controlled, but could vary considerably as a result of composite production techniques or a requirement for routine system disassembly and maintenance. For these reasons it was considered essential that analysis be conducted into the interrogator performance under varying levels of cavity loss.

Figure 5.19 shows the experimental configuration used to evaluate system performance under variable loss conditions. Due to equipment limitations two different attenuators were actually employed, for small values of attenuation a manually operated device was used, which provided loss of between 0 and 3.7dB. For larger attenuation levels (above 3.8dB), a HP8156A electronic attenuator provided better accuracy.
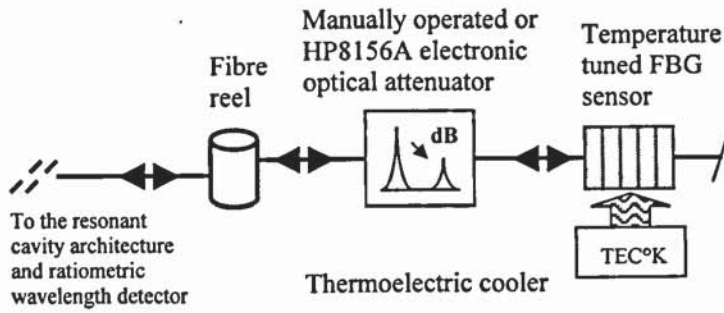
Figure 5.19 The experimental configuration used to evaluate performance of the ratiometric wavelength measurement system detector under variable loss conditions

Figure 5.20 and Figure 5.21 show two different representations of the wavelength shift reported by the ratiometric measurement system when the sensor temperature was tuned from 15°C and 30°C and the cavity attenuation was varied between 0 and 6.8dB. It can be seen that the ratiometric filter reported an exponentially increasing wavelength shift as the level of cavity attenuation increased. For attenuation changes below 3.6dB this wavelength shift was <50pm and was considered acceptable for some commercial applications, but for attenuation above 6dB an unacceptably high shift of >100pm was noted.
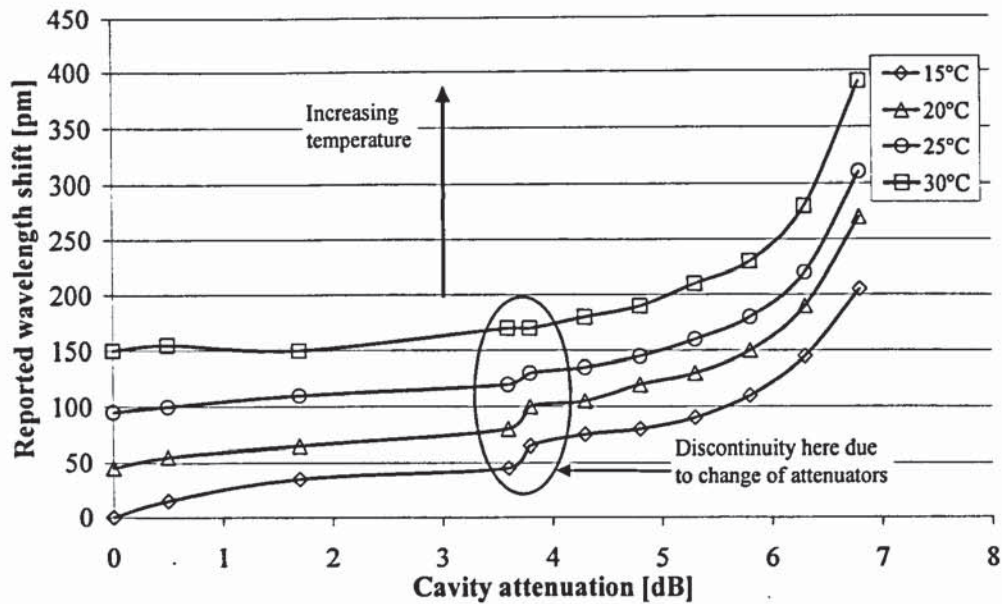
Figure 5.20 The change in reported sensor wavelength for increasing cavity attenuations, at various temperatures
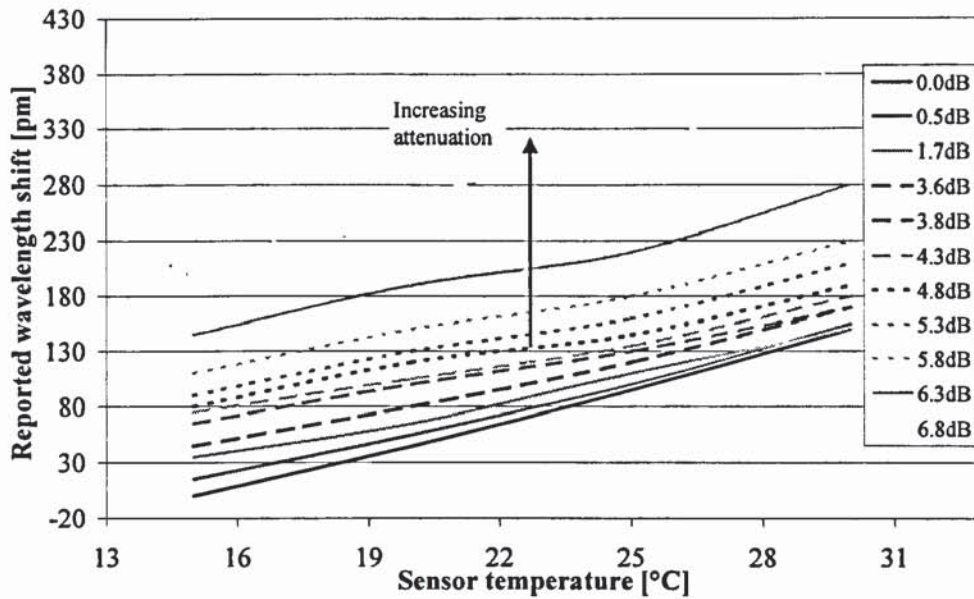
Figure 5.21 The change in reported sensor wavelength for increasing sensor temperature, for various levels of cavity attenuation

The results of the attenuation experiments of section 3.11 showed that this apparent wavelength shift resulted from a reduction in the resonant cavity signal OSNR, which occurred as the cavity loss was increased. This had the effect of causing a greater change to the edge filter photodiode signal than to the reference photodiode signal, so manifesting as a total effective change in ratio, without any actual change in signal wavelength. It was concluded that this dependence on OSNR was an inherent property of the ratiometric technique and was a consequence of having only two variables with which to provide complete analysis of the optical signal. Therefore, to improve the overall wavelength detector loss performance, research was conducted to provide additional photodiode signals to reference the level of the ASE background noise. Attempts were made to use this information to calibrate out the effects of changing OSNR, but the performance improvement was not significant.

5.7.5 Conclusion of the ratiometric measurement system evaluation

The results of the performance analysis concluded that although the component costs of the ratiometric wavelength measurement system were very low, the combination of polarisation sensitivity and response to changing loss would limit commercial success of the interrogator for some applications. Furthermore, market forecasts and a budget analysis showed that production of two variants of the interrogator that employed different wavelength detection methods was not economically viable until a requirement existed for very high volume. For this reason research and development of

the ratiometric wavelength measurement sub-system was paused, for continuation at a later time.

5.8 Development of the diffractive element spectrometer-based wavelength measurement sub-system

Following the decision to pause research and development of the ratiometric based system, focus turned to the second preferred wavelength measurement approach; the diffractive element spectrometer.

5.8.1 The channel monitor

As discussed previously, few complete spectrometer-based measurement modules were discovered that were suitable for operation at 1550nm, and of these none were directly compatible with the resonant cavity signal or considered cost-effective. Therefore, a telecommunications channel monitor was chosen for evaluation with the intention that it be used as the opto-electronic front end for a bespoke wavelength measurement sub-system. The device was an early prototype of a unit designed to monitor the optical power of 80 adjacent data channels on the 50GHz ITU grid (around 1550nm) and was based around several diffraction elements and a detector array, as depicted in Figure 5.22.
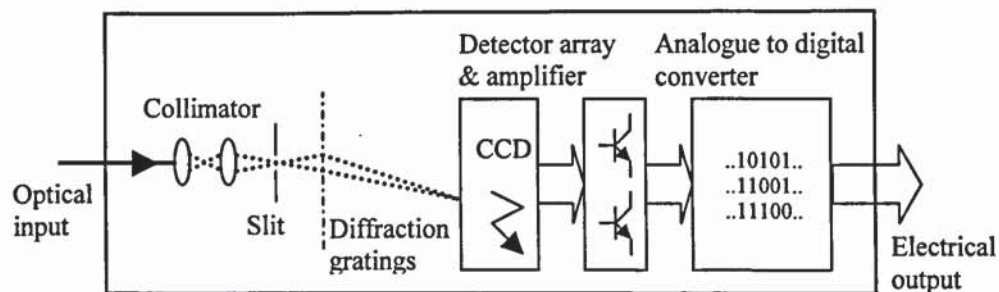
Figure 5.22 Schematic of the spectrometer based channel monitor evaluated for the opto-electronic front-end of the wavelength measurement sub-system

5.8.2 Hardware assisted synchronisation and data transfer

The prototype channel monitor was provided with basic PC evaluation software and a connectivity kit based around a standard data acquisition card. This proved sufficient for initial testing with a tuneable laser, but was not appropriate for evaluation of the device using the resonant cavity architecture, due to the lack of a trigger input for synchronisation between the channel monitor internal ADC and the pulses of the resonant cavity signal. Additionally, as the device was only intended for monitoring slowly varying signals, the electrical interface was serial in nature. This reduced the

number of connections required, but demanded considerable software overhead and so provided a very slow update rate.

Due to these limitations, a dedicated hardware interface was designed to provide synchronisation between the resonant cavity optical pulses and the channel monitor ADC. Also included in this development was circuitry for high speed, hardware assisted data fetch, serial to parallel conversion and a standard microprocessor bus interface; features that all helped to improved the interrogation rate. The schematic for this hardware, which consisted of programmable logic, configured by hardware description language (HDL), is shown in Figure 5.23.
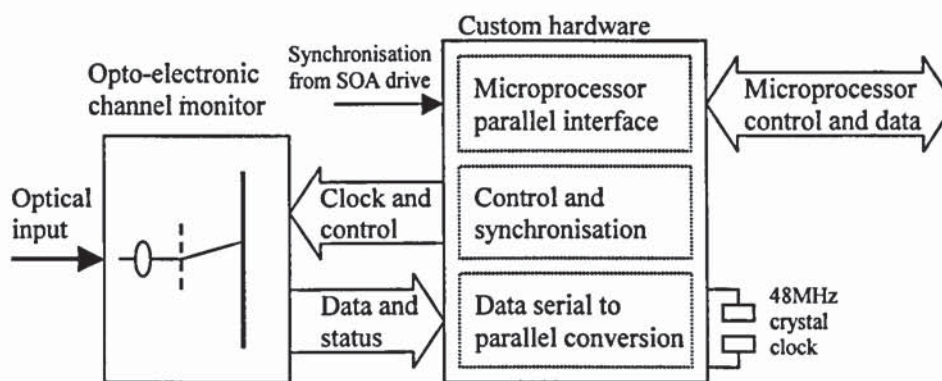
Figure 5.23 An overview schematic of the custom hardware interface developed to provide compatibility between the channel monitor and the resonant cavity optical signal

5.8.3 Integration and optimisation of the channel monitor

On completion of the synchronisation interface, integration into the resonant cavity architecture began, as shown in Figure 5.24. Due to the operation of diffractive element spectrometers, out-of-band ASE background noise was inherently filtered from the required signal and so the very high peak power configuration of the resonant architecture was employed. The coupler ratio, channel monitor analogue amplifier gain and the interface synchronisation dwell were all optimised to ensure the full working span of the channel monitor ADC was utilised. When employed with the previously developed dynamic optical gain control system, these optimisations all ensured that the usable signal strength was maximised and electrical noise minimised, but that saturation of the opto-electronics was avoided.
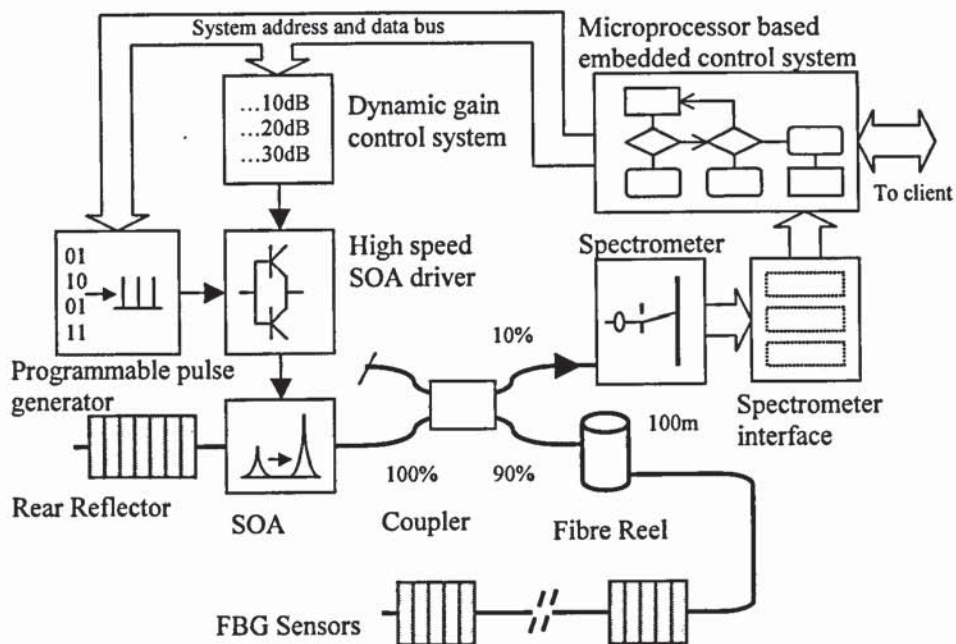
Figure 5.24 Schematic showing the channel monitor based spectrometer integrated with the resonant cavity optical circuit and other opto-electronic sub-systems

5.9 Performance evaluation of the spectrometer based wavelength measurement system

Performance evaluation of the completed system was conducted using similar experimental procedures to those used for the ratiometric-based system, but as a result of the increased system integration many of the tests were automated for efficiency.

Figure 5.25 shows a graphical view of typical measurement data for five strain-relieved, low reflectivity sensors interrogated at 50Hz each (i.e. by cycling between each sensor in turn at a rate of 250Hz and without averaging). For clarity during graphing the mean values were mathematically subtracted from each recording and then sensors 1,2,4 and 5 were offset by +10, +5, -5 and -10pm respectively.

169
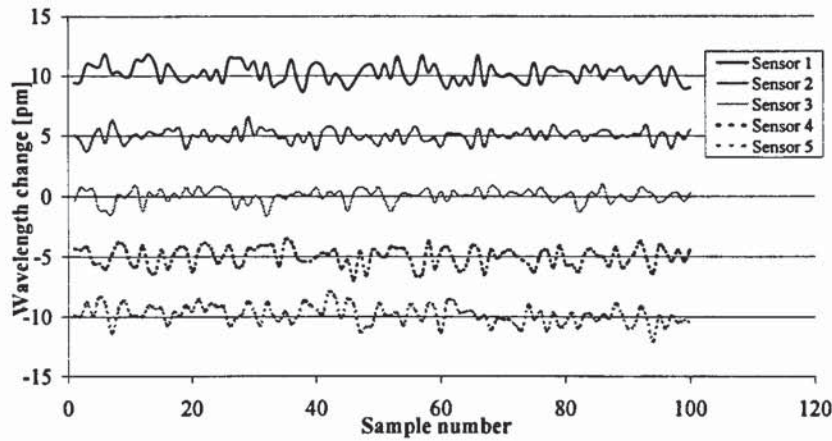
Figure 5.25 Typical data from five strain-relieved, low reflectivity sensors interrogated at 50Hz each using the spectrometer based wavelength measurement system

Table 5.4 shows an analysis of this data and highlights the extremely impressive noise performance of the system.

Fibre Bragg grating sensor number	Peak – peak sensor noise [pm]	Root-mean-square noise [pm]
1	3.1	1.00
2	2.8	0.54
3	2.5	0.91
4	3.4	0.87
5	4.1	0.96

Table 5.4 Numerical analysis of the data from Figure 5.25 showing the noise performance of the spectrometer based wavelength measurement system

Figure 5.26 shows the results of fine temperature tuning a single FBG sensor to determine the wavelength measurement resolution. Measurements were taken at 0.1°C step intervals over a 1°C total range using a sampling rate of 150Hz and a factor of 16 mean averaging. The results confirm the expected total wavelength shift of ~10pm and highlight a strong measurement linearity. Therefore, Figure 5.27 shows the calculated residual error between the measured results a linear regression best-fit line. It can be seen that the residual error confirms an impressive measurement resolution of better than 1pm for the system.

170
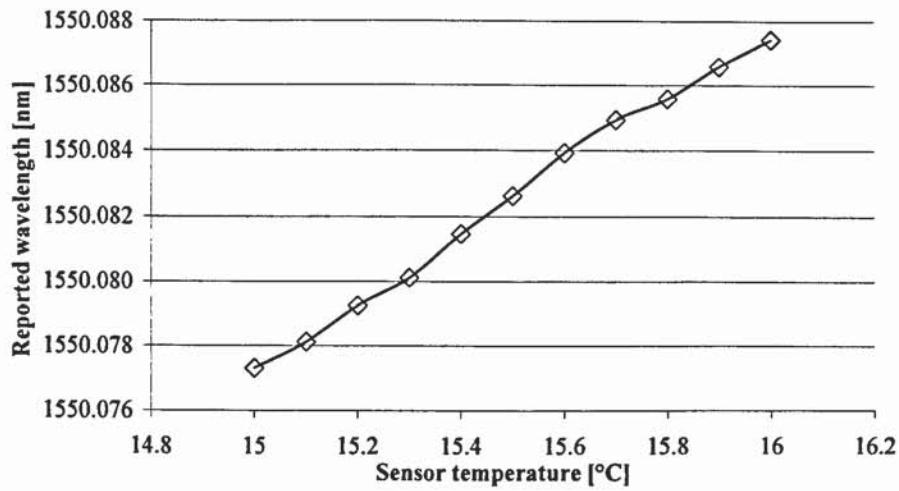
Figure 5.26 The response of the spectrometer based wavelength measurement system when a FBG sensor was temperature tuned using a thermoelectric cooler
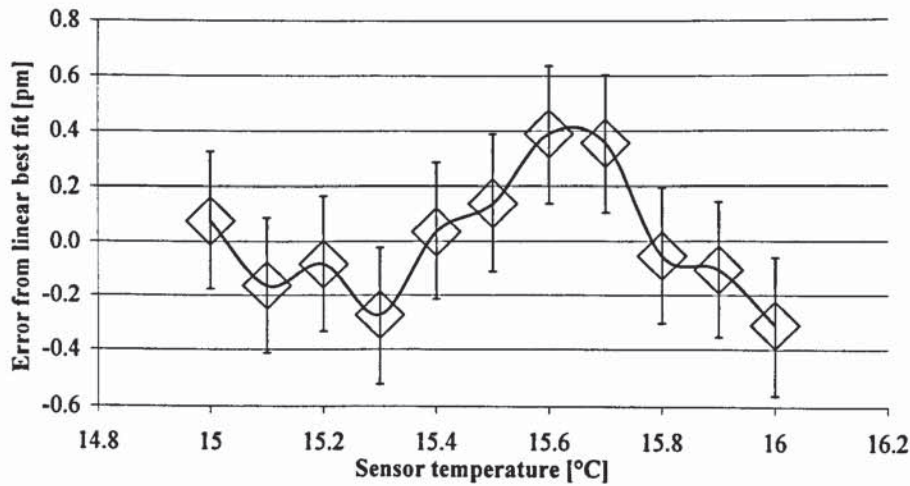
Figure 5.27 The residual error in the reported wavelength response of Figure 5.26 when compared to a linear regression best-fit line

Figure 5.28 shows the results of optical polarisation effects on reported signal wavelength for three sensors, where each has been mathematically offset for clarity. It can be seen that even under worst-case conditions, the combined effects of the polarisation change and the general signal noise still only result in 10pm peak-to-peak wavelength shift.

171
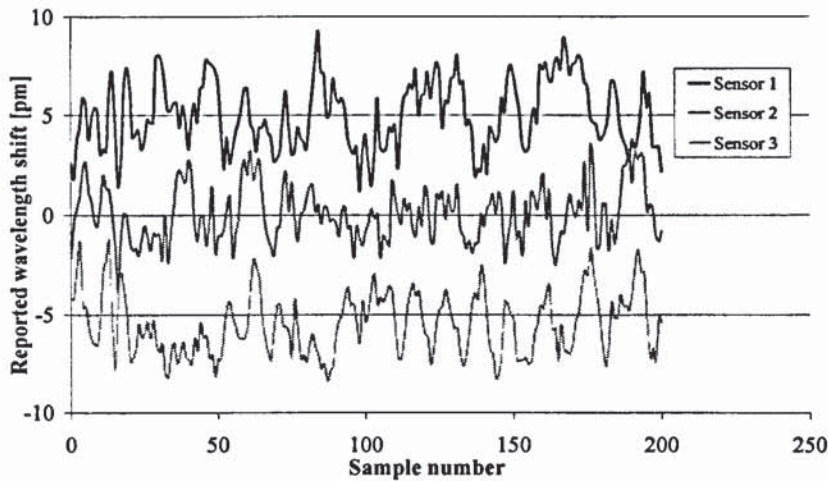
Figure 5.28 The combined noise and polarisation change reported by the spectrometer based wavelength measurement system for three low reflectivity sensors

Noise, resolution and polarisation results were better than required for all anticipated market applications, but earlier work had identified that the ability of the system to cope with significant fluctuations in optical loss was of greatest commercial importance. Therefore, a detailed experimental analysis into the effect of cavity attenuation was conducted. Figure 5.29 shows the signal noise from three strain-relieved, temperature-stabilised, 4% reflectivity sensors, as a function of increasing cavity attenuation. Exceptionally high system performance was highlighted as all sensors operated with <3pm RMS noise for attenuation up to 11.3dB and <4pm RMS noise for attenuation up to 12dB. Most importantly however, Figure 5.30 shows that the maximum reported wavelength shift for the sensors was <2pm for attenuation up to 10dB and <4pm for attenuation up to 12dB. This level of performance was exceptionally high and far better than was required for all anticipated applications.
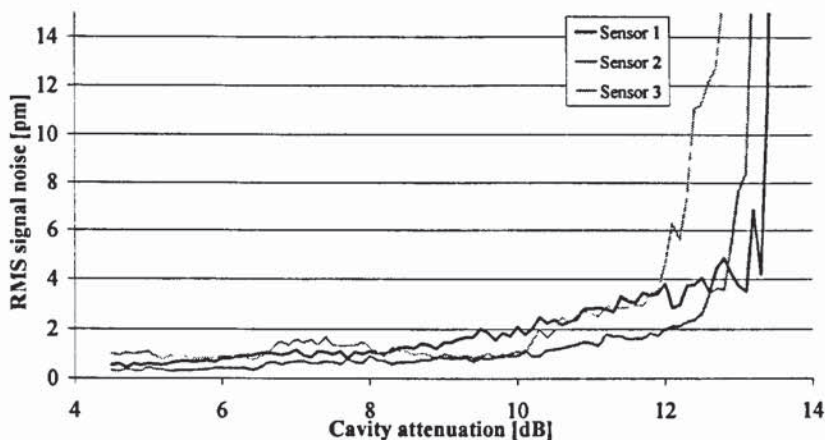
Figure 5.29 The signal noise of three low reflectivity sensors as a function of cavity attenuation when measured using the spectrometer based wavelength measurement system

172
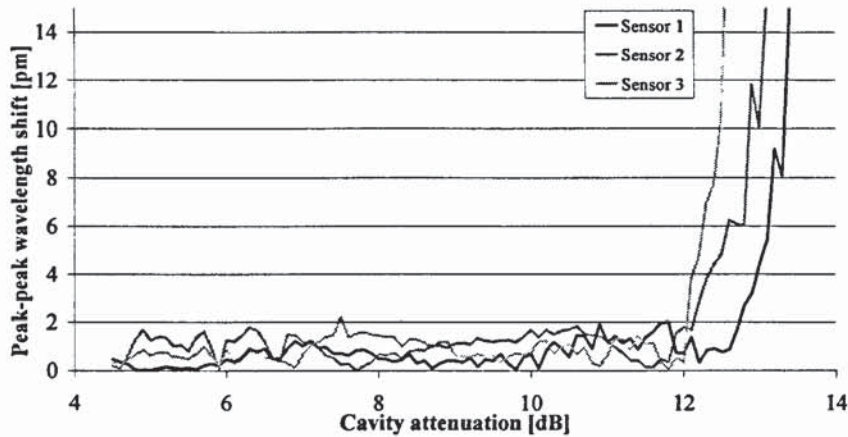
Figure 5.30 The wavelength shift for three low reflectivity sensors as a function of cavity attenuation when measured using the spectrometer based wavelength measurement system

5.10 Chapter conclusion

This chapter detailed the research and development conducted on two wavelength detection sub-systems; the ratiometric approach and the spectrometer-based wavelength detection system. Both approaches provided excellent short-range linearity, low noise and picometre resolution, but it was found that each offered a different commercial opportunity. The ratiometric approach was shown to offer great potential for a very low cost, solid-state solution for access into high volume markets such as automotive. In these markets manufacturing repeatability and the application environment are well controlled, but the high cost of current optical sensing is considered prohibitive. By contrast, the spectrometer-based wavelength measurement system developed from a channel monitor was slightly more expensive, but provided a significantly higher system performance. Exceedingly stable, low noise operation was verified for a wide range of possible operating conditions, including those of high polarisation fluctuation and large variation (>12dB) in the optical power within the resonant cavity.

1   A. D. Kersey, T. A. Kerkoff, W. W. Morey, 'Multiplexed fiber Bragg grating strain-sensor system with a fiber Fabry-Perot wavelength filter', *Opt. Lett.*, **18**, 1993, pp.1370-1372

2   Y. N. Ning, A. Meldrum, W. J. Shi, B. T. Meggitt, A. W. Palmer, K. T. V. Grattan, L. Li, 'Bragg grating sensing instrument using tunable Fabry-Perot filter to detect wavelength variations', *Meas. Sci. Technol.*, **9**, 1998, pp.599-606

3   S. M. Melle, K. Liu, R. M. Measures, 'A passive wavelength demodulation system for guided-wave Bragg grating sensors', *Photon. Technol. Lett.*, **4**, 1992, pp.516-518

4   M. A. Davis, A. D. Kersey, 'All-fiber Bragg grating strain-sensor demodulation technique using a wavelength division coupler' *Electron. Lett.*, **30**, 1994, pp.75–77

5   C. G. Askins, M. A. Putnam, 'Instrumentation for interrogating many-element fiber Bragg grating arrays embedded in fiber/resin composites', *Proc. SPIE Smart Sensing, Processing and Instrumentation*, 1995, **2444**, pp.257

6   C. Jáuregui, A. Quintela, J. M. L. Higuera, 'Interrogation unit for fibre Bragg grating sensors that uses a slanted fiber grating', *Opt. Lett.*, **29**, 2004, pp.676-678

7   K. Zhou, A. G. Simpson, X. Chen, L. Zhang, I. Bennion, 'Fiber Bragg Grating Sensor Interrogation System Using a CCD Side Detection Method With Superimposed Blazed Gratings', *Photon. Technol. Lett.*, **16**, 2004, pp.1549-1551

6 Environmental performance, Software and Applications

6.1 Chapter overview

In contrast to the previous three chapters that discussed the fundamental building blocks of the fibre sensor interrogator, this chapter concentrates on essential, peripheral elements of the system. These were required to enhance the end-user perception of the instrument and to allow its use in a diverse range of environments.

The chapter begins by discussing the environmental performance criteria required from the instrument to enable successful deployment and operation in harsh industrial applications. Details are given of the design methods used during development and the compliance testing subsequently completed to ensure market acceptance.

Embedded, Linux and Windows based software developed to automate set-up and installation of the instrument and to return measurement data for analysis is then discussed. Included is an outline of the design methodologies used and the application-programming interface (API) provided to original equipment manufacturer (OEM) customers to allow production of their own custom system extensions.

The chapter concludes with description and results from a range of applications in which the interrogator has been employed to-date. Included are details of the many electrical interfaces, data exchange protocols and software solutions that were developed. Together these enabled compatibility of the interrogator with the dynamic laboratory environment, allowed integration with industrial machinery, active control and monitoring in distributed systems and provided for self-contained, battery-powered, remote sub-sea operation.

6.2 Environmental performance

In order to ensure that the interrogator was applicable to a wide range of key commercial markets it was essential to design a system of sufficient robustness to operate under a diverse range of environmental conditions. Having designed for such conditions, it was also essential that testing was conduced to ensure compliance and that final certification was provided through assessment by a recognised independent body.

175

6.2.1 Environment performance requirements

Table 6.1 shows the environmental requirements for some of the interrogator's key market applications. The essential requirements are shown first and were those conditions under which the system was required to operate in order to be acceptable for a particular application. The ideal environmental requirements are shown in parenthesis and were harsher conditions under which the system would ideally operate, but which were not essential for market acceptance.

Market application	Storage temp. [°C]	Operating temp. [°C]	Operating humidity	Operating vibration	Operating shock
Bench top laboratory instrument	-10 / +60 (-40 / +80)	+15 / +25	0 / 70%	None (Mild)	None (Mild)
Distributed temperature monitor	-20 / +60 (-40 / +80)	0 / +50 (-20 / +70)	0 / 70% (0 / 95%)	None (Mild)	None (Mild)
Wind energy, control and monitoring	-20 / +60 (-40 / +80)	0 / +50 (-40 / +80)	0 / 70% (0 / 95%)	Mild (Severe)	Mild (Severe)
Deep sub-sea monitoring	-20 / +60 (-40 / +80)	0 / +10 (0 / +35)	0 / 10% (0 / 95%)	Mild (Severe)	Mild (Severe)

Table 6.1 The environmental requirements of the fibre sensor interrogator for different market applications. Values in parenthesis were the 'ideal' requirements

6.2.2 Design approach to meet environmental requirements

Due to the high state of maturity of electronic and mechanical components, designing for adequate humidity and temperature performance using these devices simply required selection of the correct 'industrial' or 'automotive' grade parts and adherence to the manufacturers' recommendations and example design data. However, design for compliance with regard to the opto-electronic components was significantly more difficult due to the lower maturity of the photonics industry. Liaison and significant cooperative work with manufacturers was required on many occasions to ensure an adequate, if often only modest, level of performance was possible from some devices.

Design for vibration and shock performance also required a greater degree of attention. Wind energy applications dictated the harshest operating performance, since systems were required to operate for >20 years in the hub of rotating wind turbine blades. Careful consideration was given to the mounting of all large components, both to and through the printed circuit board, to ensure adequate damping of all natural resonance

within the assembled system. To aid this design process, finite element analysis software was used to model the mass and stiffness of all components over 5 grams.

6.2.3 Environmental performance analysis and certification

Following the construction of each new prototype, performance under variable temperature conditions was usually analysed using an in-house temperature cycling chamber. Coupled with bespoke logging software this provided initial system evaluation over the range −5°C and +50°C. This was sufficient to estimate parameters such as heatsink performance, thermo-electric cooler (TEC) workload and temperature dependant wavelength error.

The final performance evaluation was conducted by a third party, dedicated, environmental testing company. The independent company operated with full compliance and traceability to national and international standards, as required by aerospace and military certification bodies. Table 6.2 shows the full environmental performance criteria that the fibre sensor interrogator was independently verified and certified as having met or exceeded. This level of certification was better than that required by the wind energy industry, which, as previously stated, dictated the harshest environmental performance of all the applications targeted to-date.

Environmental test criteria	International specification	Test summary	Equipment used	Certified result
Mechanical shock	IEC68-2-27 Test Ea	15G 11ms, 5 times per axis, 6 axis	Ling Dynamics 824 Shaker	Pass
Vibration	IEC68-2-6 Test Fc	1.5G sinusoid sweep 10-150Hz, 4mins / test, 4 tests / axis, 3 axis	Ling Dynamics 824 Shaker	Pass
High temperature storage	IEC68-2-2 Test Bb	60° C, 200 hours	Gallenkamp Hotbox 1	Pass
Low temperature storage	IEC68-2-1 Test Ab	-40° C, uncontrolled humidity, 200 hours	Ringway temperature chamber	Pass
Temperature cycling	IEC68-1-14 Test Nb	0° C to 50° C, 4° C per min ramp, 15 min dwell at extremes, 20 cycles	Ringway temperature chamber	Pass
Damp heat	IEC68-2-56 Test Cb	50° C, 80% relative humidity, 144 hours	Fisons environment chamber	Pass

Table 6.2 The independently verified and certified environmental performance of the fibre sensor interrogator

6.3 Software and programmability

6.3.1 The lower-layer software systems

As with most modern electronic equipment a large part of the total functionality of the interrogator was provided by software based systems. Employing re-programmable microprocessor based hardware in the final solution was both cost effective and versatile. Splitting of the software over a range of layers, from the top-level user application through to the lowest level hardware access drivers, provided a modular, easy to design, debug and support system that could be adapted and enhanced, without significant impact on other system components. Figure 6.1 shows an overview of the layered hardware and software components.
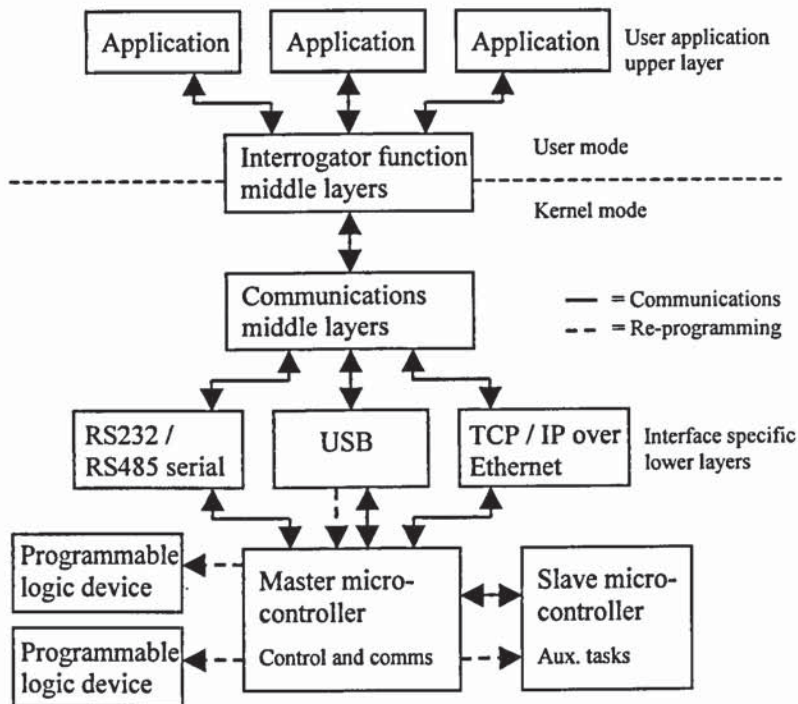
Figure 6.1 An overview of the layered system design, showing communications and re-programming paths from the low-level hardware to top-level user application software

6.3.2 The in-system re-programmable interrogator hardware

The main interrogator hardware included two fully re-programmable microprocessor systems, which operated concurrently in a master-slave configuration. Both processors executed compiled firmware that was largely written in C, with a few, small, hand-optimised assembler routines where maximum efficiency was required.

The master microprocessor provided overall system control. It also communicated with, and was in-system re-programmable by, any attached host. The slave co-processor provided a range of background support functions to the master, including monitoring and control of the semiconductor optical amplifier (SOA) TEC temperature and measurement of the ambient environment. An interconnection between these two microprocessors allowed bi-directional communication and re-programming of the slave by the master.

Two further re-programmable devices were also used in the interrogator hardware. These programmable logic elements were configured using hardware description language (HDL) and connected such that they too could be in-system re-programmed by the master microprocessor. This design meant that full in-service system upgrade was possible if required in the future.

179

6.3.3 Host-system driver-layer software

The interrogator was often connected to a host PC to either provide a graphical user interface for control and data retrieval, or to perform versatile protocol conversion and data logging, as part of a larger system. The host PC could employ either a Microsoft Windows or a GNU / Linux based operating system (OS) and so driver layer software was developed for each. To minimise the quantity of OS specific code, software was written in C and C++, with selective compilation directives employed where necessary. The lowest software layers typically operated as kernel mode device drivers, whereas upper layers were compiled into user-mode dynamically loadable and linkable libraries.

6.3.4 Middle layer software

The software middle-layers provided the link between the hardware-aware driver layer and the user-aware application layer and were also written in C and C++. An object-orientated approach was used internally, but a flat function-based application-programming interface was then exposed to allow maximum compatibility with non-object based client software. Under Microsoft Windows a standard dynamic link library (DLL) provided operation of the interrogator from C, C++, Visual Basic, Java, LabVIEW, Excel or any other DLL-aware software product.

6.3.5 Application layer software systems

The application layer software components were the most important system parts from an end-user perspective, so it was essential to provide a robust, easy to operate user interface. It was important that all demonstration applications provided the user with sufficient functionality that they were able to appreciate the performance of the interrogator, but were not so complex to burden installation and use of the system. For the majority of customers two applications were provided that acted as both system demonstrators and simple design references for inclusion of the programming interface into their own software. These applications were called 'Scan for Sensors' and 'FSI Demo'.

6.3.5.1 Scan for Sensors

Due to the time-division-multiplexed (TDM) nature of the interrogator it was essential to verify and store the spatial position and optical reflectivity of each FBG sensor when either the array or the optical circuit configuration was changed. To achieve this function quickly, reliably and with minimum user interaction, a high level application was developed called 'Scan for Sensors'. Figure 6.2 shows a typical screen shot of this

application when the user had requested the interrogator to locate and configure 15 sensors.
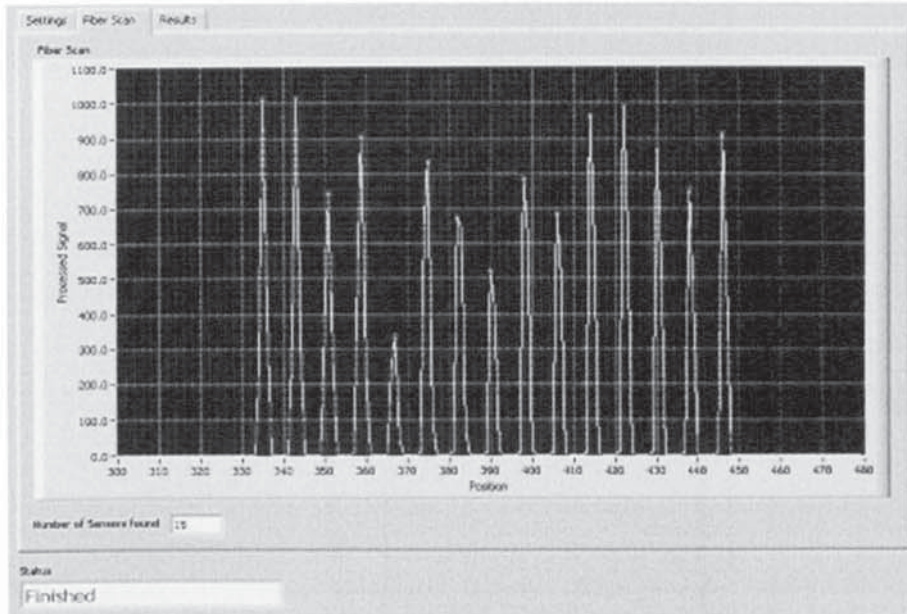
Figure 6.2 A screen shot from the 'Scan For Sensors' application when the user requested the configuration of 15 sensors
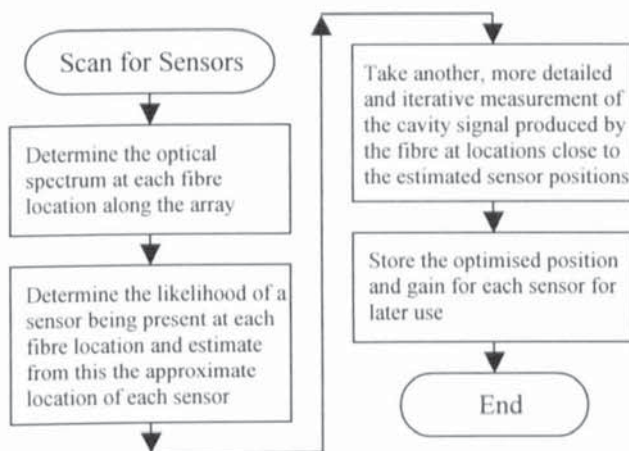
Figure 6.3 A flow chart showing the internal design of the 'Scan for Sensors' application

A flow chart showing the internal design of the 'Scan for Sensors' software is shown in Figure 6.3. Conducting this one-off operation typically took less than 30 seconds and consisted of the following four phases:

Phase 1: Determine the optical spectrum at each fibre location along the array

- The interrogator was requested to operate its programmable pulse generator, such that an attempt was made to form a resonant cavity between the rear reflector and a local fibre position close to the start of the array

181

- The interrogator then returned the optical spectrum produced by the resonant cavity signal from any reflection present at that fibre position

- This spectrum was temporarily stored in memory for later analysis

- The interrogator was then instructed to adjust its programmable pulse generator, such that it now interrogated the next spatial position (16-32cm) further along the fibre

- Again the optical spectrum of the resonant cavity signal was returned and stored for later analysis

- This process of scanning the fibre and storing the spectrum was repeated for all spatial positions between the likely start and end of the array

Phase 2: Determine the likelihood of a sensor being present at each fibre location and estimate from this the approximate location of each sensor

- Having scanned all fibre positions an analysis was made of the spectrum at each location to numerically determine the likely presence or absence of an FBG sensor at that location (as shown in Figure 6.2)

- A peak search was then conducted from this numerical data to approximately locate each of the sensors in the spatial domain

Phase 3: Take another, more detailed and iterative measurement of the cavity signal produced by the fibre at locations close to the estimated sensor positions

- Given the estimated location of each sensor, a second assessment was then made around each approximate location to determine the exact position and reflectivity of each sensor

- This step was performed with higher spatial resolution, with numerous SOA gain settings and with greater numerical analysis than that performed in phase 1

Phase 4: Store the optimised position and gain for each sensor for later use

- Finally the optimised positions and SOA gains for the sensors were stored in a configuration file and downloaded into the interrogator for later use

Options were also provided in the software to allow the user to reduce the number of active sensors used by the interrogator or to narrow the range of the fibre search.

6.3.5.2 FSI Demo

The second main application was called 'FSI Demo'. This provided a simple live view of sensor data and was primarily used for system demonstration. Figure 6.4 shows a screen shot of the application when the interrogator was set to monitor 15 sensors.
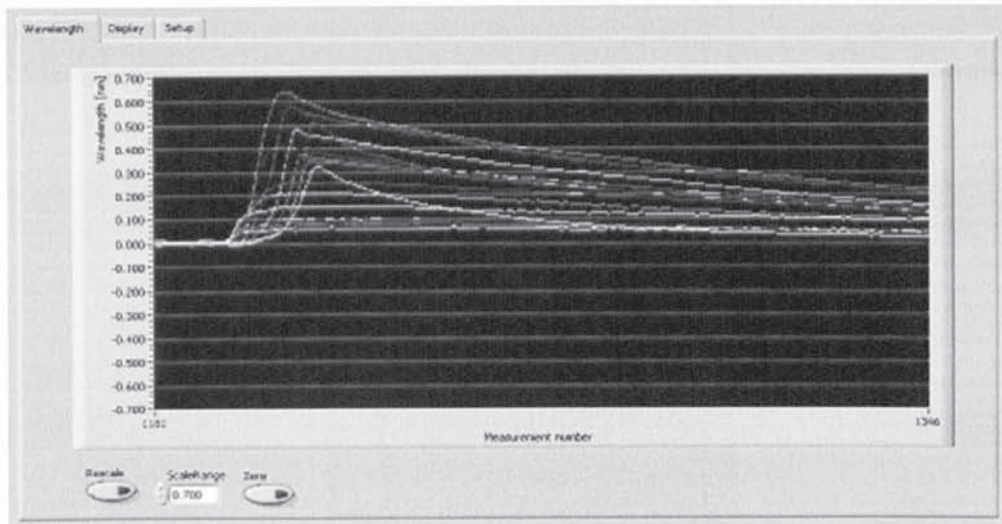
Figure 6.4 A screen shot from the 'FSI Demo' application showing live data from 15 sensors that have been briefly heated and then allowed to cool

Figure 6.5 shows the primary application-programming interface functions that were demonstrated by the application. It can be seen that interrogator initialisation and data retrieval could be achieved with just 4 simple functions. However, additional functions were also provided to allow for specialist configuration or for the return of greater levels of spectral information, as required by some custom user applications.
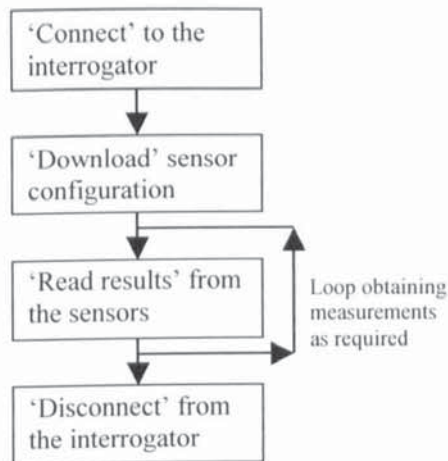
Figure 6.5 The primary application-programming interface functions demonstrated by the 'FSI Demo' software

6.4 Application examples

The resonant cavity fibre sensor interrogator has been manufactured in volume and deployed into a wide variety of applications to-date. For some of these applications very little addition development work was required, beyond that undertaken for the

basic system, but for other applications numerous extensions were required. These extensions have included:

- Numerous hardware and software interfaces for compatibility with existing customer systems

- The provision for remotely controlled interrogation

- Long term data logging to compact flash memory

- Electrical power saving and scheduled wake-up schemes

- High-speed, multi-channel measurements

- Sub-sea deployment

- Passive channel splitting

- Numerous specialist sensor deployment techniques

A brief overview of some applications is given in the sections that follow. For each application the operating scenario and environment is described and then details are provided regarding the additional research and development conducted and utilised in the implementation. Some sensor results are also included where commercially appropriate.

6.4.1 Bench top laboratory instrument

The simplest use of the fibre sensor interrogator has been as a bench top laboratory instrument for the experimental measurement of temperature or strain. Examples of experiments performed using the instrument in this manner include the measurement of railway track deformation due to locomotives, resin cure temperature monitoring in the manufacture of composite structures, break-strain measurement of materials and fatigue analysis in wind turbine blade manufacture.

Figure 6.6 shows that for general laboratory use the interrogator was packaged in a plastic enclosure and connected directly to a Microsoft Windows based host PC using a standard Universal Serial Bus (USB) connection. Electrical power was provided by a standard plug-top mains power supply. A graphical user interface (GUI) allowed the

user to control the interrogator functions and log measurements without impacting on their general use of the PC for other laboratory tasks.
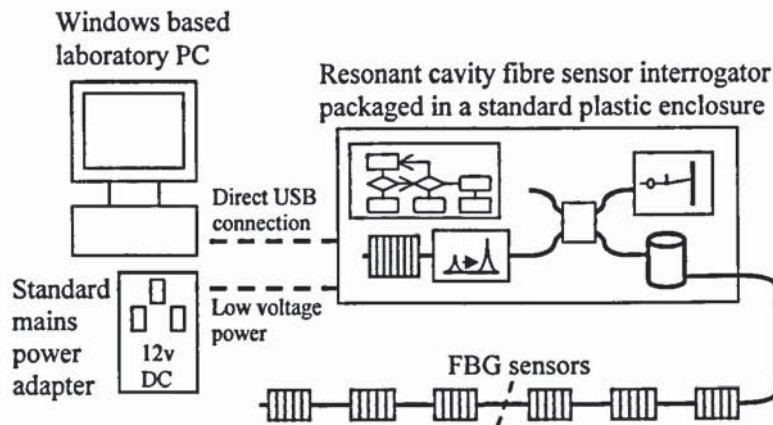
Figure 6.6 The typical configuration using the interrogator as a general laboratory instrument

6.4.2 Distributed temperature monitoring

Numerous applications have been identified for use of the resonant cavity fibre sensor interrogator as a distributed temperature monitor. To-date systems have been deployed for oil well temperature sensing, where operators use the resulting well temperature profile to ensure that pressurised steam injected from the surface during production is delivered to the correct location within the deep oil reserve.

Deep-well oil production requires temperature monitoring at distances up to 8km from the interrogation unit, so performance under high loss conditions is crucial, but interrogation rate need not be high (0.1Hz per sensor is sufficient). Therefore, connection of multiple sensing arrays to a single interrogator using an optical switch is commonplace. For this reason hardware to provide control of optical switches direct from the interrogator was included as standard for the final unit design.

Figure 6.7 shows a typical temperature monitoring system, whilst Figure 6.8 shows a very impressive level of noise from 56 temperature sensors located 4.5km from the interrogator when interrogated at 3 Hz. Typical temperature monitoring systems employ around 50 sensors at spacing >2m, but 160 sensors located at only 1m spacing have also been experimentally demonstrated.

185
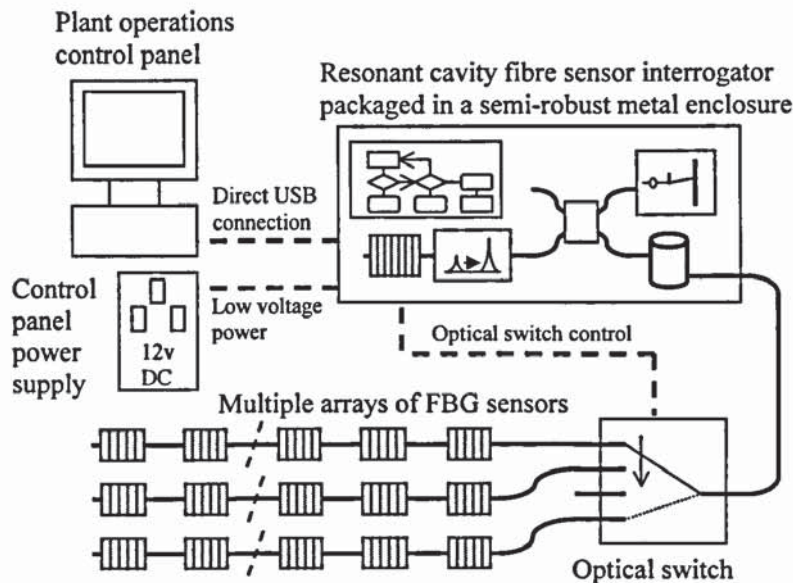
Figure 6.7 A typical configuration using the interrogator as a distributed temperature monitor for industrial process control in oil production wells
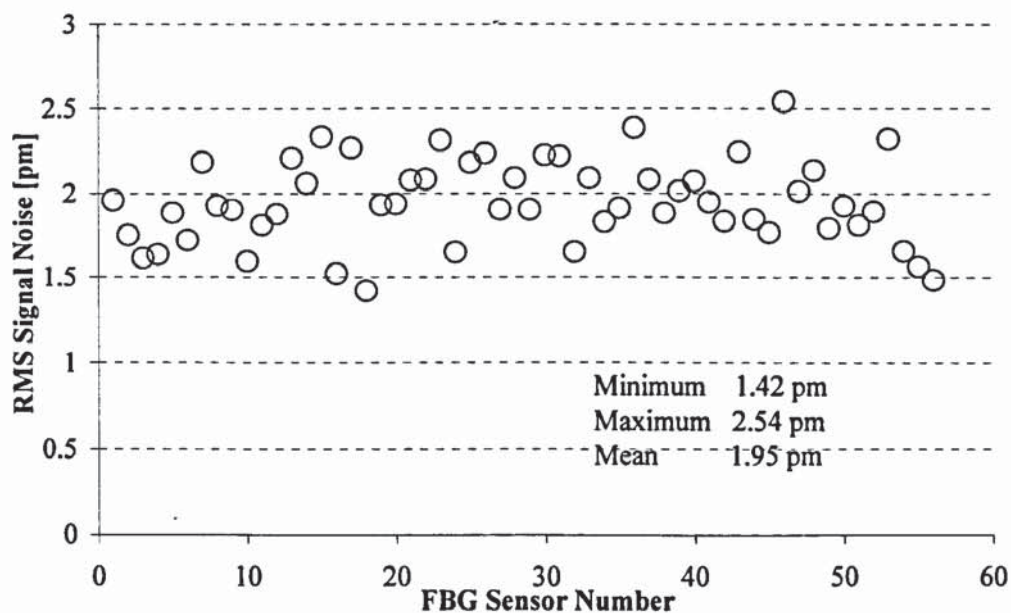
Figure 6.8 A graph showing impressively low levels of noise from 56 temperature sensors located 4480m from the interrogator in a distributed temperature monitor. Note: The reason for plotting noise is that the absolute temperature of each sensor is highly application specific

6.4.3 Applications within wind energy

The application of fibre optic strain sensing to wind energy production offers one of the largest volumes markets identified so far. FBGs offer opportunity for robust accurate remote strain sensing, which can either be retrofitted to existing turbines or installed during initial construction. A close material match between the silica sensing fibre and the host glass composite ensures structural integrity is maintained, whilst natural

186

immunity to electrical interference and metal free, low lighting risk sensors all combine to provide a significant end-user benefit, when compared to electrical alternatives.

6.4.3.1 Structural health monitoring and active blade pitch control

Fibre optic sensing using the resonant cavity fibre sensor interrogator has been identified for two primary applications in wind energy production; online monitoring of structural health and integrity of wind turbine blades, and active blade pitching control. It is intended that a single sensing system would provide both functions.

Traditionally, monitoring of the structural integrity of turbines blades has been achieved through routine visual inspection, but this is expensive and inconvenient, as it requires an engineer to visit a remote site and shutdown the turbine. Shutting down a turbine not only reduces profitability as a result of lost production, but also is only possible in calm weather for safety reasons. By contrast, online structural monitoring can be conducted continuously whilst the turbine is in operation, with the results delivered direct to an engineer's desk anywhere in the world using standard telecommunication links.

Active blade pitching and control is another new concept within the wind energy industry that is gaining considerable research interest. Traditionally turbines have operated with a near constant level of blade pitch. This provides reasonable energy production in modest conditions, but provides reduced output in calmer conditions and requires complete shutdown of the turbine during high winds to prevent damage. Active blade pitching, by contrast, uses continuous monitoring of the strain within the blades to allow a blade-control computer to actively adapt the blade pitch. This optimises energy output and limits damage risk for all weather conditions and so delivers 25%-30% increased energy productivity and reduced occurrence of mechanical failure.

6.4.3.2 Diversity of interface and protocol requirements

Due to the large number of wind energy customers and the diverse range of existing turbine equipment and control systems, it was inappropriate to produce a single bespoke interrogator solution for the entire wind energy industry. It was considered that, for cost reasons, solutions would be closely tailored to specific customer requirements in the future, but as research was still continuing within the industry a more adaptable interrogator solution was preferred for the present. An x86 based single board computer (SBC) executing an embedded GNU/Linux operating system

187

was therefore chosen to provide the interface between the standard resonant cavity fibre sensor interrogator and a variety of customer-specific hardware and software connection and protocol requirements.

Figure 6.9 shows the general configuration of the interrogator when deployed in wind energy applications. It can be seen that the optical circuit consisted of three arrays of sensors, each providing strain and temperature measurement for a single turbine blade. The arrays were connected in a star topology from a single interrogator mounted in the rotating blade hub. This configuration was favoured over serial connection of the arrays since it provided greater redundancy in the event of fibre damage and eased installation; as access was only required to one end of each array. This star connectivity was created in the interrogator enclosure using a passive optical circuit consisting of 33%:67% and 50%:50% splitting ratio fused fibre couplers and two additional spools of fibre. An additional ~5dB of cavity insertion loss occurred, but this did not reduce system performance.

The interrogator was connected to the SBC using a USB interface, whilst the SBC was interfaced to the turbine control system using either TCP/IP over wireless Ethernet, CAN Bus, RS485 Modbus or a RS232 serial connection. Electrical power was provided from the 9-36v DC blade-hub supply using a DC-DC converter.
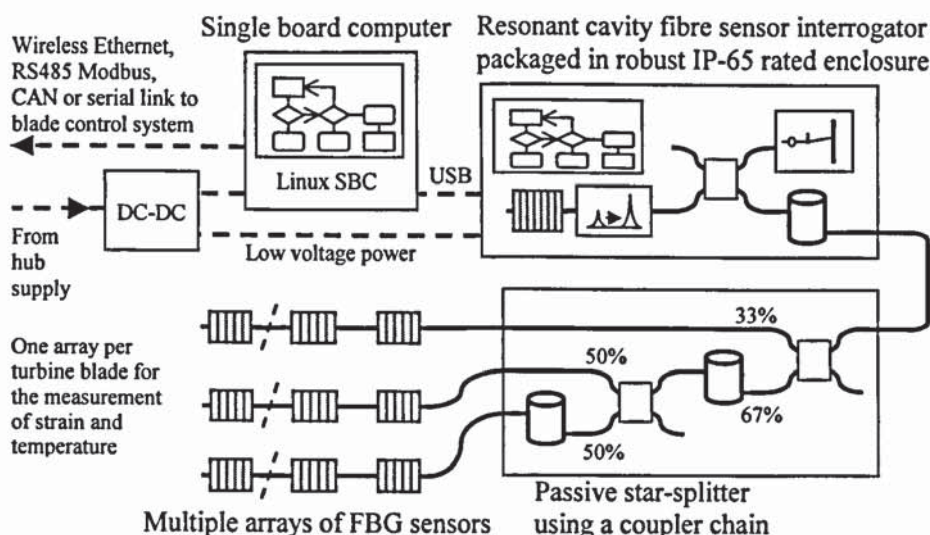

Figure 6.9 A typical configuration using the interrogator as an online strain and temperature measurement system for wind turbines

Figure 6.10 shows results of the strain in each of three wind turbine blades during moderate wind, as measured using the resonant cavity interrogator. The oscillations shown are caused by the strain changes that occur within the blades due to self–weight

forces that are a function of rotator position, the effects of wind shear as blades pass the turbine tower and from differential wind speeds that vary with height above the ground.
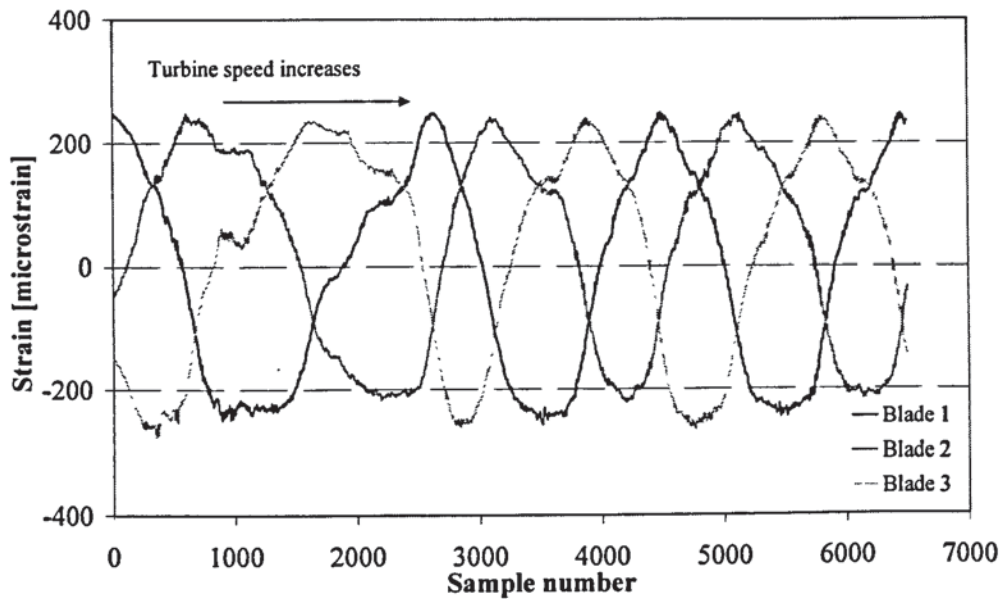
Figure 6.10 The strain measured in each of the three blades of a wind turbine during start-up in moderate wind

6.4.4 Remote battery-powered strain monitor with data logger

For the majority of system deployments a permanent electrical power supply was available and so the power consumption of the interrogator was largely insignificant. However, for applications in remote locations, where external power was not available but where measurements were required infrequently over long periods of time, a bespoke system was developed to control the standard interrogator unit.

Figure 6.11 shows the system configuration that was used for a sub-sea strain sensing deployment. This self-contained system was able to take measurements at pre-programmable intervals of several hours per day, over a period of 8 weeks. The measurement schedule, the number of sensors to interrogate and the interrogation rate were all user-selectable on a per-interval basis using a desktop PC, prior to deployment. The requested schedule was stored to a standard Compact Flash (CF) memory card (as commonly used in digital cameras), which was then inserted into the system. Measurements were then taken and stored to the same memory card, which was retrieved at the end of the analysis period for processing of the results.

189

Figure 6.11 A typical configuration using the interrogator as a remote, self-contained and battery-powered stain sensing system

In order to minimise the total system power consumption, bespoke hardware was developed to control a standard resonant cavity interrogator. This micro-controller based design executed firmware written in C to initialise the interrogator, requested the required measurements and then stored them to th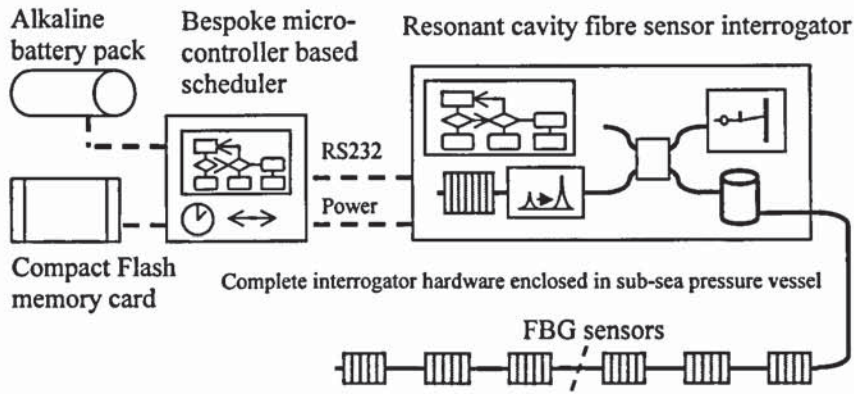e compact flash card in accordance with the specified schedule. Stand-by power consumption of the complete system was <5mW, and only 2W when taking measurements. This was adequately supplied from an inexpensive alkaline battery pack.

This battery-powered interrogator will also be used for long term monitoring of civil structures such as bridges, piers and tunnels, which are often situated in inaccessible locations.

6.4.5 High-speed multi-channel synchronised measurements

Although most applications required the use of only a single interrogator, one system was developed for a research application that employed 8 synchronised interrogators. The customer required close-tolerance, simultaneous, high-speed strain measurement from co-located sensors in 8 separate arrays for vibration analysis of an oil and gas pipeline.

Figure 6.12 shows the configuration used for this unique deployment. It can be seen that each of the 8 sensor arrays were connected to a separate resonant cavity sensor interrogator. The 8 interrogators were coupled into pairs and connected via USB to 4 Linux-based SBCs. Each SBC was networked via a standard Ethernet local area network hub to a single host PC to provide a Windows-based graphical user interface. Also included in the configuration was a dedicated hardware synchroniser, which connected to each interrogator to provide common timing and control signals.

Optimised firmware within each interrogator, bespoke Linux-based data logging software in each SBC and application-specific TCP/IP networking protocols used for communication between processes, enabled interrogation of 280 sensors. This equated to a total throughput of >16000 measurements per second.
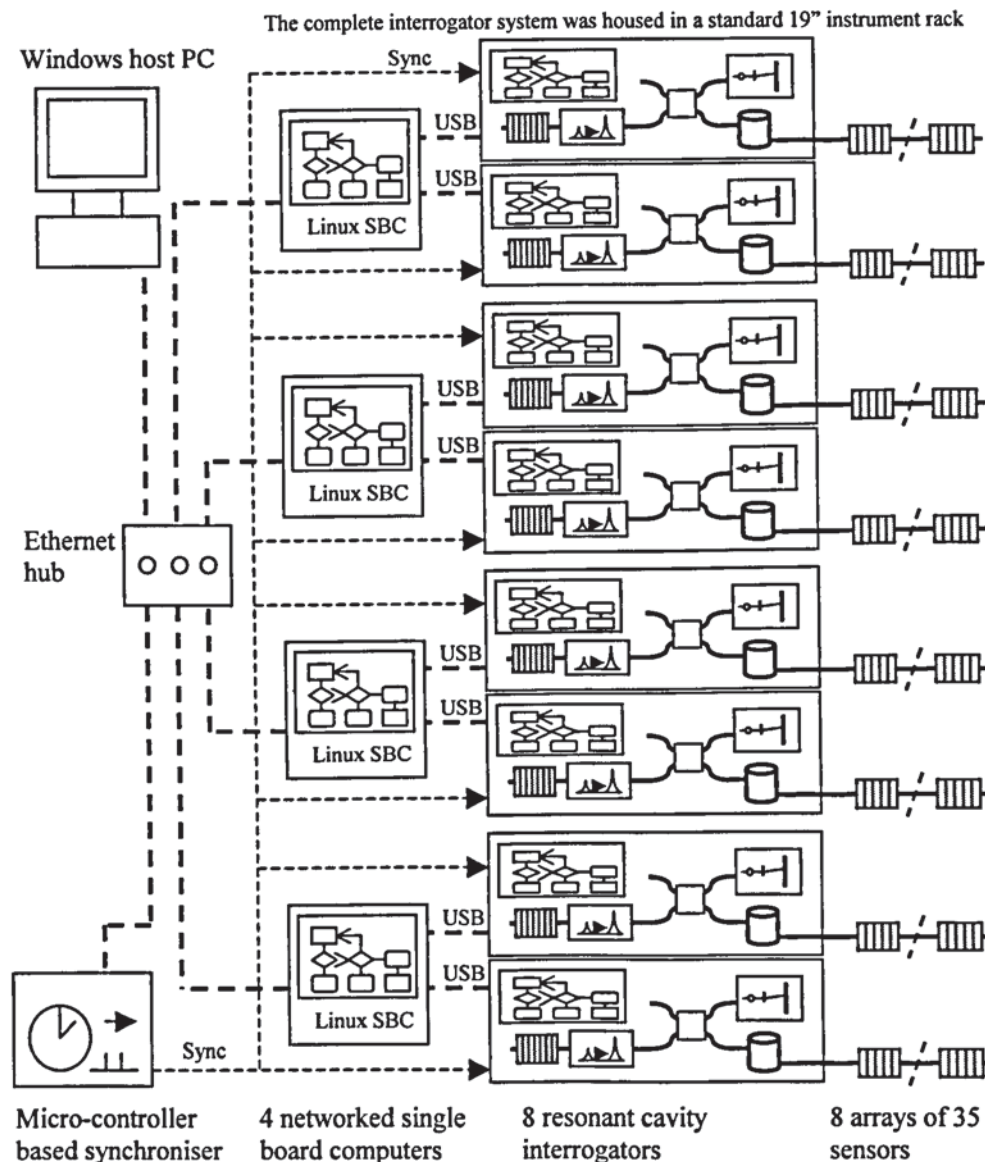
Figure 6.12 The configuration that was used to provide high-speed synchronised strain measurements across 8 separate sensor arrays, for a vibration analysis application

6.4.6 Marine, civil engineering and other pending applications

The low cost, low power, high performance and solid-state advantages of the resonant cavity fibre sensor interrogator have meant that many tens of different applications have now employed the technology. Some examples include:

- Marine projects where fibre optic strain sensing has been employed to measure the load or stress in masts, hulls, rudders and rigging of racing yachts. Live results have been delivered over wireless Ethernet to local support craft for crew training, boat design, research and development

- Civil engineering projects where sensors have been deployed along the inside of road tunnels and bridge supports to monitor for cracks or movement in structures

- Pending projects within the aerospace industry for online monitoring of struts, supports and aircraft landing equipment

- Monitoring of production riser pipes and sub-sea pipelines in the oil and gas industry to provide detection of fatigue and active lifetime estimation

6.5 Chapter conclusion

This chapter has highlighted that successful deployment of new technology into commercial applications requires a wealth of additional research and development beyond the initial fundamental core components. Cost effective production, commercial acceptance and appropriateness for purpose all require that *design for manufacture*, *design for test* and *design for environmental compliance* processes be carefully followed during product development. Robust, yet versatile, interface and access software is required to maximise a system's value to the end-user and to allow modification or extension of the core product for access into new markets.

The resonant cavity fibre sensor interrogator is now manufactured by third-party sub-contractors in volume. It has been fully independently tested and certified for environmental performance beyond the requirements of most industry sectors and has been successfully deployed in many tens of different applications. The core product is regularly sold as a complete laboratory instrument, as an OEM component for distributed temperature monitoring, for control and monitoring of strain in the wind energy sector, as a self-contained, sub-sea deployable strain recorder and as a tool for high-speed vibration research and analysis.

The advantages of the low-cost, high-sensor count, high-speed, all solid-state resonant cavity technology have ensured that new market areas continue to be identified. Research to establish new techniques for sensor deployment is ongoing and further

developments are in progress to deliver extensions to the core product as required by the applications of the future. These include the further electrical and software interface and control options and a wider variety of specialist environmental enclosures to allow operation in areas and environments where there is a high risk of explosion or ignition due to presence of flammable liquids and gases.

7 CONCLUSIONS

This thesis developed a completely novel method of time-division-multiplexing fibre Bragg grating sensors, which became known as the resonant cavity architecture. It concluded with a commercially successful high performance optical sensor interrogation product, but began with the author's original hypothesis, which was the foundation of this new technology; that 'time-division-multiplexing of fibre Bragg grating sensors should be possible using the optical gating properties of a semiconductor optical amplifier'.

This thesis concentrated on just one key topic, but the work required a breadth and depth of knowledge to deliver a novel technology and a unique product that could be repeatedly applied, with confidence, into a wide range of long-term applications in harsh industrial environments. This new technology has helped to bring a significant change to the market acceptance for fibre Bragg grating (FBG) based optical sensing and has thus created a substantially greater commercial uptake.

The initial 'proof of concept' experimental work proved three fundamentally advantageous characteristics obtained by electrically switching a semiconductor optical amplifier (SOA). Firstly, and most importantly, that it could be used to optically gate individual reflection signals from a time-division-multiplexed (TDM) FBG sensor array. Also that the amplified spontaneous emission (ASE) generated by the SOA (in the absence of an optical input signal) could be used as a source of illumination for the sensors and, finally, that the weak reflection signals received amplification whilst passing through the SOA. In this manner the SOA was shown to provide the combined functions of optical source, amplifier and gate.

The demonstration of using a rear reflector to recycle the gated reflection signals was one of the most significant experimental achievements in this thesis. When positioned at the rear of the SOA, a highly reflective, broadband, chirped fibre Bragg grating produced a 'laser-like' virtual cavity with any desired sensor in the array, under complete electronic control. The resulting cyclic, resonant cavity signal had a very high optical power (>5dBm), an exceptional optical signal to noise ratio (OSNR) (up to 50dB) and could be extracted using a number of different optical circuit configurations. This flexibility in the choice of configuration allowed wavelength measurement using a

variety of wavelength detection components, including low cost, passive techniques that are incompatible with wavelength-division-multiplexing (WDM) schemes.

Experimental verification of the resonant cavity architecture with low reflectivity (4%) FBG sensors demonstrated a high mean extracted signal power of −22dBm, an extremely impressive OSNR of >30dB, support for inline losses of >13dB and minimal crosstalk between sensors. This strong performance under high-loss conditions equated to the use of sensors with <<1% reflectivity and allowed the option of using passive splitting for support of multiple sensing fibres or looped sensor array structures (for redundancy).

Theoretical modelling of wavelength-shadowing-induced sensor crosstalk was conducted and some correlation with experimental data was determined. However, a discrepancy in the magnitude of the results indicated that the cavity dynamics are non-linear. An experimental analysis of the cavity signal evolution was therefore conducted, which showed that with each complete cycle of the cavity the peak signal power increased exponentially while the background ASE reduced, until an equilibrium was reached after ~9 cycles. This result highlights that further analysis should be conducted in the future.

Finally, preliminary experimental work was conducted using a dual-pulse SOA switching scheme, with multiple rear reflectors in a hybrid WDM / TDM architecture. This architecture was shown allow sensor spacing of less than one metre. These results are also expected to allow efficient monitoring of multiple fibre channels using a telecommunication WDM demultiplexer or support for numerous looped sensor array structures for redundancy, as required in the future.

The final conclusion of the work conducted on the configurable SOA drive system was also a very significant achievement. Early experimental verification of the operating characteristics of an SOA under pulsed conditions resulted in development of a totem pole complementary transistor SOA driver circuit. This was constructed from parallel-connected 74AC series logic gates and allowed SOA switching in just a few nanoseconds, for the close spacing of sensors (~1m). A novel pulse generator with spatial-resolution virtual sub-division was developed using programmable counters and an efficient dithering scheme, to overcome limitations in current logic speeds. When clocked at 320MHz using a frequency synthesizer this unique design allowed spatial

tuning of sensors to 0.08m, a maximum cavity length of 10.24km and the control of pulse duration in 3ns increments. Programmable control of the SOA drive current was also provided for dynamic adjustment of the optical system gain, to account for variation in cavity loss and grating reflectivity, on a per-sensor, real-time basis.

It is anticipated that with a sustained trend toward faster, higher-density, lower-power logic components, further enhancements to the programmable pulse generator will be possible in the future. In particular, additional work is envisaged in design of more advanced dual- and multi-pulse SOA drive configurations, and the ability to arbitrarily profile each pulse, to adjust the cavity gain-dynamics independently in each direction.

The research carried out on integration of the resonant cavity architecture optical demultiplexer with wavelength measurement components resulted in two successful interrogator designs with different key performance characteristics:

The simple, low-cost, passive, ratiometric design operated with a resonant cavity signal that was extracted after reflection from the rear-reflector, so removing all out-of-band ASE. This design was based around a commercial filter component, which contained a beam splitter, an edge-filter and two photodiodes. Bespoke electronics containing high-linearity analogue trans-impedance amplifiers and a dual simultaneous-sampling analogue to digital converter were designed around the filter to measure the photocurrents and return the results to a system microprocessor for conversion into wavelength, temperature or strain. This ratiometric design was demonstrated to provide a measurement rate of 4.4kHz, a resolution of 1pm, and has good linearity after calibration, but its operation with a cavity loss variation >3.6dB was not recommended. The design was expected to be of greatest commercial successful for future very high volume, high repeatability applications, such as automotive.

The second wavelength measurement technique researched was a diffractive element spectrometer. This was based on a telecommunications channel monitor and was integrated with an alternative variant of the resonant cavity architecture, which extracted the high power cavity signal from the front of the SOA. This pulsed optical signal was synchronised with the acquisition cycle of the spectrometer using bespoke interface electronics. This hardware also provided acceleration of serial-to-parallel data transfer and enabled high measurement speed. Detailed performance analysis showed exceptional results, with a resolution of ~1pm, an RMS noise of <1pm, a polarisation

dependant wavelength shift of <10pm and a loss-induced wavelength shift of <2pm (for 10dB change in cavity loss), using only 4% reflective sensors. The high performance spectrometer-based resonant cavity sensor interrogator design was considered appropriate for all targeted applications and so was chosen for mass production, but it was noted that a wide variety of other wavelength detection techniques are also compatible with the resonant cavity architecture and so could be utilised in future designs.

The work conducted on the mass manufactured interrogator in *design for environmental performance compliance*, *design for manufacture* and *design for test* all demonstrated that successful deployment of new technology into commercial applications requires significantly more effort than simply concentrating on the initial fundamental core components. A target of ease of installation, ease of integration, confidence in long term performance and true end-user value for money were all demonstrated through a environmental performance test program and the development of a variety of versatile installation, control and data interfacing protocols and software systems.

Similarly, the goal of developing a core interrogation system capable of benefiting from economies of scale through the mass manufacture of a single high performance design was successfully demonstrated. The core resonant cavity interrogator was deployed, with ease, as a bench top instrument, as a unit for distributed temperature monitoring in oil production, for health monitoring and control in wind energy, for sub-sea battery powered strain monitoring and for synchronised high-speed vibration analysis in a cluster of 8 interrogators and 280 sensors.

Despite the highly significant success of the resonant cavity interrogator design further work is possible as the technology can be extended on many levels. At the fundamental level the resonant cavity architecture is likely to be improved as new optical configurations are analysed, stronger theoretic models are constructed and new optical components are developed. At a developmental level the physical construction, fibre layout, electronics, control and software systems could all be improved to lower manufacturing costs, reduce electrical power consumption, improve reliability or provide application level parametric data analysis. At an application level the advantages delivered by the novel, high sensor count, low complexity, low cost FBG

sensor interrogation technology provide a strong potential for the development of optical sensing solutions into entirely new disciplines.

With the success that has occurred so far, and the potential that is still to be explored, the future for resonant cavity time-division-multiplexed FBG sensor interrogation looks very bright indeed.

8 PUBLICATIONS

G. D. Lloyd, L. A. Everall, 'Optical Interrogation System and Sensor System' European Patent 2258640.8, Filed 16th December 2002

G. D. Lloyd, L. A. Everall, 'Optical Interrogation System and Sensor System', US Patent 2004/0113056-A1, Published 17th June 2004

G. D. Lloyd, L. A. Everall, K. Sugden, I. Bennion, 'A high-performance miniaturized time-division-multiplexed sensor system for remote structural health monitoring', *Proc. SPIE Photonics Europe 2004, Strasbourg, France*, 2004, 5459-17

G. D. Lloyd, L. A. Everall, K. Sugden, I. Bennion, 'Novel resonant cavity TDM demodulation scheme for FBG sensing', *Proc. Conference on Lasers and Electro-optics (CLEO) 2004, San Francisco, USA*, 2004, CWD4

G. D. Lloyd, L. A. Everall, K. Sugden, I. Bennion, 'Resonant Cavity Time-Division-Multiplexed Fiber Bragg Grating Interrogator', *Photon. Technol. Lett.*, **16**, (10), 2004, pp.2323-2325

G. D. Lloyd, L. A. Everall, K. Sugden, I. Bennion, 'Resonant cavity based fibre Bragg grating interrogation using ratiometric detection', *Opt. Commun.*, **244**, (1-6), 2004, pp.193-197

G. D. Lloyd, L. A. Everall, K. Sugden, I. Bennion, 'Re-configurable, multi-channel, high-speed FBG strain sensing system for vibration analysis in oil risers', *17th Conference on Optical Fibre Sensing, Bruges, Belgium* 2005 (submitted for publication)

Yicheng Lai, W. Zhang, G. D. Lloyd, J.A.R. Williams, I. Bennion, "A novel cavity mode assessment technique for fibre lasers" *Proc. 29th European Conference on optical Communications (ECOC/IOOC), Rimini, Italy*, 2003, We2.6.4

X. Shu, K. Sugden, P. Rhead, J. Mitchell, I. Felmeri, G. D. Lloyd, K. Byron, Z. Huang, I. Khrushchev, I. Bennion, 'Tunable Dispersion Compensator Based on Distributed Gires-Tournois Etalons', *Photon. Technol. Lett.*, **15**, (8), 2003, pp.1111-1113

P. Rhead, X. Shu, G. D. Lloyd, 'Tuneable optical waveguide grating transmission filter' US and Worldwide Patents from PCT/GB03/01117